The Chukchi Region - Arctic Ocean - Tectonic and Sedimentary Evolution

Dissertation

zur Erlangung des akademischen Grades doctor rerum naturalium
(Dr. rer. nat.)

vorgelegt dem Rat der Chemisch-Geowissenschaftlichen Fakultät der
Friedrich-Schiller-Universität Jena

von Diplom-Geophysikerin Anne Hegewald
geboren am 11. Januar 1985 in Erfurt

Gutachter:

1. Prof. Dr. Gerhard Jentzsch, Friedrich-Schiller-Universität Jena

2. Prof. Dr. Michael Korn, Universität Leipzig

3. PD Dr. Thomas Jahr, Friedrich-Schiller-Universität Jena

Tag der öffentlichen Verteidigung: 19. Oktober 2012

The Chukchi Region - Arctic Ocean - Tectonic and Sedimentary Evolution

Dissertation

Anne Hegewald

Summary

The Arctic Ocean is an area of increasing interest for research. Variations in the sensitive polar ecosystem influence the environment of the global Earth system and climate change. Therefore, reviews of modern Arctic Ocean system thereby provide the basis to interpret the Arctic Ocean evolution through its past. Regarding the bathymetry, the Arctic Ocean consists of two major basins: the Eurasian Basin (the smaller and geologically younger basin) and the Amerasian Basin (the larger and geologically older basin). The evolution of the Eurasian Basin is well understood, based on magnetic spreading anomalies. In contrast, the opening of the Amerasian Basin remains controversial and multiple oceanic rift models still exist. The data acquisition in the Arctic Ocean and particularly in the western Arctic Ocean (Amerasian Basin), however, has been complicated by the limited accessibility due to the perennial ice cover and short summer season.

During the ARK-XXIII/3 expedition in the summer of 2008, the Alfred Wegener Institute (Bremerhaven, Germany) could acquire the first seismic data set - consisting of seismic reflection lines as well as wide-angle reflection and refraction data - in the northern Chukchi region and the southern part of the Mendeleev Ridge, Amerasian Basin. In addition, further data sets (logging information from exploration wells, additional seismic lines from the southern Chukchi region, gravity data of the entire Arctic Ocean) were available and used for the investigations within this thesis.

Summarising the results, we could date the sediments which cover the research area (northern Chukchi region and southern part of the Mendeleev Ridge), using the age control from the exploration wells. Furthermore, with the interpretation of the tectonic elements (e.g. faults, graben structures, erosion events) the ages of evolution of the southern Mendeleev Ridge, the Chukchi Abyssal Plain and the Chukchi Plateau were derived. In addition, a complex 3D gravity model of the research area was calculated and allowed the development of two tectonic models for the origin of the Chukchi Borderland and the Mendeleev Ridge. Moreover, two already existing oceanic rift models

for the opening of the Amerasian Basin were modified based on our results. On the other hand, we used the prograding sediment horizons on the northern Chukchi Shelf to reconstruct the first relative sea level curve for the Chukchi region, beginning in the Late Eocene. This curve led to conclusions about the existence of gateways between the Arctic Ocean and the other global oceans. Therefore, we suggest an isolated Arctic Ocean from the Eocene/Oligocene boundary to the Early Miocene. In this period, the relative sea level in the isolated Arctic basin was higher than in the global oceans. With the opening of the Fram Strait in the Early Miocene, the Arctic Ocean water flowed into the Atlantic Ocean causing an increase in the North Atlantic sea level.

Zusammenfassung

Der Arktische Ozean rückt zunehmend in den Fokus wissenschaftlichen Interesses, da klimatische Veränderungen in diesem hoch empfindlichen Ökosystem tiefgreifende globale Auswirkungen zur Folge haben. Die Erstellung globaler Klimaprognosen setzt dabei das Verständnis früherer Umweltbedingungen voraus. Noch immer bestehen Unklarheiten über entscheidende Prozesse der klimatischen und geologischen Geschichte dieser Region.

Der zentrale Bereich des Arktischen Ozeans besteht aus zwei Tiefseebecken, dem Eurasischen und dem Amerasischen Becken. Die Entstehung des geologisch jüngeren Eurasischen Beckens ist durch datierte magnetische Spreizungsanomalien weitestgehend verstanden. Im Gegensatz dazu ist die Entstehung des geologisch älteren Amerasischen Beckens größtenteils unklar. In diesem Zusammenhang existieren verschiedene Modelle, die die Öffnung des Amerasischen Beckens auf unterschiedliche Weise beschreiben.

Die Erhebung neuer Daten, die mögliche Antworten auf diese Fragen liefern könnten, ist jedoch stark durch die permanente Meereisbedeckung sowie die kurze Sommersaison eingeschränkt. Besonders der westliche Teil des Arktischen Ozeans gehört zu den am wenigsten erforschten Meeresregionen der Erde.

Die dieser Arbeit zu Grunde liegenden geophysikalischen Daten, aus der nördlichen Chukchi Region und dem südlichen Mendeleev Rücken, wurden im Sommer 2008 im Rahmen der Schiffsexpedition ARK-XXIII/3 vom Alfred-Wegener-Institut erhoben. Dabei handelt es sich um die ersten reflexionsseismischen Daten in dieser Region. Zusätzlich zu den seismischen Daten standen drei weitere Datensätze zur Verfügung und wurden in die Interpretation mit einbezogen: (1) Informationen über Sedimenteigenschaften und -alter von fünf Explorationsbohrungen, (2) weitere seismische Profile von der südlichen Chukchi Region, sowie (3) Schwerefelddaten vom gesamten Arktischen Ozean.

Die Ergebnisse dieser Arbeit umfassen die erstmalige Datierung von Sedimenthorizonten im Bereich der nördlichen Chukchi Region und dem südlichen Mendeleev Rücken.

Die datierten Sedimenthorizonte konnten anhand seismischer Profile und der Explorationsbohrungen im Untersuchungsgebiet identifiziert werden. Darauf basierend wurden Entstehungsalter für das Chukchi Plateau, die Chukchi Tiefseeebene und den Mendeleev Rücken abgeleitet. Darüber hinaus konnte mittels verfügbarer Schwerefelddaten ein komplexes 3D Schweremodell entwickelt werden, auf dessen Grundlage zwei Entstehungsmodelle für das Chukchi Grenzland und den Mendeleev Rücken abgeleitet und diskutiert wurden. Zusätzlich wurden zwei bereits bestehende Modelle für die Öffnung des Amerasischen Beckens modifiziert.

Des Weiteren konnte, basierend auf progradierenden Sedimenthorizonten auf dem nördlichen Chukchi Schelf, eine relative Meeresspiegelschwankungskurve für die Chukchi Region rekonstruiert werden. Diese Kurve beginnt im späten Eozän und ist die erste relative Meeresspiegelschwankungskurve für den Arktischen Ozean. Daraus abgeleitet war der Arktische Ozean vom Eozän/Oligozän Übergang bis in das frühe Miozän ein von der globalen Meerwasserzirkulation abgeschlossener Wasserkörper, dessen relativer Meeresspiegel höher war als in den angrenzenden globalen Ozeanen. Mit der Öffnung der Framstraße im frühen Miozän strömte das arktische Meerwasser in den Atlantik. Dies führte zu einem Anstieg des Meeresspiegels im Nordatlantik wie anhand von Daten im Bereich der New Jersey Küstenebene dokumentiert wurde.

Contents

Summary i

Zusammenfassung iii

Contents v

List of Figures vii

List of Tables ix

Abbreviation xi

1 Introduction 1

1.1 Motivation 1

1.2 Outline 3

2 The Chukchi Region 5

2.1 Regional Setting (Bathymetry, Gravity, Magnetics) 5

2.2 Geological Evolution 9

2.3 Geological Stratigraphy 12

3 Seismic Data 15

3.1 Multi Channel Seismic Data 15

3.1.1 Processing 16

3.1.2 Age Control for Seismic Data 18

3.2 Sonobuoy Data 22

3.2.1 Processing 23

3.2.2 Results 23

3.3 Main Geological Framework 27

3.3.1 The Chukchi Plateau 27

3.3.2 The Chukchi Abyssal Plain 32

3.3.3 The Mendeleev Ridge 33
3.3.4 The Chukchi Shelf 40
3.4 Sediment Source Area 42
3.5 Relative Sea Level Variations 44
3.5.1 Seismic Sequence Stratigraphy 45
3.5.2 Relative Sea Level Variations in the Chukchi Region 49

4 Gravity Data **55**
4.1 The Arctic Gravity Project (ArcGP) 55
4.2 Sedimentary Thickness and Basement Depth 55
4.3 Calculation of Moho Depth 59
4.4 Gravimetric 3D Modelling 62
4.4.1 Boundary Conditions 63
4.4.2 The 3D Model 65
4.4.3 Residuals 73

5 Models for the Origin of the Chukchi Region **79**

6 Conclusion and Discussion **85**

7 Outlook **91**

8 References **93**

Acknowledgment **I**

Selbstständigkeitserklärung **III**

Curriculum Vitae **V**

List of Figures

2.1 Map of the Arctic Ocean 7
2.2 Bathymetry, gravity, magnetics of the Chukchi region 8
2.3 Four main oceanic rift models for the Amerasian Basin 10
2.4 Main structural features below the Chukchi and East Siberian Shelf . . 11
2.5 Geological stratigraphy of the Chukchi region 13
3.1 Locations of the AWI seismic lines 16
3.2 Workflow for seismic data processing 17
3.3 Locations of exploration wells and additional seismic lines 19
3.4 Extrapolated seismic horizons over "data gap" on Chukchi Shelf 20
3.5 AWI line 60 including dated horizons 20
3.6 Locations of dated horizons in the AWI seismic network 21
3.7 Locations of the AWI sonobuoys 22
3.8 Processing steps shown at sonobuoy SB09 24
3.9 2D velocity-depth models of the AWI sonobuoys 25
3.10 TWT-depth relation for the study area 26
3.11 Seismic lines across the Chukchi Plateau 28
3.12 Sediment filled channel on the Chukchi Cap 31
3.13 Syntectonic sediments on the Chukchi Rise 31
3.14 Seismic lines across the Chukchi Abyssal Plain 34
3.15 Dipping basement reflectors in the Chukchi Abyssal Plain 35
3.16 Dipping basement reflectors at eastern slope of the Mendeleev Ridge . . 35
3.17 Seismic lines across the Mendeleev Ridge 38
3.18 Subbasement reflectors on the Mendeleev Ridge 39
3.19 Top Oligocene unconformity on the Mendeleev Ridge 39
3.20 Seismic lines on the Chukchi Shelf 41
3.21 Shelf margin shape between Chukchi Plateau and Mendeleev Ridge . . 43
3.22 Main sediment source area 44

3.23 AWI seismic lines across the shelf margin 46
3.24 Method of seismic sequence stratigraphy 47
3.25 Interpreted prograding sequences in the AWI MCS lines 48
3.26 Relative sea level curve from the Arctic Ocean 50
4.1 Arctic Gravity Project (ArcGP) map 56
4.2 Data sets for the calculation of the basement depth 57
4.3 Basement depth map 58
4.4 Sedimentary thickness map 58
4.5 Areas of Moho depth calculation and 3D gravity model 60
4.6 Spectral analysis of the gravity field 61
4.7 Calculated Moho depth 61
4.8 Locations of model sections on bathymetry map 63
4.9 Locations of model sections on free-air anomaly map 64
4.10 Location of crustal model bodies 65
4.11 Model section 1 69
4.12 Model section 7 70
4.13 Model section 12 71
4.14 Model section 19 72
4.15 Gravity effects of sediments, crust and mantle 75
4.16 Measured, modelled free-air anomalies and residuals 76
4.17 Calculated, modelled basement depths and residuals 77
4.18 Calculated, modelled Moho depths and residuals 78
5.1 Evolution models for Chukchi Borderland and Mendeleev Ridge 81

List of Tables

3.1 Technical specifications of the used streamers and air gun array 15
3.2 Maximum offsets of the AWI sonobuoys 22
4.1 Moho depth values from several data sets 62
4.2 Sediment densities received from logging information 64
4.3 Densities of the geological model bodies 66
4.4 Modelled Moho depth and published values 73

List of Tables

Abbreviation

AACM	Arctic Alaska-Chukotka Microplate
AGC	Automatic Gain Control
AR	Alpha Ridge
ArcGP	Arctic Gravity Project
AWI	Alfred Wegener Institute
BGR	Federal Institute for Geosciences and Natural Resources
BS	Beaufort Sea
CAP	Chukchi Abyssal Plain
CB	Canada Basin
CBL	Chukchi Borderland
CDP	Common Depth Point
Chevron USA	Oil Company
CP	Chukchi Plateau
CS	Chukchi Shelf
EMAG	Earth Magnetic Anomaly Grid
ESS	East Siberian Shelf
FSST	Falling Stage Systems Tract
FSU	Friedrich Schiller University Jena
HST	Highstand Systems Tract
IBCAO	International Bathymetric Chart of the Arctic Ocean
ION-GXT	Geophysical Company
JU	Jurassic Unconformity
LCU	Lower Cretaceous Unconformity
LR	Lomonosov Ridge
LST	Lowstand Systems Tract
MB	Makarov Basin
MBU	Mid Brookian Unconformity

MCS	Multi Channel Seismic
MFS	Maximum Flooding Surface
Moho	Mohorovičić discontinuity
MR	Mendeleev Ridge
MRS	Maximum Regressive Surface
NR	Northwind Ridge
PO	Pliocene
RMS	Root Mean Square
RSL	Relative Sea Level
RV	Research Vessel
SB	Sonobuoy
Shell	Oil Company
TGS-NOPEC	Geophysical Company
TST	Transgressive Systems Tract
TWT	Two-Way Time
UAF	University of Alaska, Fairbanks
USGS	United States Geological Service
WesternGeco	Geophysical Company
WGS	World Geodetic System
WHA	Wrangel-Herald Arch
WI	Wrangel Island

1 Introduction

1.1 Motivation

The Arctic Ocean is surrounded by continents and the world's largest shelf seas. Furthermore, the Arctic Ocean itself is seasonally to permanently covered by sea ice, and the Arctic Ocean water is strongly influenced by huge river discharge from the surrounding continents. These characteristics have a large influence on the environment of the Arctic Ocean itself, the global Earth system and climate change (Stein 2008). Therefore, the Arctic Ocean is an area of increasing interest. However, the opening of the Arctic Ocean, especially the Amerasian Basin, is highly controversial according to the few available geophysical data and the missing of significant magnetic seafloor spreading anomalies in this basin (Lane 1997). This is why a variety of models describe the opening of the Amerasian Basin (Lawver & Scotese 1990, Miller et al. 2006). The most widely accepted one is the rotation model where Arctic Alaska and Chukotka moved away from the Canadian Arctic by a counterclockwise rotation in Jurassic to Early Cretaceous time (Rowley & Lottes 1988, Grantz et al. 1990, Embry 1990, Plafker & Berg 1994, Lawver et al. 2002). Moreover, the current knowledge about the Chukchi region (part of the Amerasian Basin) is poor and bases on very few data. Therefore, new geophysical data would have a huge impact on the understanding of the evolution of the Chukchi region, and subsequently the opening of the Amerasian Basin.

In the 2008 summer expedition, the Alfred Wegener Institute (AWI) carried out the ARK-XXIII/3 expedition with the German research ice breaker "Polarstern" to the Chukchi region and southern part of the Mendeleev Ridge (Jokat et al. 2009). Main objective of this expedition was to acquire and collect geoscientific data and material to deepen our understanding of the older geological evolution as well as the younger glacial history of this region.

However, the geophysical data acquisition in the Amerasian Basin is quite difficult because of heavy ice conditions all over the year. Therefore, data from only one expedition during 2005 exist and show the sediment and basement structures of the Northwind

Ridge (Arrigoni 2008) and the northern part of the Mendeleev Ridge (Dove et al. 2010). In addition, the stratigraphy of the Northwind Ridge was reconstructed from 15 piston cores and one box core that sampled bedrock outcrops on the Northwind Escarpment carried out by the American expeditions in 1988, 1992 and 1993 (Grantz et al. 1998). During the 2008 expedition, the AWI could acquire multi channel seismic (MCS) data (using a 3000 m and a 600 m streamer) as well as wide-angle reflection and refraction data (using 12 sonobuoys) in the Chukchi region and southern part of the Mendeleev Ridge (Jokat et al. 2009). These data represent the first seismic data set in this region of the Arctic Ocean. In addition, we used three other data sets in this thesis to develop a geodynamic model for the Chukchi region: (1) public-domain gravity data from airborne, submarine, ship and from ERS-1 and -2 satellite altimetry are available as a compilation of the gravity field in the Arctic Gravity Project (ArcGP, Kenyon et al. 2008), (2) public-domain seismic reflection data (located on Chukchi Shelf, Northwind Ridge, northern Mendeleev Ridge) are available from the National Archive of Marine Seismic Surveys (USGS 2012), and (3) logging information from five exploration wells drilled on the Chukchi Shelf near the coast of Alaska (Sherwood et al. 2002).

In general, geophysical data (e.g. seismic and gravity data) give an insight into the structure of the earth's crust and its upper mantle. Sediment and basement structures as well as tectonic elements, like faults and folds can be imaged with MCS data. The absolute age control for seismic horizons, the character of subground material and several physical material parameters can be received from analysed well data. Using gravity data a 3D model can be calculated. Within this 3D model the basement topography, the crustal thickness and structures as well as the Moho topography can be displayed. Therefore, interpreted seismic data have been used as boundary conditions to reduce the ambiguity of the gravity potential field solution.

Based on all these data it might be possible to understand the tectonic evolution of the Chukchi region in the Arctic Ocean. Furthermore, such results could lead to the conclusions about the opening of the Amerasian Basin, and subsequently the history of the Arctic Ocean.

1.2 Outline

This thesis bases on two geophysical data sets - seismic and gravity - from the Chukchi region and southern part of the Mendeleev Ridge. During the AWI 2008 expedition more than 3300 km of seismic lines and data sets of 12 sonobuoys were acquired (Jokat et al. 2009). Furthermore, the gravity grid (ArcGP) has a resolution of 5' x 5' and covers the entire study area (Kenyon et al. 2008). In addition, the logging information of five exploration wells near the coast of Alaska (Sherwood et al. 2002) were used for the dating of the seismic horizons.

First steps were the processing of the MCS data (Chapter 3.1) as well as the modelling of the sonobuoys wide-angle reflection and refraction data (Chapter 3.2). Prominent horizons of the processed seismic lines were dated using the five exploration wells and additional seismic lines acquired by other international institutes and companies between 1969 and 2006 (Chapter 3.1.2). The processed and dated AWI MCS data were interpreted for the four main geological provinces in the study area: the Chukchi Plateau, the Chukchi Abyssal Plain, the southern part of the Mendeleev Ridge and the northern Chukchi Shelf (Chapter 3.3). Furthermore, the main sediment source area could be inferred from prograding sediment structures on the Chukchi Shelf (Chapter 3.4). Based on prograding sequences in the upper sediments on the Chukchi Shelf the relative sea level variations for the Arctic Ocean, beginning in the Late Eocene (40 Ma), could be calculated (Chapter 3.5). This Arctic relative sea level curve leads to the conclusions about the existence of marine gateways between the Arctic Basin and the other global oceans since the Late Eocene.

On the basis of the interpreted seismic lines, the sediment thickness and the basement depth for the entire Chukchi region could be calculated (Chapter 4.2). Furthermore, the depth of the Mohorovičić discontinuity (Moho) was estimated by using gravity inversion (Chapter 4.3). These results of the data processing and interpretation (listed above) were used as boundary conditions for the calculation of a 3D gravity model of the Chukchi region and adjacent areas (Chapter 4.4).

Conclusively, the results of this thesis, including published data by Grantz et al. (1998), Dove et al. (2010) and Arrigoni (2008), allow the development of two possible models for the origin of the Chukchi region. Moreover, these models lead to the conclusion about the tectonic evolution of the Arctic Ocean (Chapter 5).

2 The Chukchi Region

The Arctic Ocean is the smallest of the global oceans and surrounded by large shelf areas of the North American and Eurasian continents (Fig. 2.1). Two gateways connect the Arctic Ocean with the global oceans: firstly, the deep Fram Strait between the Arctic and the Atlantic Ocean, and secondly, the shallow Bering Strait between the Arctic and the Pacific Ocean. Furthermore, the Arctic Basin is divided into two subbasins which are separated by the continental and shallow Lomonosov Ridge (Stein 2008). The evolution of the geologically younger basin - the Eurasian Basin - is well understood, based on magnetic spreading anomalies (Kristofferson 1990). However, the evolution of the geologically older basin - the Amerasian Basin - remains controversial (Lawver & Scotese 1990). Therefore, the Alfred Wegener Institute (AWI) carried out a ship expedition into the Amerasian Basin in the summer of 2008.
The main research area of this expedition - the Chukchi region - is located in the Amerasian Basin (Fig. 2.1). This region consists of the Chukchi Shelf, the Chukchi Borderland which is divided into the Chukchi Plateau and the Northwind Ridge, and the Chukchi Abyssal Plain. During the 2008 expedition, the AWI could acquire and collect geophysical and geological data in the research area (Jokat et al. 2009).

2.1 Regional Setting (Bathymetry, Gravity, Magnetics)

The Chukchi region is located in the Amerasian Basin north of Alaska and Siberia (Fig. 2.1). Using the International Bathymetric Chart of the Arctic Ocean (IBCAO) with a resolution of 2 km x 2 km (Jakobsson et al. 2008a), the bathymetry of this region and its adjacent areas shows a large and shallow shelf, deep oceanic basins as well as submarine plateaus and ridges (Fig. 2.2A). The Chukchi and East Siberian Shelf is the largest shelf area worldwide. The water depth ranges between 40 m and 200 m. Over the steep shelf margin, the water depth increases to more than 4000 m in the Canada Basin, about 3000 m in the Makarov Basin and around 2300 m in the Chukchi Abyssal Plain. Between the Canada Basin and the Chukchi Abyssal Plain, the

Chukchi Borderland rises as much as 3400 m above its surroundings. Therefore, the Chukchi Plateau is about 500 m and the Northwind Ridge is about 800 m below the sea surface. The graben system between the Chukchi Plateau and the Northwind Ridge is more than 2000 m below the sea surface. The water depth above the Mendeleev Ridge ranges between 800 m and more than 2000 m. Furthermore, the area of the Mendeleev Ridge shows a rough seafloor topography as well as the area of the Northwind Ridge, the Chukchi Plateau and the graben system inbetween. In contrast, the seafloor of the Makarov Basin, the Canada Basin and the Chukchi Abyssal Plain looks flat. These observations correlate with variations in sediment thickness: an area with a rough seafloor topography shows a thin sediment coverage, and an area with a flat seafloor shows a thick sediment coverage (for more details see Chapter 3.3).

Using the public-domain Arctic Gravity Project (ArcGP) grid with a resolution of 5' x 5' (Kenyon et al. 2008), the gravity field for the Chukchi region and adjacent areas was plotted on the bathymetric relief (Fig. 2.2B). The reference level for the gravity data is the sea level, which is defined as an equipotential surface. Therefore, the free-air anomaly data were used for this study (Chapter 4). These free-air anomaly values range between -600 $\mu m/s^2$ and 700 $\mu m/s^2$ for the entire study area. High gravity values of more than 500 $\mu m/s^2$ exist along the shelf edge, on the Northwind Ridge, on the Chukchi Plateau and on the high mountains of the Mendeleev Ridge. The basins (Canada Basin, Chukchi Abyssal Plain, Makarov Basin) are dominated by gravity values between -250 $\mu m/s^2$ and 100 $\mu m/s^2$, whereas the Chukchi and East Siberian Shelf are characterised by gravity values between -100 $\mu m/s^2$ and 250 $\mu m/s^2$. The lowest gravity values are reached along the foot of the continental margin around the Canada Basin.

Using the public-domain Earth Magnetic Anomaly Grid (EMAG2) with a resolution of 2' x 2' (Maus et al. 2009), the magnetic field for the Chukchi region and adjacent areas was plotted on the bathymetric relief (Fig. 2.2C). The reference level for the magnetic data is 4 km above the sea level. The total magnetic intensity values range between -400 nT and 450 nT. The region of the Alpha and Mendeleev Ridge is characterized

by the highest magnetic values in the Amerasian Basin. The Canada Basin as well as the Chukchi Shelf area are dominated by magnetic values of less than 100 nT, and the Chukchi Borderland by values of less than -100 nT.

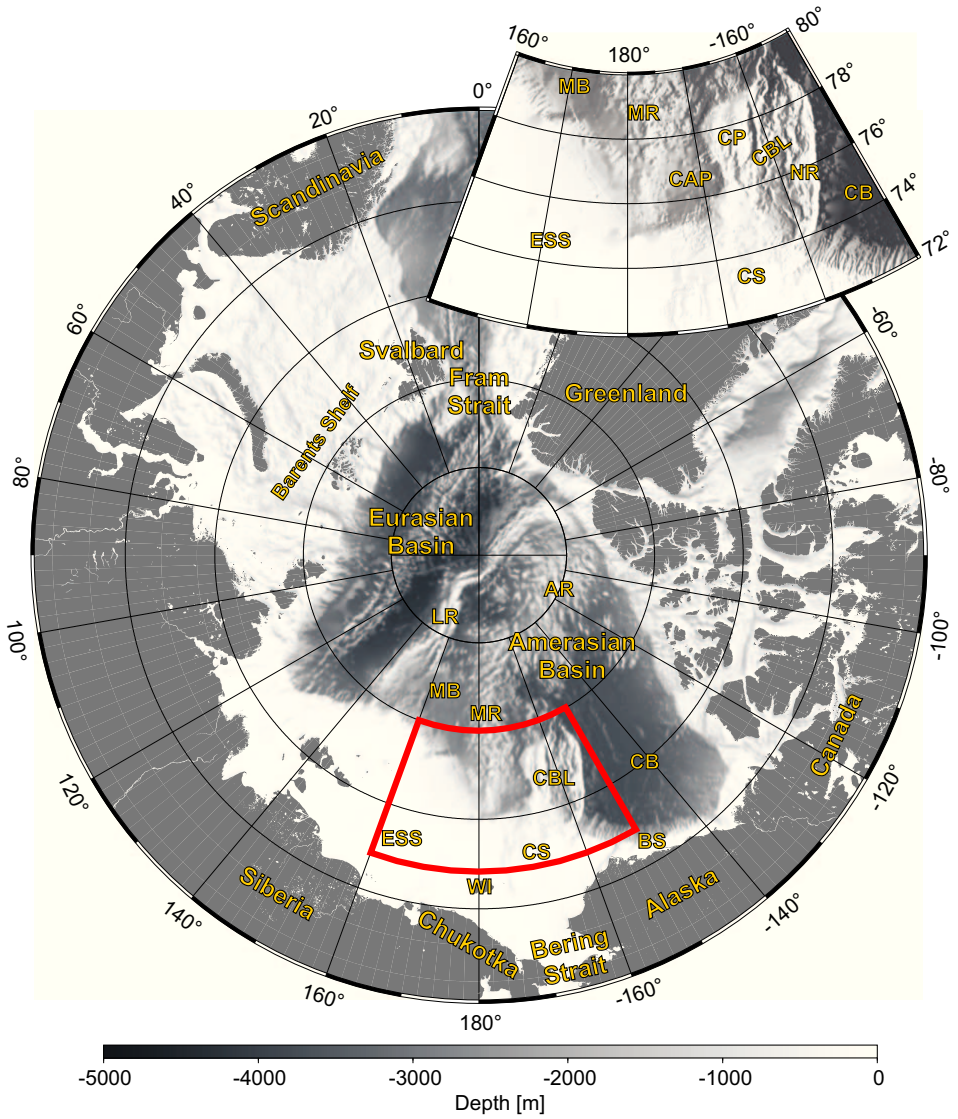

Figure 2.1: Bathymetric map (IBCAO, Jakobsson et al. 2008a) showing the Arctic Ocean with the two major basins - Eurasian and Amerasian Basin - and the main study area (red frame and small map). AR - Alpha Ridge, BS - Beaufort Sea, CAP - Chukchi Abyssal Plain, CB - Canada Basin, CBL - Chukchi Borderland, CP - Chukchi Plateau, CS - Chukchi Shelf, ESS - East Siberian Shelf, LR - Lomonosov Ridge, MB - Makarov Basin, MR - Mendeleev Ridge, NR - Northwind Ridge, WI - Wrangel Island.

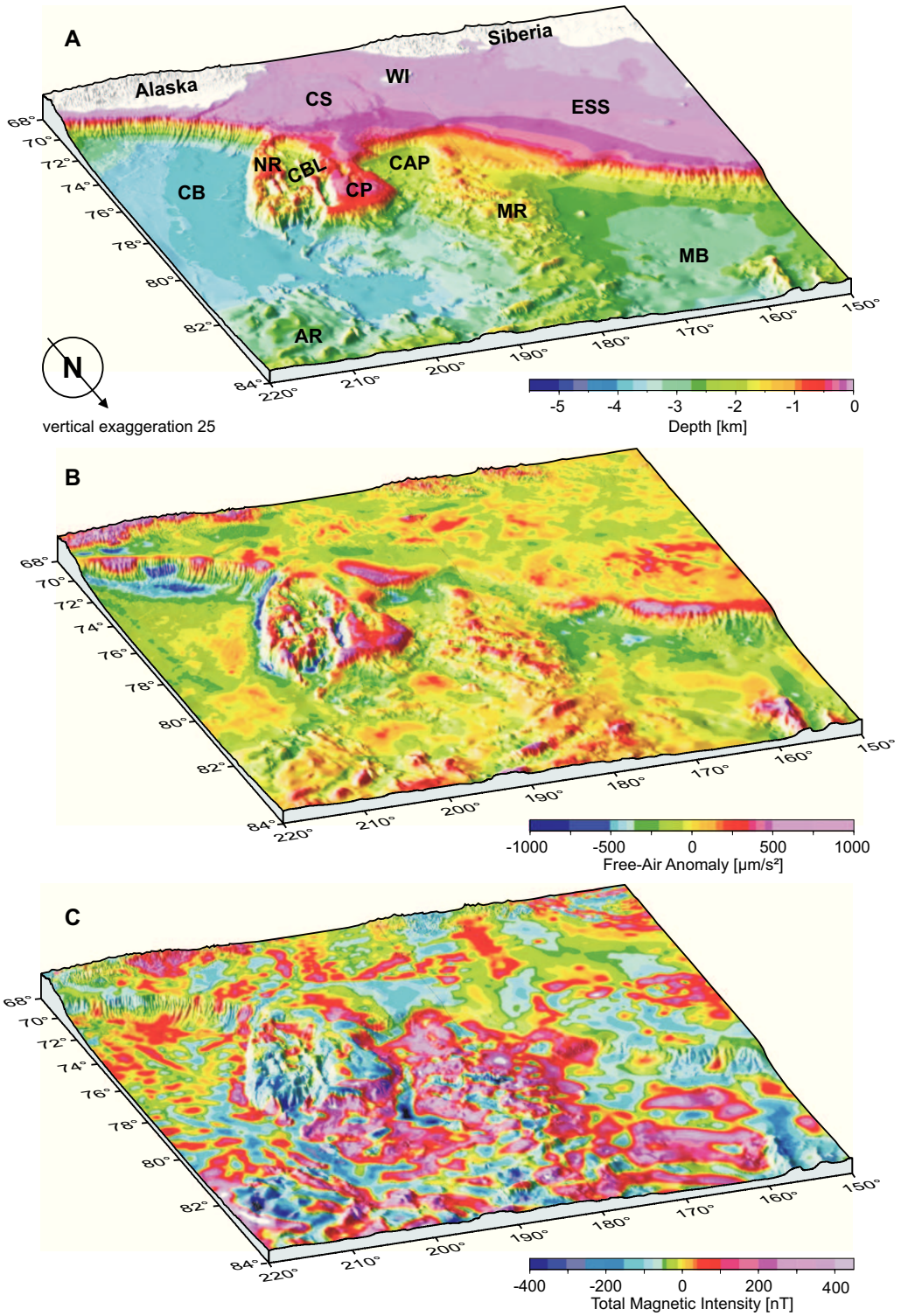

Figure 2.2: Maps of the Chukchi region and adjacent areas showing: (A) the bathymetry (IBCAO, Jakobsson et al. 2008a), (B) the gravity (ArcGP, Kenyon et al. 2008), and (C) the magnetics (EMAG2, Maus et al. 2009).

2.2 Geological Evolution

The Arctic Ocean consists of two major basins (Fig. 2.1) with different ages of evolution. The basins are separated by the Lomonosov Ridge, which is a continental fragment rifted off the Barents Shelf by the opening of the Eurasian Basin. This geologically younger basin was formed by seafloor spreading which started about 56 Ma ago (Ostenso & Wold 1973, Vogt et al. 1979, Kristofferson 1990). The evolution of the geologically older Amerasian Basin remains controversial (Lawver & Scotese 1990, Lane 1997). This deep basin is almost certainly made of oceanic crust and is most likely Jurassic to Early Cretaceous in age (Baggeroer & Falconer 1982, Grantz & May 1982, Grantz et al. 1990). Multiple tectonic reconstructions, however, disagree in the number and orientation of spreading centres. In all rifting models, the Amerasian Basin opened by moving the Arctic Alaska-Chukotka microplate (AACM) - consisting of Chukchi Borderland, Chukchi Shelf, North Slope of Alaska, north-eastern part of Siberia - off the Arctic Canada or off the Barents Shelf (Lawver & Scotese 1990). The four main oceanic rift models for the Amerasian Basin are (Figs. 2.3): (A) the counterclockwise rotation of the AACM from the Arctic Canada where the pole of rotation is located in the Mackenzie Delta after Grantz et al. (1979), (B) the simultaneously rotation of the AACM from the Arctic Canada and the Barents Shelf where two poles of rotation are located in the Mackenzie Delta and in the Laptev Sea after Miller et al. (2006), (C) the strike-slip model where the Lomonosov Ridge is an early spreading centre after Dutro (1981), and (D) the strike-slip model where the AACM moved off the Arctic Canada after Herron et al. (1974). The Chukchi Borderland, however, is difficult to place in all these models.

Following Grantz et al. (1998), the continental basement of the Chukchi Borderland is of Phanerozoic age (Cambrian, Ordovician, and Carboniferous to Cretaceous) which bases on analysed rocks from the Northwind Ridge. Permian red bed sediments and other dredged rocks correlate with coeval rocks of the Canadian Arctic Archipelago, supporting the theory that the Chukchi Borderland was originally attached to the

Arctic Canada. The earliest syn-rift sediments recovered from the Northwind Ridge are of Early Jurassic age which correlates with the beginning of rifting in the Amerasian Basin in Jurassic to Early Cretaceous time (Grantz et al. 1998).

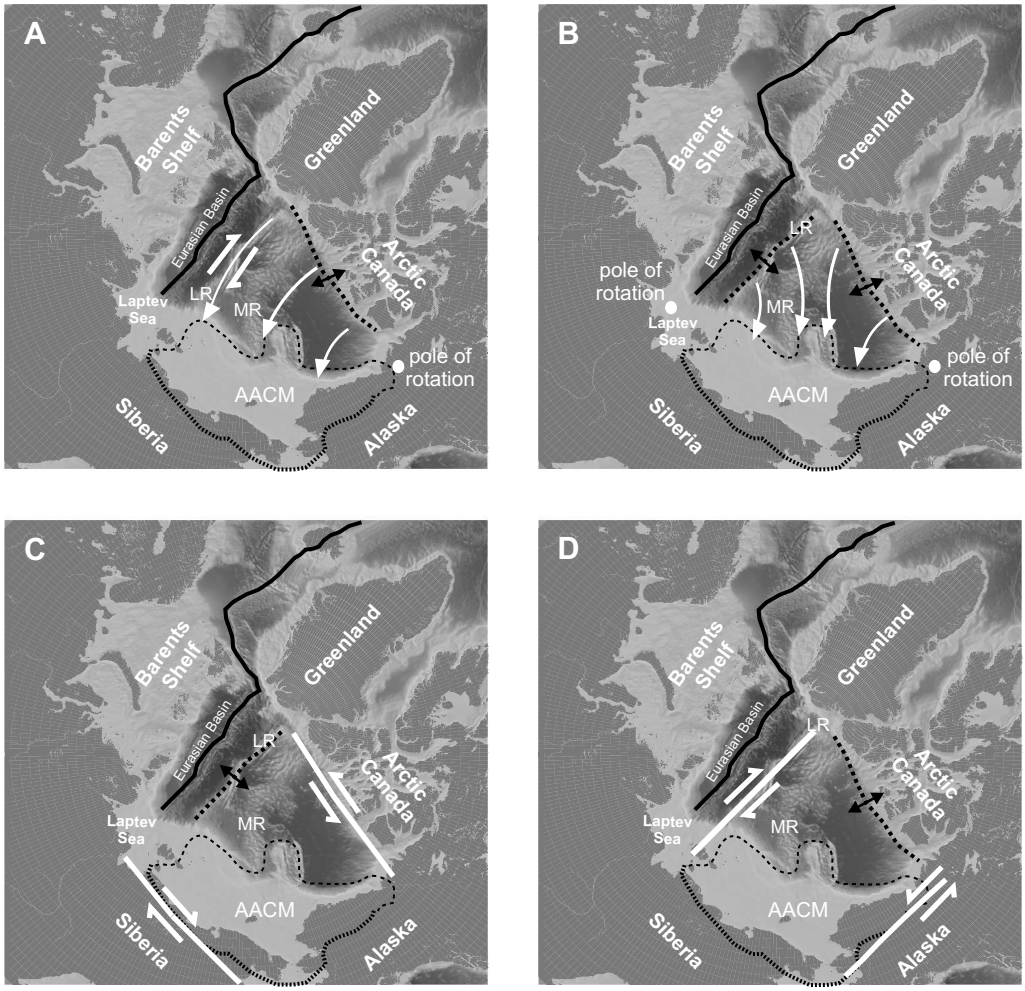

Figure 2.3: Bathymetric map (IBCAO, Jakobsson et al. 2008a) showing the four main oceanic rift models for the opening of the Amerasian Basin after Miller et al. (2010). The black line marks the recent oceanic spreading centre of the North Atlantic mid-ocean ridge and the Gakkel Ridge in the Eurasian Basin.

Regarding the four main geological structures below the thick sediment covered Chukchi and East Siberian Shelf (Fig. 2.4) - Vilkitskii Basin, North Chukchi Basin, Wrangel-Herald Arch (WHA) and Hope Basin - their geological evolutions are still controversial

(Drachev et al. 2010). Following Drachev et al. (2010) about the four main structures, there are no data about the Vilkitskii Basin to infer the sediment age and composition in the basin, or to infer the scale and timing of possible crustal extension. Furthermore, the North Chukchi Basin was probably initiated as an Early to Mid Jurassic rift basin which opened during an extensional stage precursor to the opening of the Canada Basin (Drachev et al. 2010). In Late Jurassic to Early Cretaceous time, a major collision occurred between the AACM and the Eurasian and North American continental margins (Figs. 2.3A-D), followed by orogeny (Moore et al. 1994) and formation of the WHA (Verzhbitsky et al. 2008). Conclusively, the final North Chukchi Basin formed as foreland basin north of the deformation front (Drachev et al. 2010). As a result of plate realignment in the Late Cretaceous and early Tertiary, compressional tectonism associated with strong convergence between the North American and the Eurasian plate was superseded by an extensional/transtensional regime. This resulted in the evolution of the Hope Basin as a pull-apart basin (Tolson 1987).

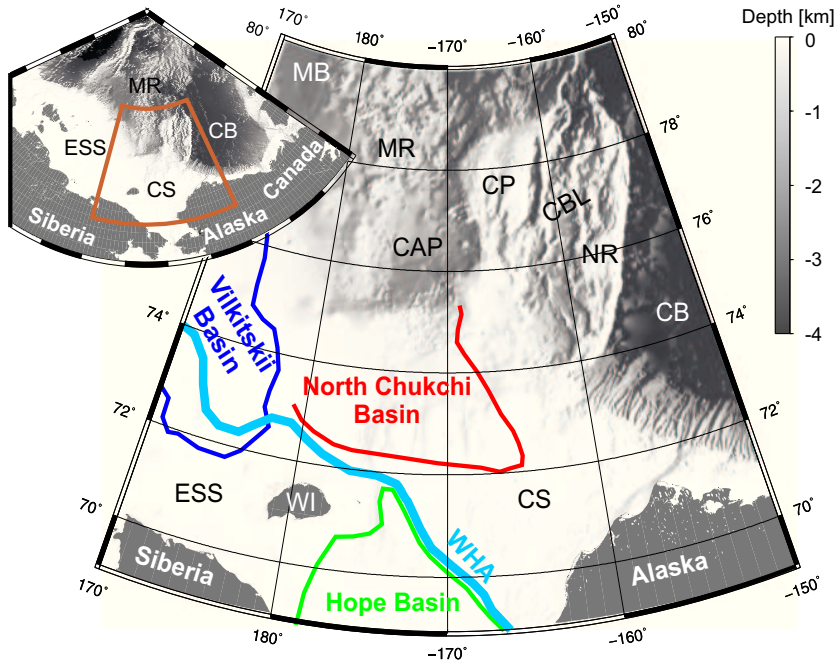

Figure 2.4: Bathymetric map (IBCAO, Jakobsson et al. 2008a) showing the four main geological structures below the sediment covered shelf after Grantz et al. (2011).

In northwest direction, the AACM is bordered by the Mendeleev Ridge (Figs. 2.3A-D). The geological evolution of the Mendeleev Ridge remains controversial (Dove et al. 2010), like the history of the entire Amerasian Basin. Three tectonic models exist for its origin: (1) a rifted volcanic continental margin (Lebedeva-Ivanova et al. 2006), (2) a single oceanic plateau created by hotspot volcanism (Forsyth et al. 1986, Lawver & Müller 1994), and (3) an oceanic plateau formed at a spreading centre which was located in parallel to the Mendeleev Ridge (Hall 1970). Based on the mentioned publications, the age of the Mendeleev Ridge varys between Paleozoic and Early Tertiary.

2.3 Geological Stratigraphy

Based on five exploration wells from the Chukchi Shelf (Chapter 3.1.2), the lithology was derived (Sherwood et al. 2002). Hence, most of the rocks consist of shale and Sandstone. In the Quaternary, mainly conglomerate was deposited (Fig. 2.5).

Following Sherwood et al. (2002), the rocks that underlie the Chukchi Shelf can be divided into four main sequences regarding to the regional stratigraphy of northern Alaska: (1) the oldest sequence consists of deformed and metamorphosed rocks of Late Devonian and older age that are assigned to the Franklinian sequence (Lerand 1973), (2) from Late Devonian (?) to Late Jurassic time the deposited sediments are assigned to the Ellesmerian sequence which was concluded with the development of a Jurassic regional unconformity (JU, Fig. 2.5), (3) from Late Jurassic to Early Cretaceous the strata represent the opening of the Canada Basin and have been distinguished along the Beaufort margin as the Rift sequence (Craig et al. 1986) and was concluded by the development of the Lower Cretaceous unconformity (LCU, Fig. 2.5), (4) the Cretaceous and Tertiary rocks are assigned to the Brookian sequence and consist of sediments from mountain belts created during the orogeny (Moore et al. 1994, Fig. 2.5).

Moreover, Figure 2.5 also shows the horizons which we were able to date in the AWI seismic data from the 2008 expedition, and in additional seismic lines (Chapter 3.1.2). The geologically oldest horizon is the Lower Cretaceous unconformity of Barremian to

Hauterivian age. The Mid Brookian unconformity (MBU) developed at the Cretaceous-Tertiary boundary. In Early Eocene, the Azolla horizon was deposited and represents a fresh water event in the Arctic Ocean (Brinkhuis et al. 2006). The geologically youngest horizons are the Top Eocene, the Top Oligocene and the Top Miocene.

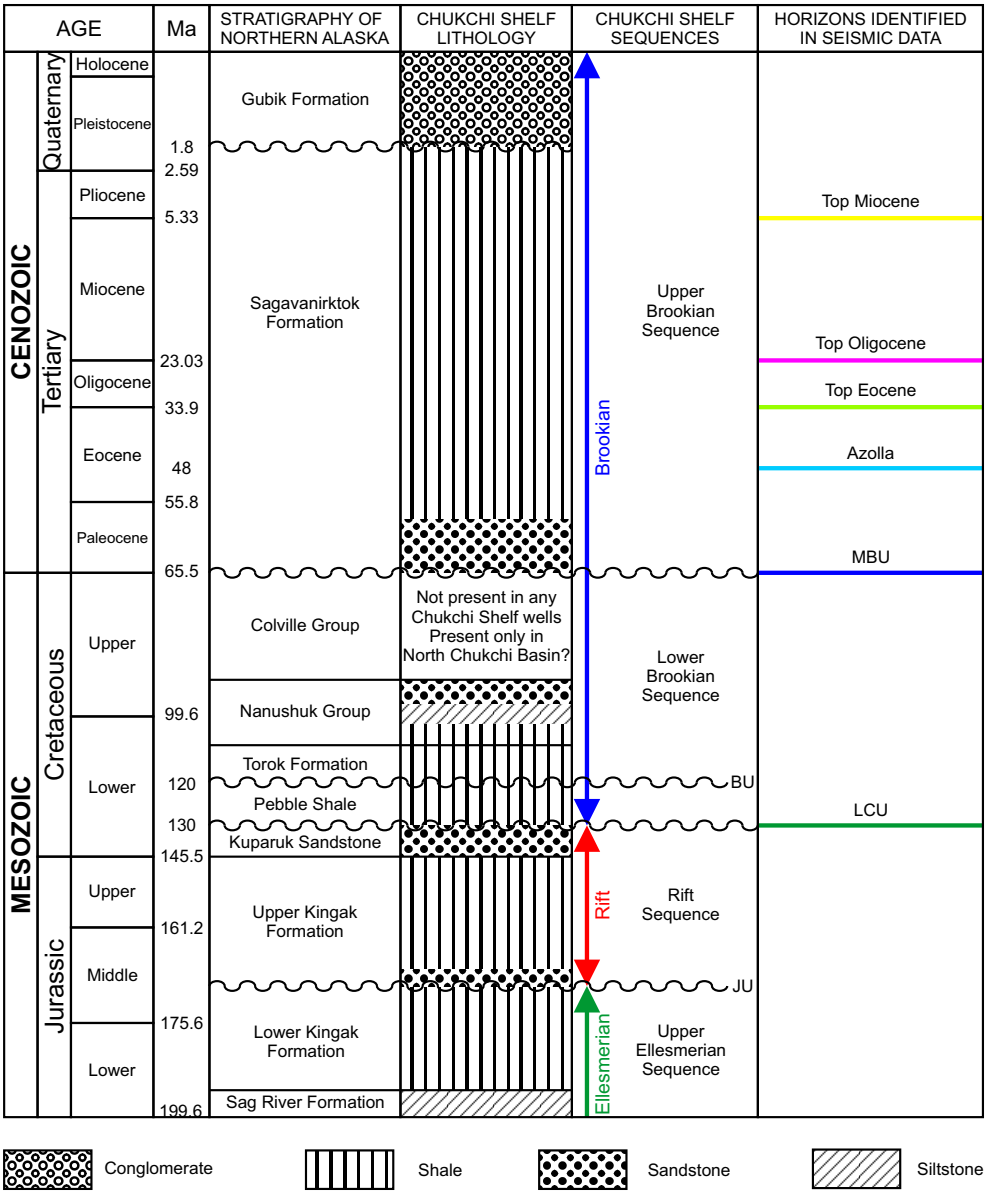

Figure 2.5: Geological stratigraphy of the Chukchi region from five exploration wells near the coast of Alaska after Sherwood et al. (2002); time scale is after Gibbard et al. (2010). The last column shows the identified horizons in the seismic lines (Chapter 3.1.2).

3 Seismic Data

In the summer of 2008, the Alfred Wegener Institute (AWI) collected more than 3300 km of multi channel seismic (MCS) data (using a 3000 m and a 600 m streamer) as well as wide-angle reflection and refraction data (using 12 sonobuoys) during the expedition ARK-XXIII/3 (Jokat et al. 2009). The main study area was the Chukchi region and the southern part of the Mendeleev Ridge (Chapter 2.1, Fig. 2.1). Subsequent investigations are based on this seismic network.

3.1 Multi Channel Seismic Data

For the data acquisition two different streamers were used depending on the sea ice coverage during the expedition. The seismic energy was consistently generated with an air gun array. For technical specifications of both streamers as well as the air gun array see Table 3.1. The locations of the AWI MCS lines recorded with both streamers in the Chukchi region and the southern part of the Mendeleev Ridge are shown in Figure 3.1.

Table 3.1: Technical specifications of the two streamers and the air gun array used for the MCS data acquisition during the 2008 expedition.

	Streamers			Air Gun Array
Length	3000 m	600 m	No. Air Guns	4 G-Guns
No. Active Channels	240	96	Total Volume	32 l
Group Distance	12.5 m	6.25 m	Pressure	200 bar
Record Length	12 s	12 s	Shot Interval	15 s
Sample Rate	2 ms	2 ms		

The vertical and horizontal resolution of seismic data are characterised by the Fresnel zone (Militzer & Weber 1987). The resulting vertical resolution of the AWI MCS data is about 15 m below the seafloor (using a seismic velocity of 1.8 km/s and a peak

frequency of 35 Hz) and decreases to about 100 m in a depth of 8 km (using a seismic velocity of 5.0 km/s and a peak frequency of 13 Hz). Horizontal resolution refers to how close two reflecting points can be situated horizontally, and yet be recognised as two separate points rather than one. The horizontal resolution of the AWI MCS data is about 40 m in a depth of 50 m below the seafloor (using a seismic velocity of 1.8 km/s and a peak frequency of 35 Hz).

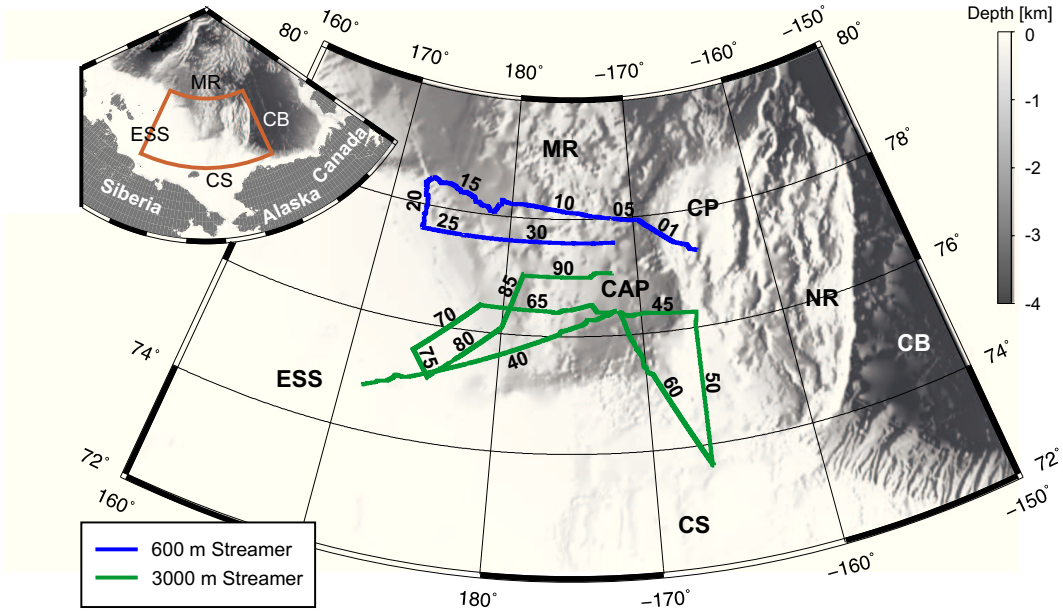

Figure 3.1: Bathymetric map (IBCAO, Jakobsson et al. 2008a) showing the locations of all AWI MCS lines (with annotated line numbers) in the main study area of the Chukchi region and the southern part of the Mendeleev Ridge.

3.1.1 Processing

After acquisition, the MCS data were demultiplexed and CDP sorted (25 m CDP distance). Afterwards, a processing workflow was created (Fig. 3.2) and has been applied to all seismic lines using the software package DISCO/FOCUS 5.4 developed by Paradigm (Houston, Texas, USA). Fundamental knowledge about the different processing steps are described by Yilmaz (2001).

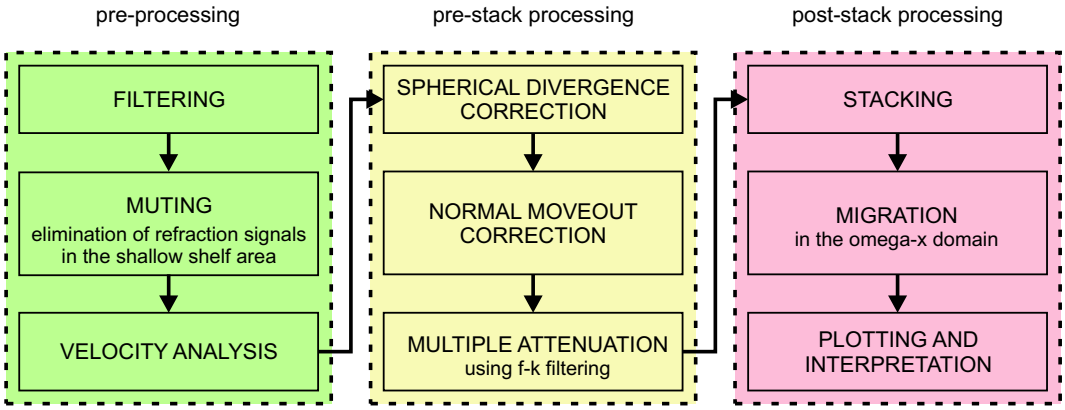

Figure 3.2: Workflow for the MCS data processing after demultiplexing and CDP sorting.

Firstly, the aim of the pre-processing is to create velocity models for the seismic data (Fig. 3.2). Therefore, the data were filtered with a band pass filter of 10 - 100 Hz. Afterwards, in case of shelf data, the signals of refraction waves were eliminated by applying a manual mute along the ocean bottom hyperbola. Due to several velocity analyses, the best fitting root mean square (RMS) velocities were calculated. Based on these velocity models the pre-stack processing of the MCS data was done (Fig. 3.2): after the corrections of the spherical divergence and the normal moveout, the multiple signals of the ocean bottom and lower horizons with high impedance contrast were attenuated. The multiple attenuation proved extremely difficult, especially for the data acquired on the shallow shelf. Due to the low water depth, the ocean bottom multiple arrives with a small time delay behind its primary signal and covers the primary signals of the sediments with the same travel time. Following Verschuur (2006) several methods for the multiple elimination were tested (predictive deconvolution, filtering in the Radon domain, modelling of surface related multiples, filtering in the f-k domain). Conclusively, we decided to attenuate the multiples by filtering all data in the f-k domain. This method works sufficiently for data acquired in deep sea regions. However, the filtering in the f-k domain attenuated the multiples in the seismic lines acquired on the shelf so that the primary signal of the sediments is visible and interpretable. Moreover, the application of this method to all seismic lines would guarantee that the seismic

amplitudes are still comparable after processing. Hereafter, the signal-to-noise ratio was increased by stacking of the MCS data. Finally, in the post-stack processing the data were migrated in the omega-x domain and saved as grey-scale images (Fig. 3.2).

3.1.2 Age Control for Seismic Data

On the Chukchi Shelf, northwest of the coast of Alaska, five exploration wells were drilled by Chevron USA and Shell between 1989 and 1991 (Fig. 3.3). The maximum drilling depth varies between 2000 m and 3600 m, and the geologically oldest sediments were dated to Permian time (Sherwood et al. 2002). Most of the drilled sediments consist of sandstone, siltstone and shale (Chapter 2.3, Fig. 2.5). However, for this study several logging information were available: e.g. depth log, bulk density log, sonic log, resistivity log, gamma ray log, age dating based on biostratigraphy.
Furthermore, many seismic reflection lines on the Chukchi Shelf are available which we used to get the logging information from the wells into the AWI data over a distance of more than 200 km (Fig. 3.3). These additional data were acquired by TGS-NOPEC (Verzhbitsky et al. 2008), ION-GXT (Dinkelman et al. 2008), USGS (public-domain data, Grantz et al. 2004, Dove et al. 2010, USGS 2012) and WesternGeco (public-domain data, USGS 2012) between 1969 and 2006. For some of these lines published interpretations with dated horizons were also used for this working step (Sherwood et al. 2002, Verzhbitsky et al. 2008, Drachev et al. 2010, Kumar et al. 2011).
The correlation of the logging information (Sherwood et al. 2002) with the seismic data required to transform the depth values into two-way time values (TWT). For each well the transformation was carried out with the velocity-depth function, based on the sonic log. Consequently, six prominent horizons between the Lower Cretaceous and the Top Miocene were selected (Chapter 2.3, Fig. 2.5) and correlated with the seismic data on the Chukchi Shelf. These marker horizons were followed trough the southern seismic network up to the north. The dated horizons were extrapolated over the “data gap” of about 70 km (Fig. 3.3) using seismic interval velocities of the sediments as well as reflection characteristics of the seismic horizons (Fig. 3.4).

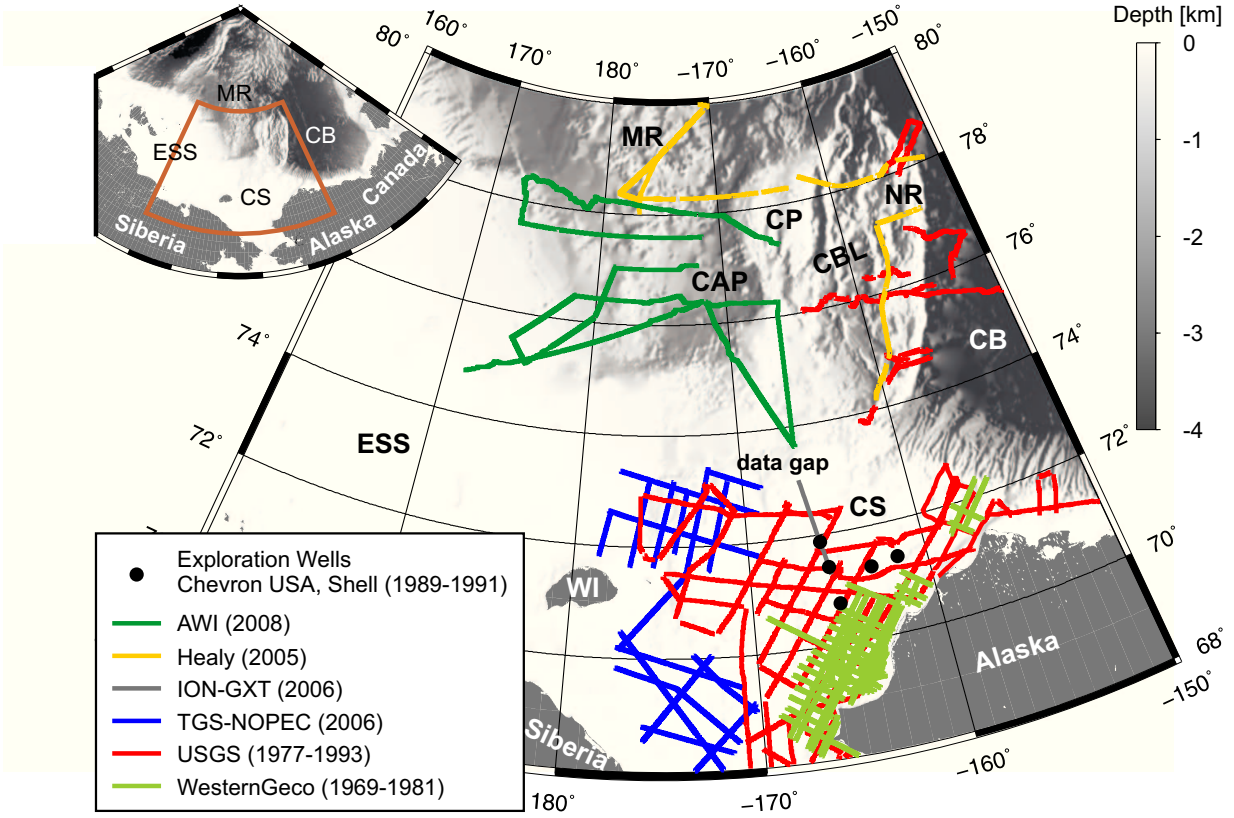

Figure 3.3: Bathymetric map (IBCAO, Jakobsson et al. 2008a) showing the locations of the five exploration wells (Sherwood et al. 2002) and the additional seismic lines on the Chukchi Shelf (Verzhbitsky et al. 2008, Kumar et al. 2011, USGS 2012) and the Chukchi Borderland (Grantz et al. 2004, Arrigoni 2008, Dove et al. 2010).

Six horizons (Chapter 2.3, Fig. 2.5) could be dated in the upper 6 s TWT (equates to 11 km depth) of the shelf part of line 60 (Fig. 3.5). However, it was not possible to follow each horizon trough the entire AWI seismic network because of basement highs, faults, sediment erosions and variations in the sediment thickness. Specifically, the Top Eocene and the Azolla horizon (fresh water horizon deposited in the Early Eocene, Brinkhuis et al. 2006) got lost near the Chukchi Shelf edge (Fig. 3.6). The Lower Cretaceous unconformity (Barremian-Hauterivian) got lost in the Chukchi Abyssal Plain by pinching out against the basement of the Mendeleev Ridge and Chukchi Plateau. The other three horizons (Top Miocene, Top Oligocene, Mid Brookian unconformity) could be identified in all AWI MCS lines (Fig. 3.6).

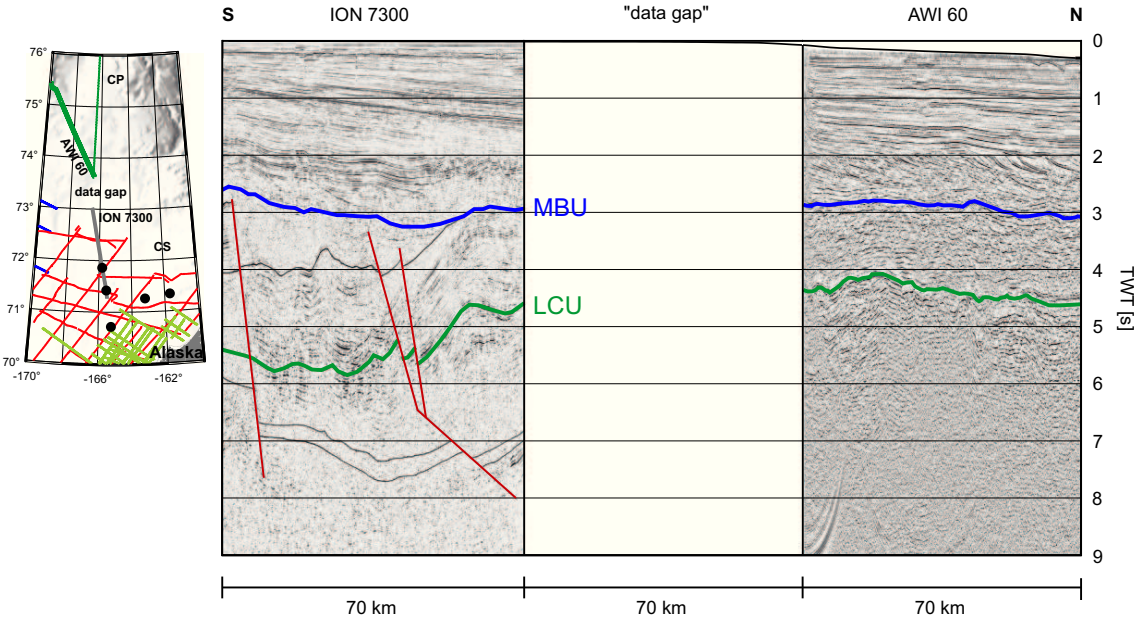

Figure 3.4: Extrapolation of the Mid Brookian unconformity and the Lower Cretaceous unconformity from the ION-GXT profile (ION 7300, Kumar et al. 2011) to the AWI profile (AWI 60) over the "data gap" of about 70 km. The small overview map is a map section of Figure 3.3.

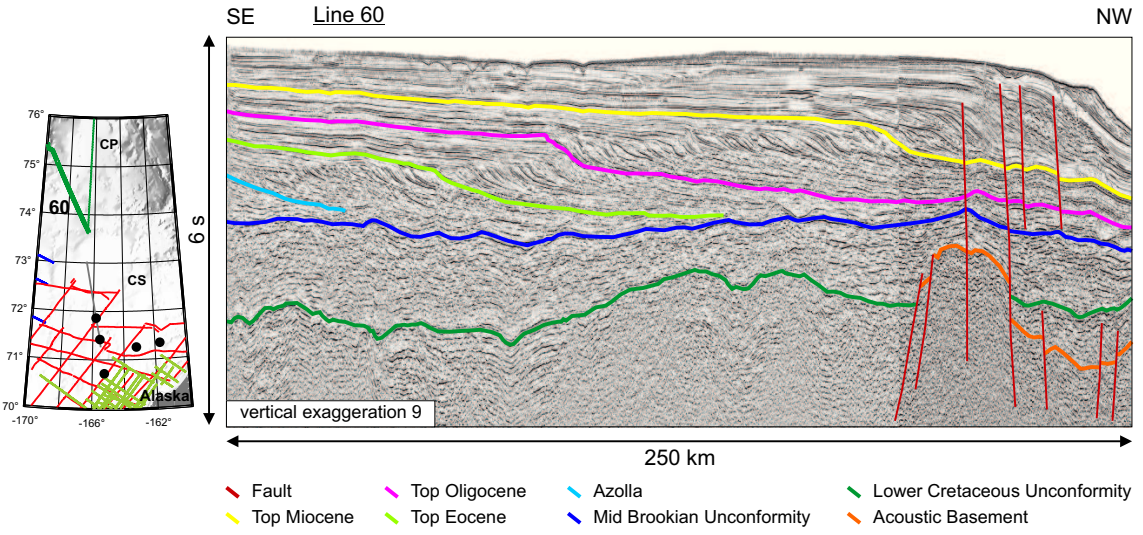

Figure 3.5: Shelf part of line 60 (Fig. 3.1) including six dated horizons (Chapter 2.3, Fig. 2.5) with ages between the Lower Cretaceous and the Top Miocene (after Hegewald & Jokat 2012). The small overview map is a map section of Figure 3.3.

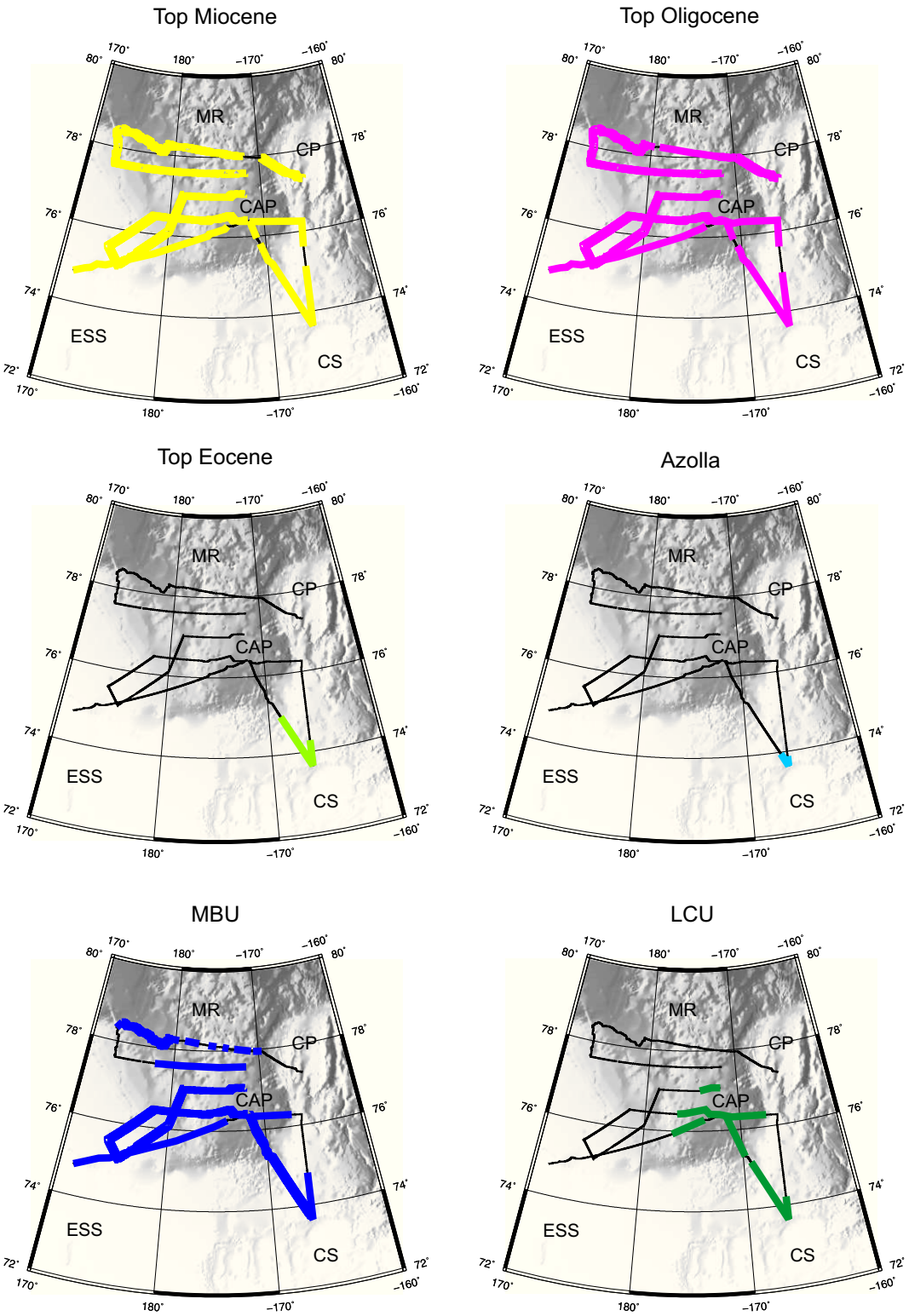

Figure 3.6: The coloured lines show the locations where the six marker horizons were identified in the AWI MCS lines (black and coloured lines; Fig. 3.1).

3.2 Sonobuoy Data

Wide-angle reflection and refraction data were acquired using 12 sonobuoys (SB) in parallel to the AWI MCS data (Fig. 3.7). The sonobuoy data were recorded with a sample rate of 10 ms and a record length between 3 h and 5 h. Table 3.2 includes the MCS line numbers on which the sonobuoys were used and the maximum offset of seismic information in each sonobuoy data set.

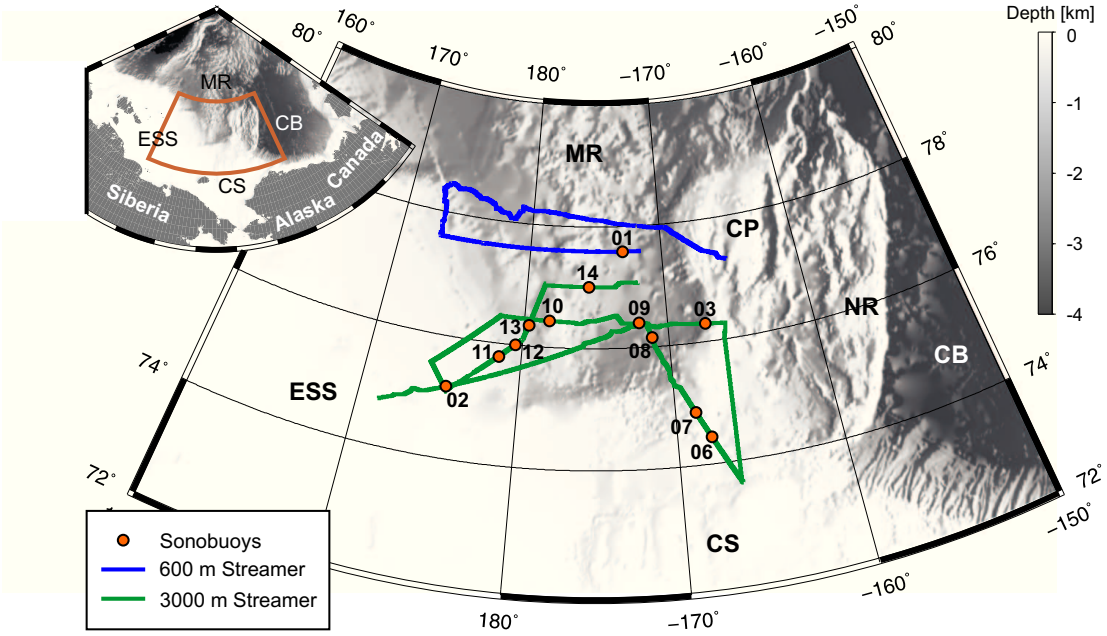

Figure 3.7: Bathymetric map (IBCAO, Jakobsson et al. 2008a) showing the locations of the AWI sonobuoys (with annotated buoy numbers) acquired in 2008.

Table 3.2: Numbers of the 12 sonobuoys, MCS line numbers (Fig. 3.1) on which the sonobuoys were used, and maximum offset of seismic information in each sonobuoy data set.

No. Sonobuoy	01	02	03	06	07	08	09	10	11	12	13	14
No. MCS line	30	40	45	60	60	60	65	65	80	80	85	90
Max. offset [km]	21	31	30	23	25	34	27	29	30	30	23	26

3.2.1 Processing

Firstly, the sonobuoy data were filtered with a band pass filter of 5 - 20 Hz, and an automatic gain control (AGC) with a time window of 0.7 s was applied (Fig. 3.8a). Furthermore, the hyperbolas of the reflection waves and the straight lines of the direct and refraction waves were digitized (Fig. 3.8b), and the 2D velocity-depth models were calculated by ray tracing using the software package RAYINVR (Zelt & Smith 1992, Fig. 3.8c). From the MCS data, additional information about horizon topography, tectonic structures as well as the depth of horizons with high impedance contrast were used as boundary conditions for the modelling (Fig. 3.8d).

3.2.2 Results

Focusing on our interpretation, Figure 3.9 shows the 2D velocity-depth models for each sonobuoy, sorted from the shelf to the basin area. The modelled interval velocities vary between 1.7 km/s for the ocean bottom and about 5.2 km/s for the basement. The sediment thickness decreases from more than 12 km on the Chukchi Shelf to about 4 km in the Chukchi Abyssal Plain (SB09) and less than 1 km on the Mendeleev Ridge (SB01 and SB14). Most of the modelled horizon depths fit well to seismic horizons with high impedance contrast and the dated marker horizons in the MCS data (Chapter 3.3).
In Figure 3.9, the sonobuoys located on the shelf (SB02, SB06, SB07) do not show the basement, whereas SB03, SB14 and SB01 were acquired over basement highs. The Lower Cretaceous sediments (below LCU, interval velocities 4 - 5 km/s) decreases in thickness from more than 6 km on the shelf to less than 1 km in the basin. These sediments were only deposited in basement depressions and were totally eroded on the basement highs. The thickness of the Upper Cretaceous sediments (below MBU, interval velocities 3 - 4 km/s) decreases from 3 km on the shelf to 1 km in the basin. The Eocene sediments (interval velocity 3.8 km/s) were only found in sonobuoy SB06. The Oligocene (interval velocities 2.5 - 3.6 km/s) and Miocene sediments (interval velocities 2 - 3.2 km/s) are similar in thickness and decrease from about 2 km on the

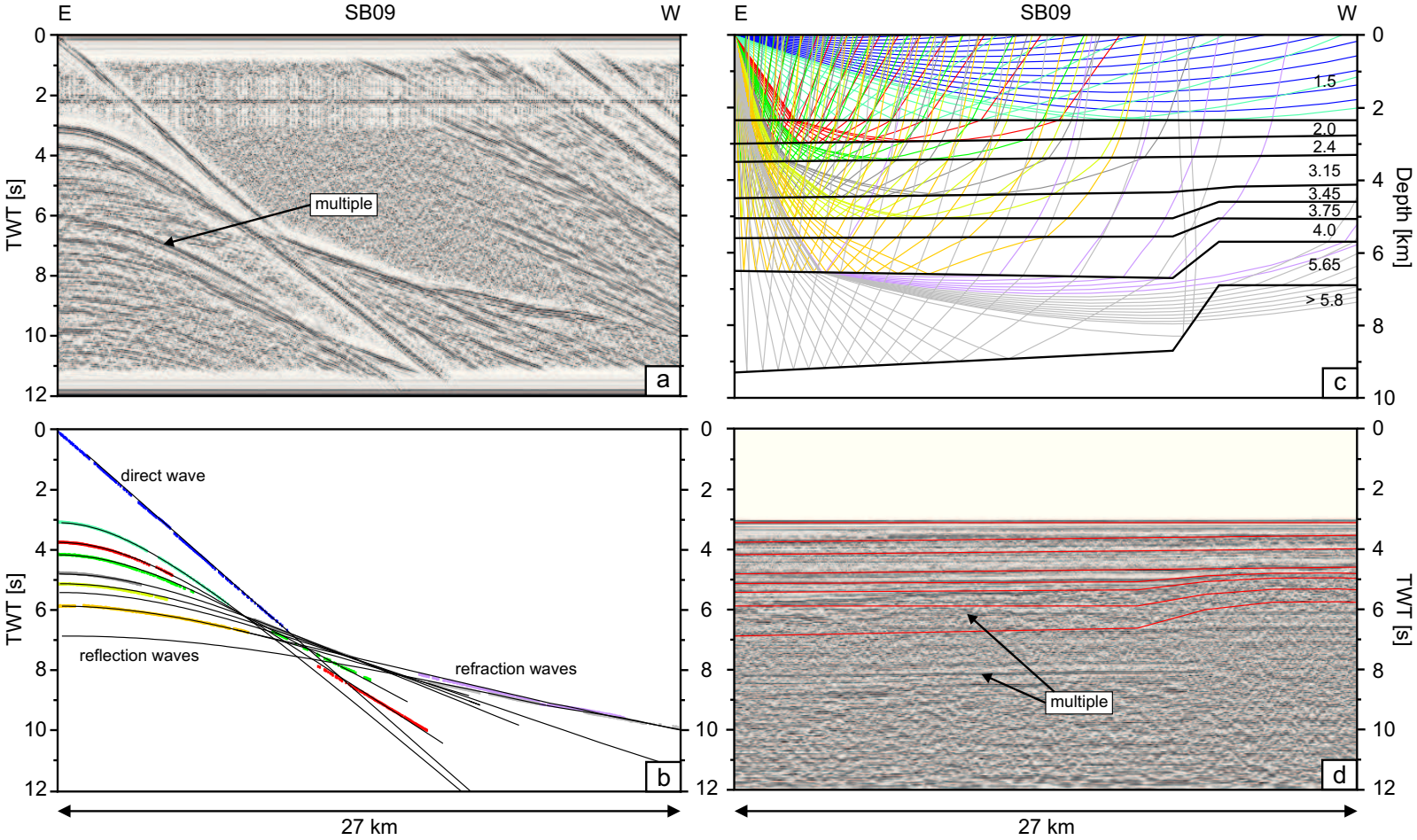

Figure 3.8: Main processing steps used for the sonobuoy data, here shown for sonobuoy SB09. (a) Sonobuoy data after band pass filtering and applying of AGC. (b) Digitized waves (coloured) and modelled waves (black). (c) 2D velocity-depth model calculated by applying ray tracing; the interval velocity values are given in [km/s]. (d) Time section of MCS line 65 (Fig. 3.1), which was acquired in parallel to SB09 (Fig. 3.7). Red lines showing the modelled horizons resulting from Figure c.

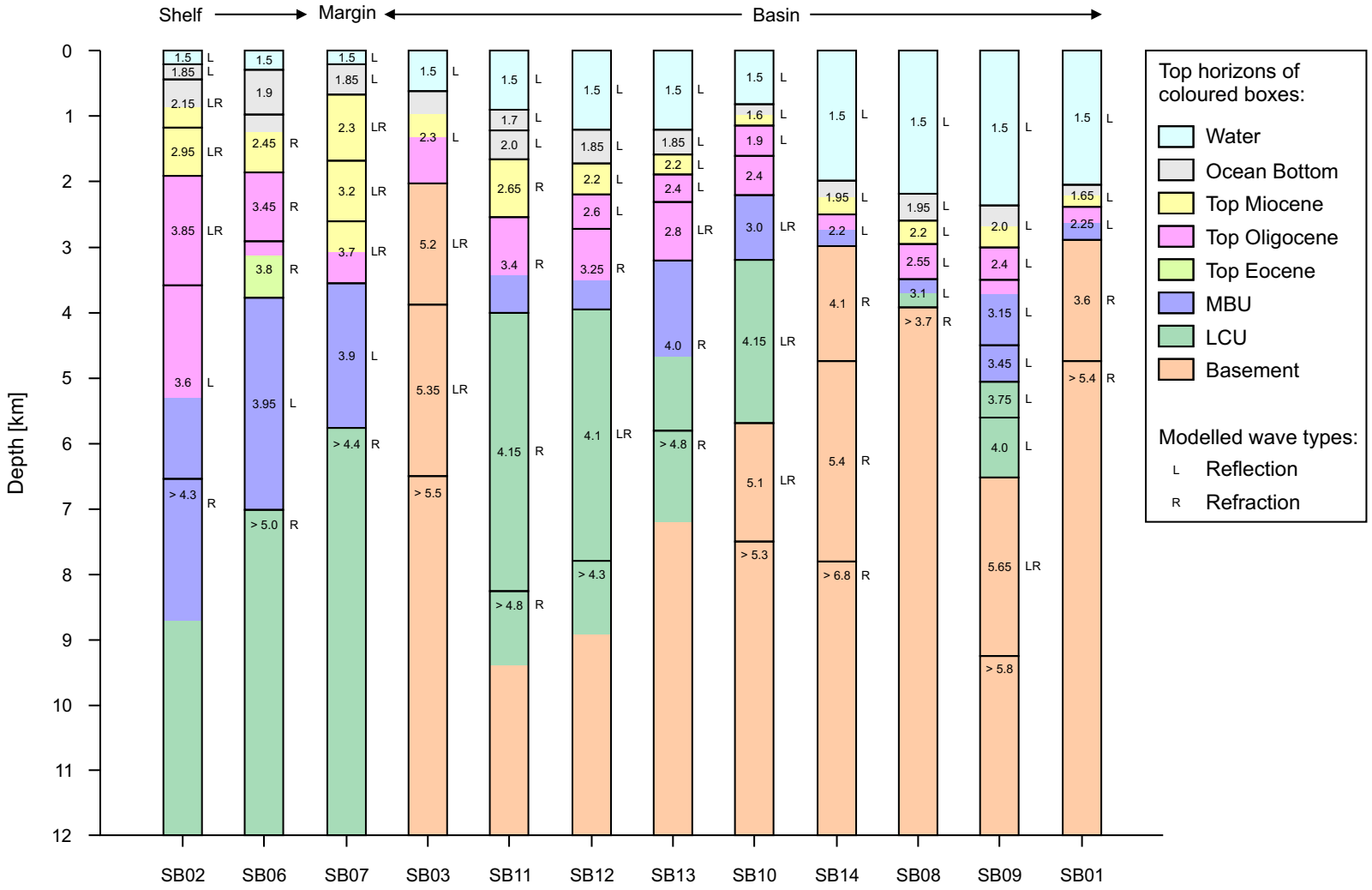

Figure 3.9: 2D velocity-depth models from the AWI sonobuoys acquired in the Chukchi region, sorted from the shelf to the basin area. The wave types (L - reflection, R - refraction) mark the character of the waves which were identified in the sonobuoy data and travelled trough the associated layer. The values show the average interval velocity [km/s] for each layer. The colours and horizon names base on the dated horizons in the MCS data (Fig. 3.5).

shelf to less than 1 km in the basin. The youngest and uppermost sediments below the seafloor surface (interval velocities 1.7 - 2 km/s) have a thickness of less than 1 km in the entire study area.

Based on the modelled sonobuoy data (Fig. 3.9) we could calculate the TWT-depth relation for the Chukchi region. Therefore, the water column was subtracted from the velocity-depth model of each sonobuoy. Afterwards, the velocity-depth models were transformed into TWT-depth models and plotted (Fig. 3.10). The TWT-depth values were fitted by a polynomial of degree 3:

$$Depth = 0.107 + 0.215 \cdot TWT + 0.672 \cdot TWT^2 - 0.065 \cdot TWT^3. \tag{3.1}$$

This equation (Eq. 3.1) was used for the subsequent investigations to transform the interpreted seismic horizons from TWT [s] values to depth [km] values (Chapter 3.5.2).

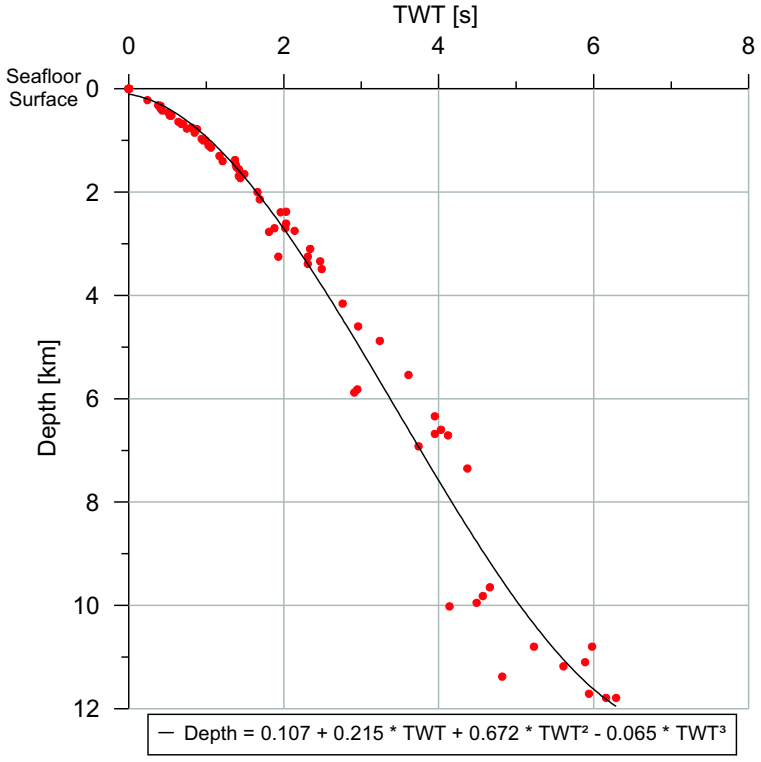

Figure 3.10: TWT-depth relation based on the modelled sonobuoy data (Fig. 3.9). The modelled values (red) and the fitted polynomial function (black) show the TWT-depth relation of the deeper ground beginning at the seafloor surface.

3.3 Main Geological Framework

The study area consists of four main geological provinces (Fig. 2.1): the Chukchi Plateau as part of the Chukchi Borderland, the Chukchi Abyssal Plain, the Mendeleev Ridge and the Chukchi Shelf. Using the software package LANDMARK developed by Halliburton (Dallas, Texas, USA), the seismic reflection data were interpreted.

3.3.1 The Chukchi Plateau

The Chukchi Plateau is part of the Chukchi Borderland and divided into a southern part (Chukchi Rise) and a northern part (Chukchi Cap, Fig. 3.11). These plateaus rise as much as 3400 m above their surroundings. They are relatively shallow (less than 300 m below sea surface) and have steep flanks. In south direction, the Chukchi Plateau is bounded by the shallow Chukchi Shelf (Jakobsson et al. 2008a, Fig. 2.1). Following Grantz et al. (1998), the basement of the Chukchi Borderland is of Phanerozoic age (Cambrian, Ordovician, and Carboniferous to Cretaceous) which is based on analysed rocks from the Northwind Ridge (Fig. 2.1). During the 2008 expedition, three MCS lines were acquired across the Chukchi Plateau. Figure 3.11 shows line 50 which runs from the Chukchi Shelf to the Chukchi Rise and ends at line 45 which crosses the western flank of the Chukchi Rise. Line 01 crosses the Chukchi Cap.

Focusing on our interpretation of these lines (Fig. 3.11), the basement of the Chukchi Plateau looks compact without any internal structures. Its top shows dissected reflection pattern which indicate a crystalline nature. Based on the sonobuoy SB03 data the interval velocity of the basement is 5.2 km/s. This value corresponds to modelled velocities of elastic waves in magmatic rocks like granite or basalt as suggested by Schön (2004). The basement is highly fragmented by numerous normal faults building horst and graben structures. Furthermore, a basement height below the Chukchi Rise (Fig. 3.11, line 50) and two grabens below the Chukchi Cap (Fig. 3.11, line 01) could be seen. Towards the Chukchi Shelf, the basement deepened and could not be detected in the seismic data anymore (Fig. 3.11, southern end of line 50). The steep western

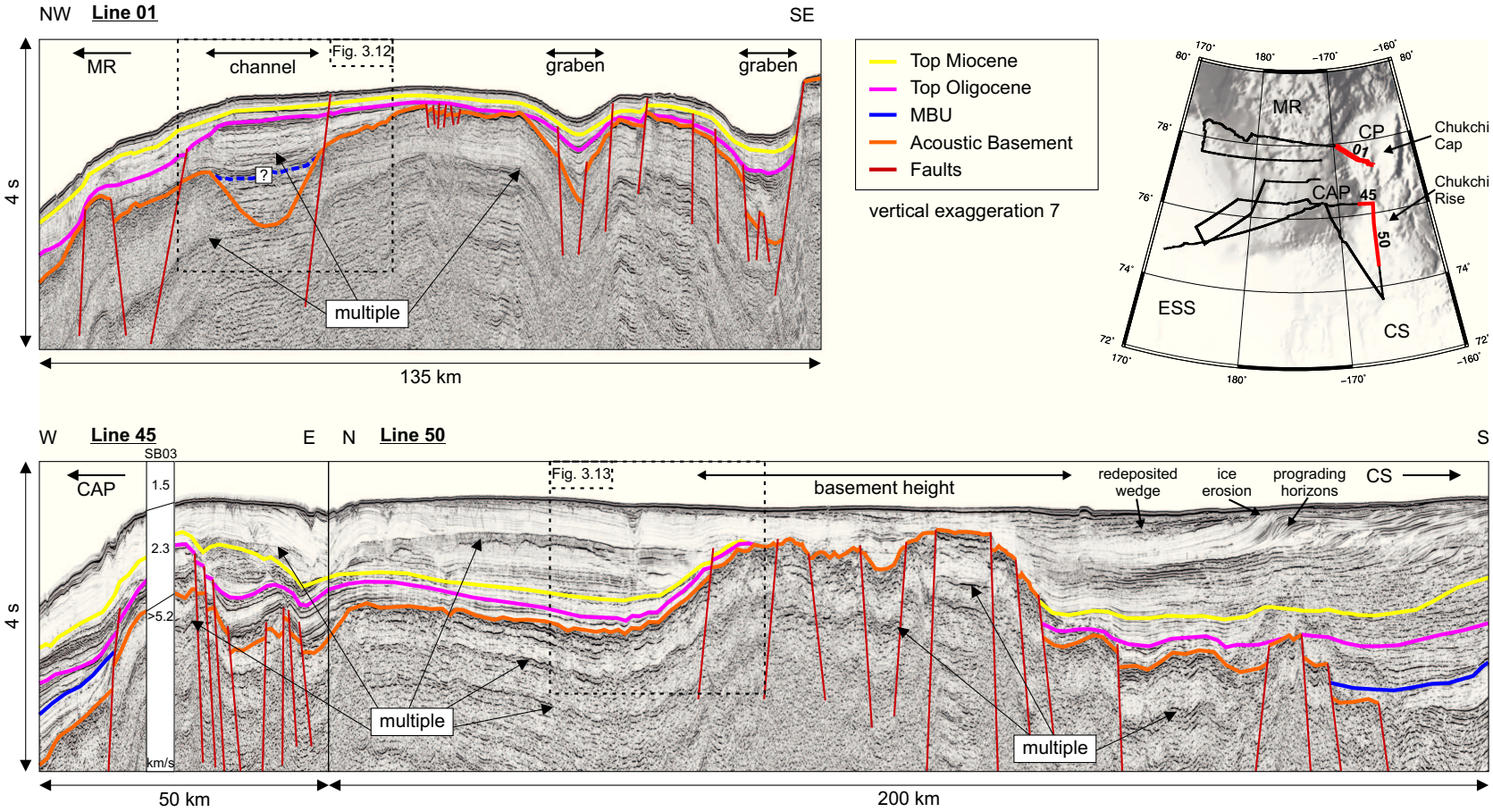

Figure 3.11: Three interpreted AWI MCS lines showing the deeper structures of the Chukchi Plateau, which is divided into the Chukchi Rise and the Chukchi Cap. The age control for the sediment horizons is described in Chapter 3.1.2.

flank of the Chukchi Rise (Fig. 3.11, line 45) is dominated by normal faults which produced a maximum basement offset of about 300 m. Following Grantz et al. (1979), Hall (1990), Vogt et al. (1998), Klemperer et al. (2002) and our observations described above, the Chukchi Shelf basement consists of continental crust and evolved in an E-W directed extensional regime. Several normal faults of the western flank of the Chukchi Rise (line 45), the Chukchi Cap (line 01) as well as the Northwind Ridge (Arrigoni 2008) affected the overlying sediments. Some of these normal faults are reaching up to the seafloor surface (Fig. 3.12). These faults show that the regional extensional stress field is still active until modern time.

The sediments overlying the Chukchi Plateau came from the Chukchi Shelf as can be seen by the prograding sediment horizons at the southern end of line 50 (Fig. 3.11). The thickness of the sediment cover varies across the Chukchi Plateau. Above the basement height, the average sediment thickness is about 600 m and increases to about 1.6 km next to the height on the Chukchi Rise (line 50). In north direction, the average sediment thickness decreases to 400 m, and to about 1 km in the two grabens on the Chukchi Cap (line 01). The average interval velocity for the sediment cover is 2.3 km/s resulting from the sonobuoy SB03 data. Totally, three seismic reflectors with known ages of Base Tertiary, Top Oligocene, and Top Miocene could be identified (age control see Chapter 3.1.2). The Mid Brookian unconformity (Base Tertiary) is the geologically oldest of the interpreted horizons on the Chukchi Plateau. Usually in the entire research area, the Mid Brookian unconformity builds the basis of a seismic reflector band with high amplitudes which is lying above a transparent, thick seismic reflector band. This horizon could only be seen at three locations on the Chukchi Plateau (Fig. 3.11): firstly, between the Chukchi Shelf and the basement height of the Chukchi Rise (southern end of line 50), secondly, at the western flank of the Chukchi Rise (line 45), and supposedly in the deep channel on the Chukchi Cap (Fig. 3.12). The Mid Brookian unconformity follows the basement topography and was dissected by the basement faulting. On the other hand, the Top Oligocene horizon builds the top of a thin seismic reflector band with high amplitudes and represents an erosional surface on

the Chukchi Cap (Fig. 3.12). The Top Miocene horizon is characterised by a seismic reflector with high amplitudes, deposited in the middle of a mostly transparent and undisturbed seismic reflector band (Fig. 3.12). Both horizons were found on the entire Chukchi Plateau, excluding the area above the basement height of the Chukchi Rise (Fig. 3.11). Furthermore, the Top Oligocene and Top Miocene horizon are less affected by basement faulting and the Oligocene and Miocene sediments overly the basement horst and graben structures with a constant thickness (Fig. 3.11). Therefore, both horizons were deposited after the main tectonic events, where the Chukchi Plateau rifted and drifted to its recent position. In some cases, however, both horizons are dissected by faults (Fig. 3.12, Fig. 3.13), and the Oligocene and Miocene sediments are thinning out against the normal faults of the basement height (Fig. 3.13). These are clearly evidences for syntectonic sediment depositions and lead to the conclusion that the tectonic activity in the Chukchi Plateau region was ongoing at least until the Pliocene. The uppermost sediments (above Top Miocene horizon, Fig. 3.11) decreases in thickness from south (about 3 km) to north (about 300 m). These geologically young sediments of Pliocene and Quaternary age cover the basement height (Fig. 3.11, line 50). Moreover, evidences for glaciations of the Chukchi Plateau in Quaternary time were found. These include sediment filled, small channels below the ocean bottom of the Chukchi Rise (Fig. 3.13) as well as eroded sediment horizons and redeposited sediments in a more chaotically wedge on the Chukchi Rise (Fig. 3.11, line 50). These indications for glaciation on the Chukchi Plateau are corresponding to published data about an ice covered Chukchi Borderland in the Quaternary by Jakobsson et al. (2008b).

Summarising the above, the Chukchi Plateau consists of continental crust and moved to its recent position in an E-W directed extensional regime most likely with the opening of the Canada Basin (Grantz et al. 1998). The entire region is covered by Tertiary sediments which came from the Chukchi Shelf and decrease in thickness from south to north across the Chukchi Plateau. Furthermore, the faulted geologically young sediments are an indication of tectonic activity at least until the Pliocene. Moreover, various facts indicate that the Chukchi Plateau was temporary glaciated in the Quaternary.

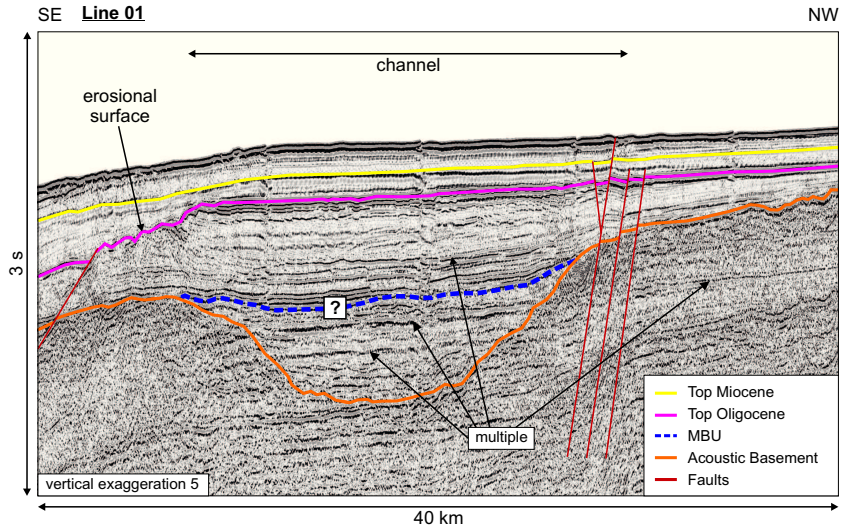

Figure 3.12: Part of the AWI line 01 showing the sediment filled channel on the Chukchi Cap. The Top Oligocene horizon partly represents an erosional surface. The Mid Brookian unconformity was supposedly archived in the channel. For the exact location of this picture detail see Figure 3.11.

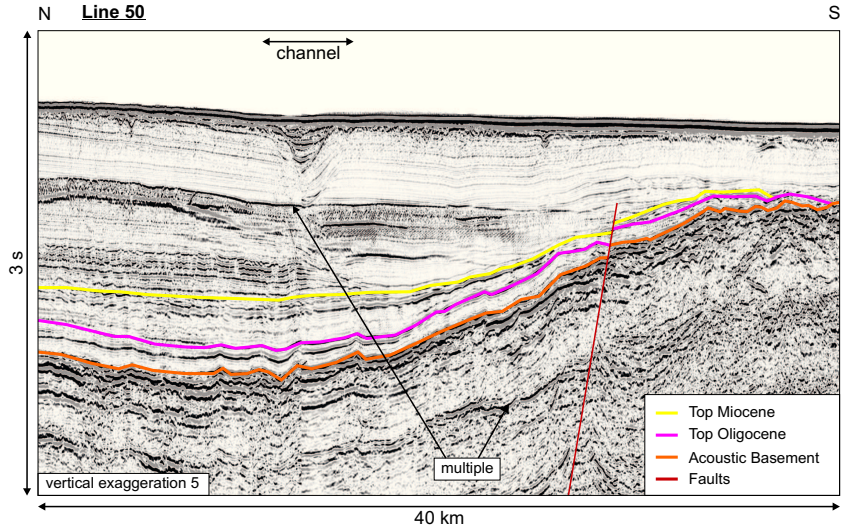

Figure 3.13: Part of the AWI line 50 showing the Oligocene sediments - deposited in a pretectonic regime - and the Miocene sediments - deposited in a syntectonic regime - overlying the acoustic basement of the Chukchi Rise. Conclusively, the Chukchi Plateau was tectonically active at least until the Pliocene. For the exact location of this picture detail see Figure 3.11.

3.3.2 The Chukchi Abyssal Plain

The Chukchi Abyssal Plain is bounded by the Chukchi Plateau, the Mendeleev Ridge and the Chukchi Shelf. In north direction, the Chukchi Abyssal Plain is linked by a narrow abyssal gap with the Canada Basin (Fig. 3.14). The water depth above the flat ocean bottom is about 2.3 km (Jakobsson et al. 2008a). During the 2008 expedition, five MCS lines were acquired across the Chukchi Abyssal Plain. Figure 3.14 shows the lines 65, 45 and 90 which cross the Chukchi Abyssal Plain. The lines 10 and 05 are displaying the structures of the abyssal gap.

Focusing on our interpretation of these five lines, the basement of the Chukchi Abyssal Plain looks mostly compact, however, several subbasement dipping reflectors could be seen below the Chukchi Abyssal Plain (Fig. 3.15) and at the eastern slope of the Mendeleev Ridge (Fig. 3.16). Furthermore, the basement is topped by a high amplitude seismic reflector band which indicates a high impedance contrast between the sediments and the basement. Based on the data of two sonobuoys (SB09, SB14), the minimum interval velocity of the basement is 5.4 km/s. Regarding the area of the subbasement dipping reflectors an average interval velocity of 4.1 km/s was modelled (Fig. 3.14). In general, the basement is characterised by horst and graben structures (Fig. 3.14) like the basement of the Chukchi Plateau (Fig. 3.11) and the Northwind Ridge (Arrigoni 2008). Along these normal faults, the maximum basement offsets are about 1 km.

The sediment cover which overlays the Chukchi Abyssal Plain basement (Fig. 3.14) varies in thickness from 4 km next to the Chukchi Plateau (line 45) and 2.5 km next to the Mendeleev Ridge (line 65) to about 1 km in the abyssal gap (line 10). Concerning the ages of the sediments, the geologically oldest of the identified horizons is the Lower Cretaceous unconformity (Barremian-Hauterivian). Geologically younger in age are the Mid Brookian unconformity (Base Tertiary), the Top Oligocene horizon and the Top Miocene horizon (Fig. 3.14). Furthermore, the basement faulting affected the Lower Cretaceous unconformity and the Mid Brookian unconformity in the western part of the Chukchi Abyssal Plain next to the Mendeleev Ridge (Fig. 3.14, lines 65

and 90). Moreover, the Jurassic and Lower Cretaceous sediments (below the Lower Cretaceous unconformity) become thinner from east to west and pinch out against the basement of the Chukchi Plateau and the Mendeleev Ridge (Fig. 3.14, lines 45, 65 and 90). In the abyssal gap, however, the Lower Cretaceous unconformity could not be identified and the Mid Brookian unconformity is significant affected by faulting (Fig. 3.14, lines 10 and 05). On the other hand, in the eastern part of the Chukchi Abyssal Plain next to the Chukchi Plateau the sediment horizons are not affected by the basement faulting (Fig. 3.14, line 45). Furthermore, the thickness of the Jurassic and Lower Cretaceous sediments as well as of the Upper Cretaceous sediments (below the Mid Brookian unconformity) is much higher in the eastern part than in the western part of the Chukchi Abyssal Plain (Fig. 3.14, lines 45 and 65).

Summarising the above, we conclude that the Chukchi Abyssal Plain evolved in a mainly E-W directed extensional regime shown by the basement horst and graben structures. The basement consists very likely of oceanic crust due to the high impedance contrast between the sediments and the basement, the high interval velocity of more than 5.6 km/s resulting from the sonobuoy SB09 data (Fig. 3.14), as well as the sub-basement dipping reflectors which might be associated with magmatism (Mutter 1985) in the Chukchi Abyssal Plain. Concerning the sediment cover, the south-eastern part of the Chukchi Abyssal Plain is geologically older than the western part based on the thickness and the faulting of the lower sediment layers. The geologically youngest part is the abyssal gap because of the absence of Jurassic and Lower Cretaceous sediments and the faulted Mid Brookian unconformity.

3.3.3 The Mendeleev Ridge

The Mendeleev Ridge separates the Canada Basin from the Makarov Basin (Fig. 2.1). In the research area, the Mendeleev Ridge is characterised by a rough topography and rises as much as 2500 m above its surrounding basins. Hence, the highest mountains of the Mendeleev Ridge reach up to 800 m below the sea surface (Jakobsson et al. 2008a). During the 2008 expedition, four MCS lines were acquired across the Mendeleev Ridge.

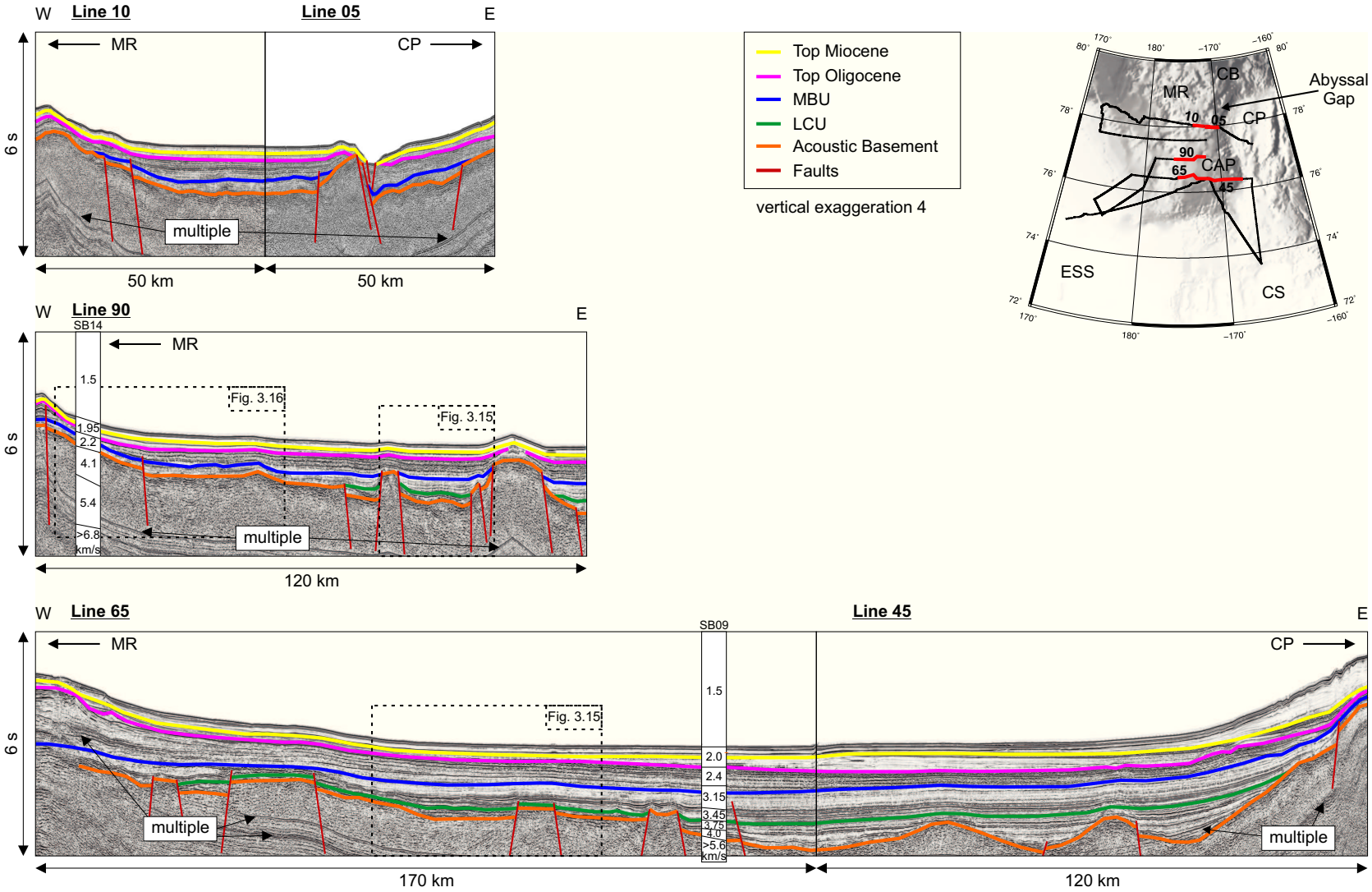

Figure 3.14: Five interpreted AWI MCS lines showing the deeper structures of the Chukchi Abyssal Plain. The age control for the sediment horizons is described in Chapter 3.1.2.

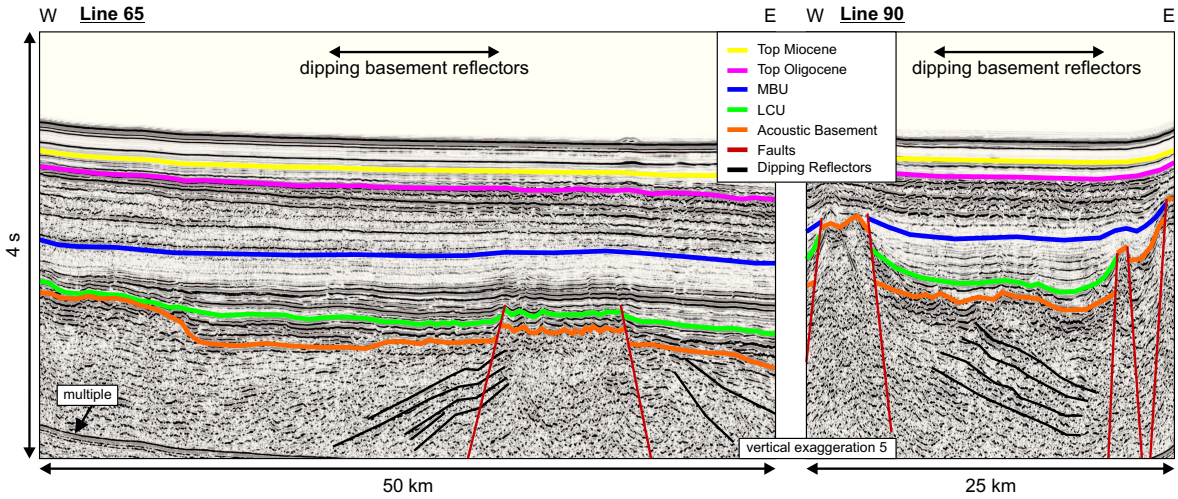

Figure 3.15: Parts of the AWI MCS lines 65 and 90 showing subbasement dipping reflectors in the Chukchi Abyssal Plain next to the Mendeleev Ridge. For the exact location of this picture detail see Figure 3.14.

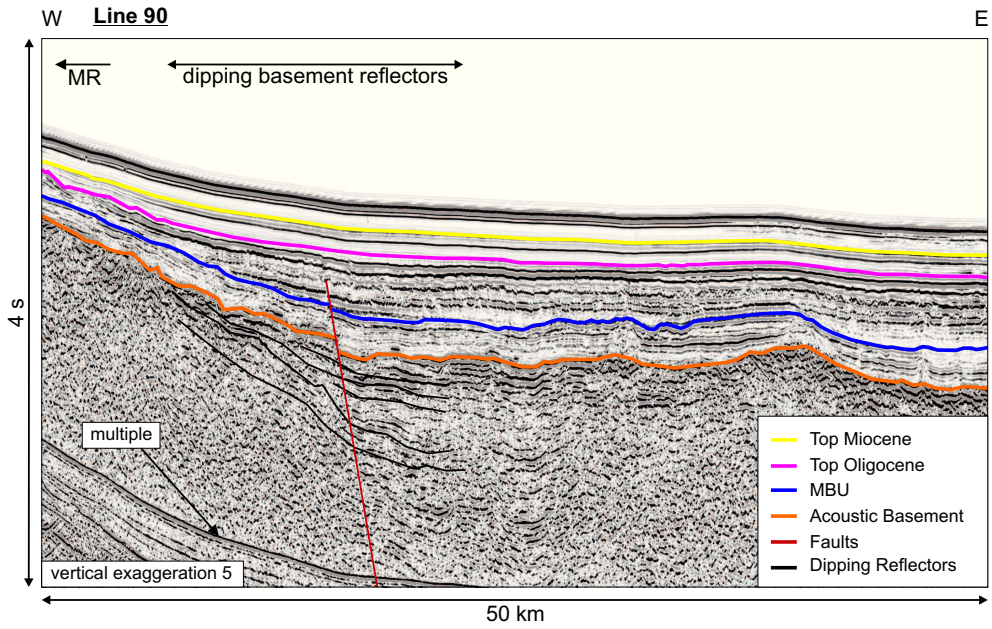

Figure 3.16: Part of the AWI MCS line 90 showing subbasement dipping reflectors at the foot of the eastern slope of the Mendeleev Ridge. For the exact location of this picture detail see Figure 3.14.

Figure 3.17 shows the lines 90, 30 and 10 which cross the Mendeleev Ridge in W-E direction from south to north. Line 85 runs from the East Siberian Shelf to the Mendeleev Ridge.

Focusing on our interpretation of the seismic data, the basement is dominated by several normal faults forming horst and graben structures (Fig. 3.17). Based on the sonobuoy data (SB01, SB14), the basement can be divided into two subunits. Below the top basement seismic reflectors, the upper unit is characterised by interval velocities between 3.6 km/s and 4.1 km/s and a thickness of about 2 km (Fig. 3.17). Below this unit, the interval velocity increases to 5.4 km/s, which relates to the typical average basement velocity of the research area (Fig.3.9). Corresponding results from four sonobuoys, located at the eastern flank of the Mendeleev Ridge, were published by Dove et al. (2010). Hence, the upper subbasement unit was modelled with interval velocities between 3.5 km/s and 4.0 km/s. Moreover, subbasement reflectors could be identified at the top of the Mendeleev Ridge (Fig. 3.18).

The sediment cover overlying the Mendeleev Ridge has a thickness of about 1 km and increases to approximately 6 km next to the East Siberian Shelf (Fig. 3.17, line 85). The average interval velocities of the sediments (1.6 km/s - 2.3 km/s) are similar to those from the Chukchi Plateau and the Chukchi Abyssal Plain. In total, three horizons with known ages (Mid Brookian unconformity, Top Oligocene, Top Miocene) could be identified in the entire southern Mendeleev Ridge region (Fig. 3.17). The Mid Brookian unconformity is the geologically oldest horizon. This unconformity was affected by basement faulting, whereas the offsets of the Mid Brookian unconformity along the normal faults are similar to those of the basement. However, the absence of the Mid Brookian unconformity at the tops of several basement heights lead to the conclusion that the unconformity was eroded at this positions (Fig. 3.17, line 10). Furthermore, the geologically younger Top Oligocene and Top Miocene horizons were not affected by the basement faulting. Figure 3.19 shows the Top Oligocene horizon which cuts into the geologically older sediments at the flanks of the Mendeleev Ridge heights. This type of flank erosion could be seen at all steep flanks of the southern Mendeleev Ridge

(Fig. 3.17). Moreover, the Top Oligocene horizon is covered by geologically younger, undisturbed sediments with a constant thickness in the entire southern Mendeleev Ridge region (Fig. 3.17). In these uppermost sediments the Top Miocene horizon was identified.

The special type of flank erosion and the subsequent covering by geologically younger, undisturbed sediments were also described by Dove et al. (2010) for the northern Mendeleev Ridge and by Bruvoll et al. (2010) for the northwestern Alpha Ridge. However, both authors did not present any age control for the unconformity or any other sediment horizon. Bruvoll et al. (2010) propose two age models based on the correlation of seismic images from the northern Mendeleev Ridge, the northwestern Alpha Ridge and the central Lomonosov Ridge with the IODP core from the ACEX expedition 302 to the central Lomonosov Ridge (Jakobsson et al. 2007). Depending on the model, the age of the unconformity is older than Early Eocene ($>$ 49.7 Ma, model 1) or younger than Mid Eocene ($<$ 45.4 Ma, model 2). Our dated unconformity age of Top Oligocene corresponds to the model 2 proposed by Bruvoll et al. (2010).

Summarising the above, the Mendeleev Ridge evolved after the opening of the Canada Basin (maybe in the Early Tertiary) because of the absence of the Lower Cretaceous unconformity and the highly faulted Mid Brookian unconformity. The upper basement of the Mendeleev Ridge most likely consists of flood basalts which we conclude from the three following facts: (1) the subdivision of the basement into a upper unit (interval velocity 3.6 km/s - 4.1 km/s) and a lower unit (minimum interval velocity 5.4 km/s) which correspond to the seismic properties of flood basalts from the southeast Greenland margin published by Planke & Cambray (1998), (2) the existence of subbasement reflectors which might be associated with magmatism (Mutter 1985), and (3) the size of the Alpha-Mendeleev Ridge area and the time of evolution are similar to the Deccan Traps in India (Vandamme et al. 1991). Furthermore, the flank erosions which occurred at the Miocene-Oligocene boundary might be the result of a changing in the Arctic Ocean currents associated with the beginning of the opening of the Fram Strait at that time (Fig. 2.1, Engen et al. 2008).

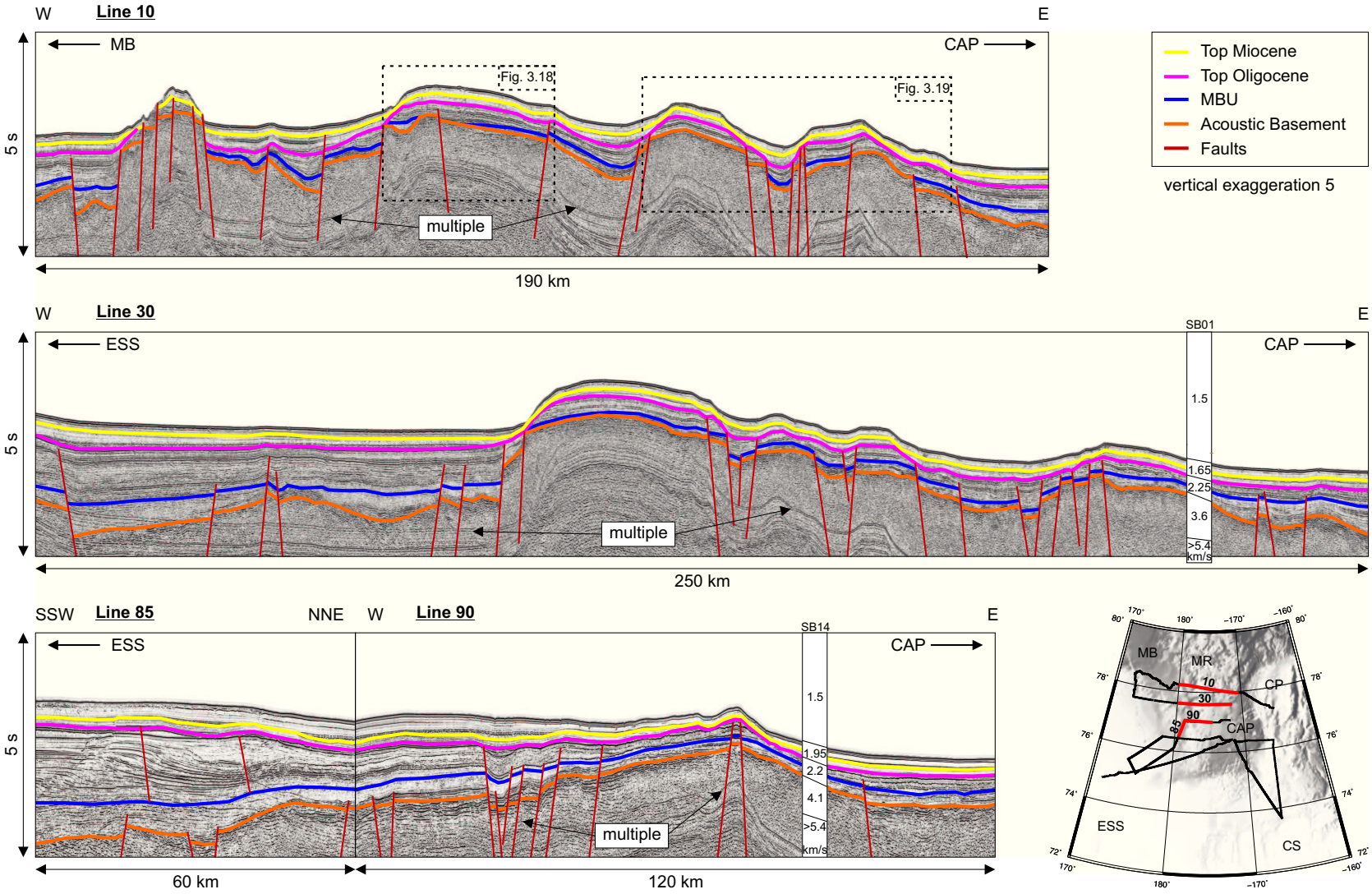

Figure 3.17: Four interpreted AWI MCS lines showing the southern part of the Mendeleev Ridge. The age control for the sediment horizons is described in Chapter 3.1.2.

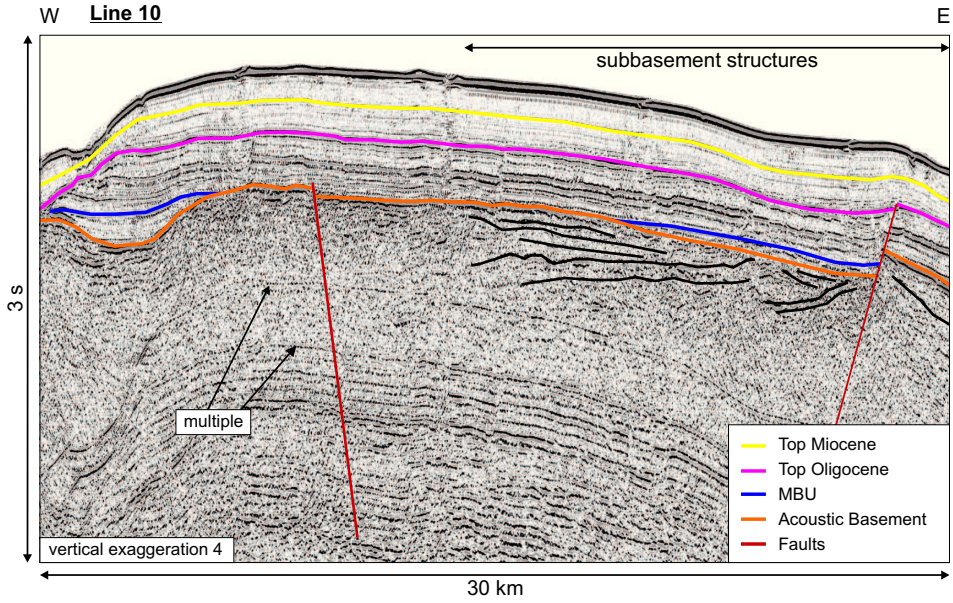

Figure 3.18: Subbasement seismic reflectors (black) on the Mendeleev Ridge might be associated with magmatism in this region. For the exact location of this picture detail see Figure 3.17.

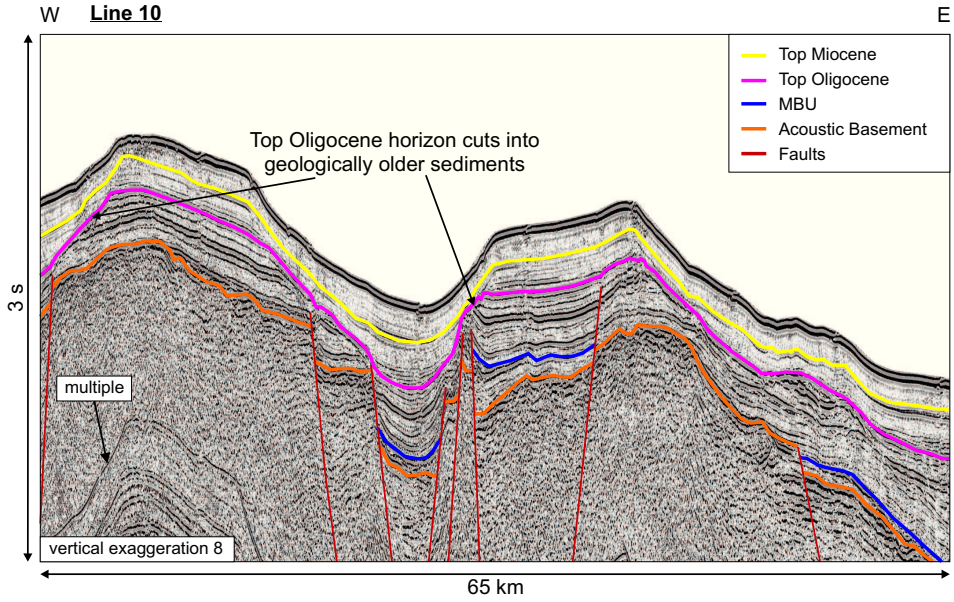

Figure 3.19: The Top Oligocene horizon cuts into the geologically older sediments. Moreover, this horizon also marks the basis of the upper sediment drape which covers the entire southern Mendeleev Ridge. For the exact location of this picture detail see Figure 3.17.

3.3.4 The Chukchi Shelf

The Chukchi Shelf is bounded to the south by northeast Siberia, northwest Alaska and the Bering Strait inbetween, to the east by the Beaufort Sea, to the north by the Chukchi Plateau, the Chukchi Abyssal Plain and the Mendeleev Ridge and to the west by the East Siberian Shelf (Fig. 2.1). The average water depth on the Chukchi Shelf is about 200 m (Jakobsson et al. 2008a). During the 2008 expedition, six MCS lines were acquired on the Chukchi Shelf and across the continental margin to the north (Figs. 3.20 and 3.21).

Focusing on our interpretation, the Chukchi Shelf basement could not be identified in the seismic lines because of the thick sediment cover of more than 12 km (Grantz et al. 2011). However, near the shelf edge the sediment thickness is about 8 km and the basement shows horst and graben structures like in the entire study area (Fig. 3.20, lines 50 and 60).

The sediment cover overlying the Chukchi Shelf is much thicker than in other parts of the Chukchi region. Based on several sonobuoy data (Fig 3.7 and 3.9) the interval velocities of the shelf sediments range between 1.7 km/s and 5 km/s (Fig. 3.20). The two geologically oldest identified horizons on the Chukchi Shelf are the Lower Cretaceous unconformity and the Mid Brookian unconformity. In the area of the shelf margin these two unconformities are affected by the basement faulting. Furthermore, the Tertiary sediments above the Mid Brookian unconformity consist of prograding horizons. These sediment structures are associated with the progradation of the Chukchi Shelf edge from south to north over time. Chapter 3.5.1 gives a detailed description and interpretation of the Tertiary prograding sediment horizons.

Concerning the continental margin at the northern boundary of the Chukchi Shelf, the shape of the slope vary from the Chukchi Plateau to the Mendeleev Ridge (Fig. 3.21). Next to the Chukchi Plateau, the continental margin consists of one slope (Fig. 3.21, lines 45 and 60). In contrast, next to the Mendeleev Ridge, the continental margin consists of two slopes separated by a horizontal section (Fig. 3.21, lines 40, 65 and 70).

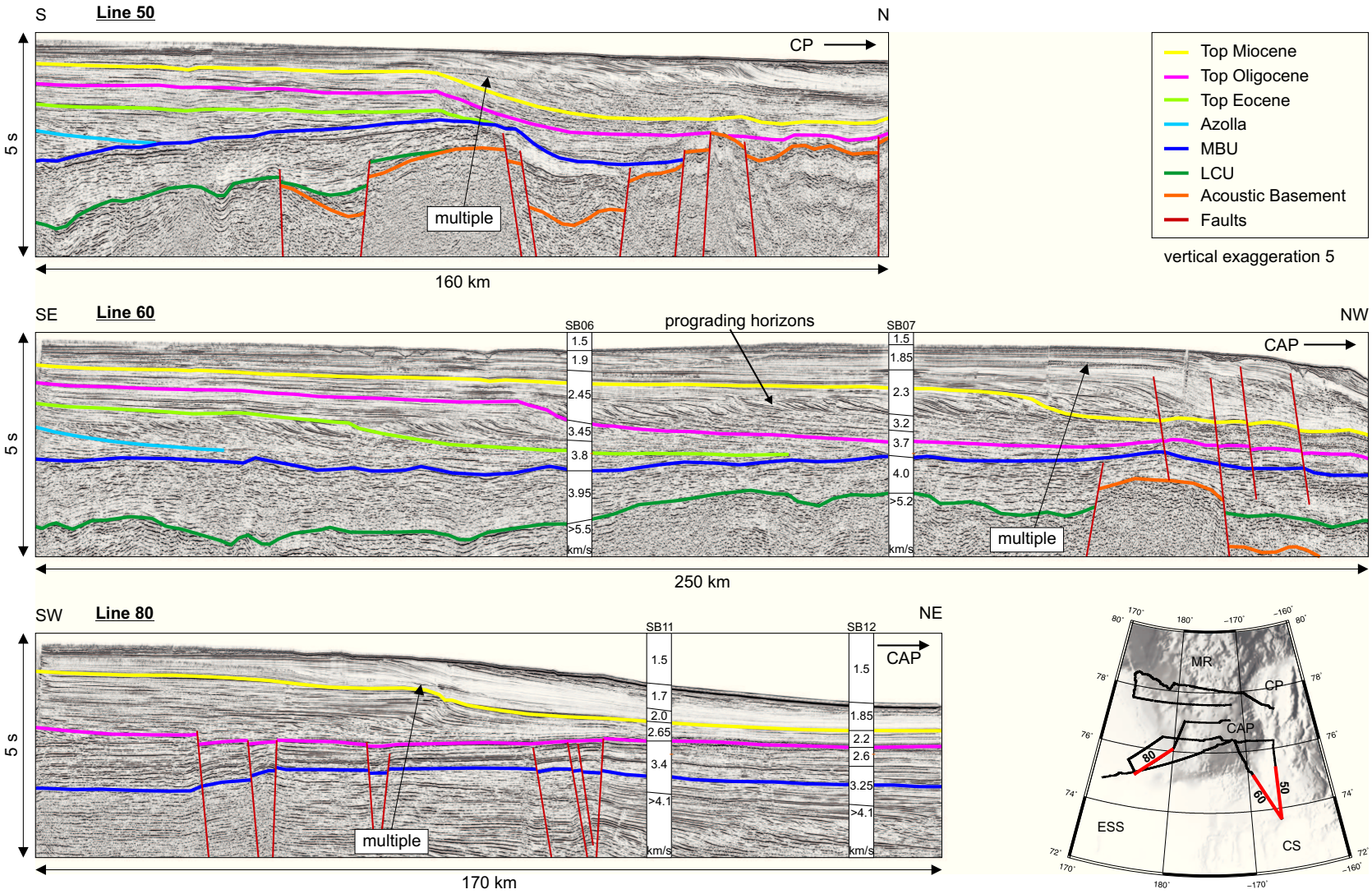

Figure 3.20: Three interpreted AWI MCS lines showing the northern part of the Chukchi Shelf. The age control for the sediment horizons is described in Chapter 3.1.2.

However, following the directions of the Tertiary prograding sediment horizons at the continental margin (Fig. 3.21, black arrows) a significant relocation of the slope next to the Mendeleev Ridge was observed. Hence, the slope moved shelf-ward over a distance of about 160 km along the Top Oligocene horizon (Fig. 3.21).
Summarising the above, the Chukchi Shelf basement is covered by more than 12 km of sediments (Grantz et al. 2011). Therefore, we could not identify the basement in the AWI MCS data. However, the geologically oldest horizon dates back to the Lower Cretaceous. Regarding the sediments, Tertiary prograding sediment horizons represent the progradation of the Chukchi Shelf edge to the north over time. Finally, the variation in the slope shape of the continental margin shows that, next to the Mendeleev Ridge the shelf edge moved south-ward in the Late Oligocene-Early Miocene. The relocation of the shelf edge was most likely caused by a tectonic event of the Mendeleev Ridge concluded from the highly faulted Mid Brookian unconformity and Top Oligocene horizon above the Mendeleev Ridge (Fig. 3.21, lines 65 and 70).

3.4 Sediment Source Area

The main sediment source area could be inferred from the directions of the prograding sediment horizons in the AWI MCS data acquired on the Chukchi Shelf (Fig. 3.20). Moreover, published seismic profiles from the Chukchi Shelf (Verzhbitsky et al. 2008, Houseknecht & Bird 2011) and a modelled section across the Wrangel-Herald Arch which is based on seismic and gravity data (Drachev et al. 2010) were used in addition to the AWI MCS lines (Fig. 3.22). All these mentioned data suggest that the main sediment transportation direction in the Tertiary was from south-southeast to north-northwest (Fig. 3.22). Hence, the main sediment source area was the north-western Alaska and north-eastern Siberia hinterland as well as the region of the Bering Strait before its opening at the end of the Miocene (Gladenkov et al. 2002). Consequently, the sediments were transported from the hinterland to the Chukchi Shelf edge over a distance of more than 400 km and filled the North Chukchi Basin (Fig. 3.22).

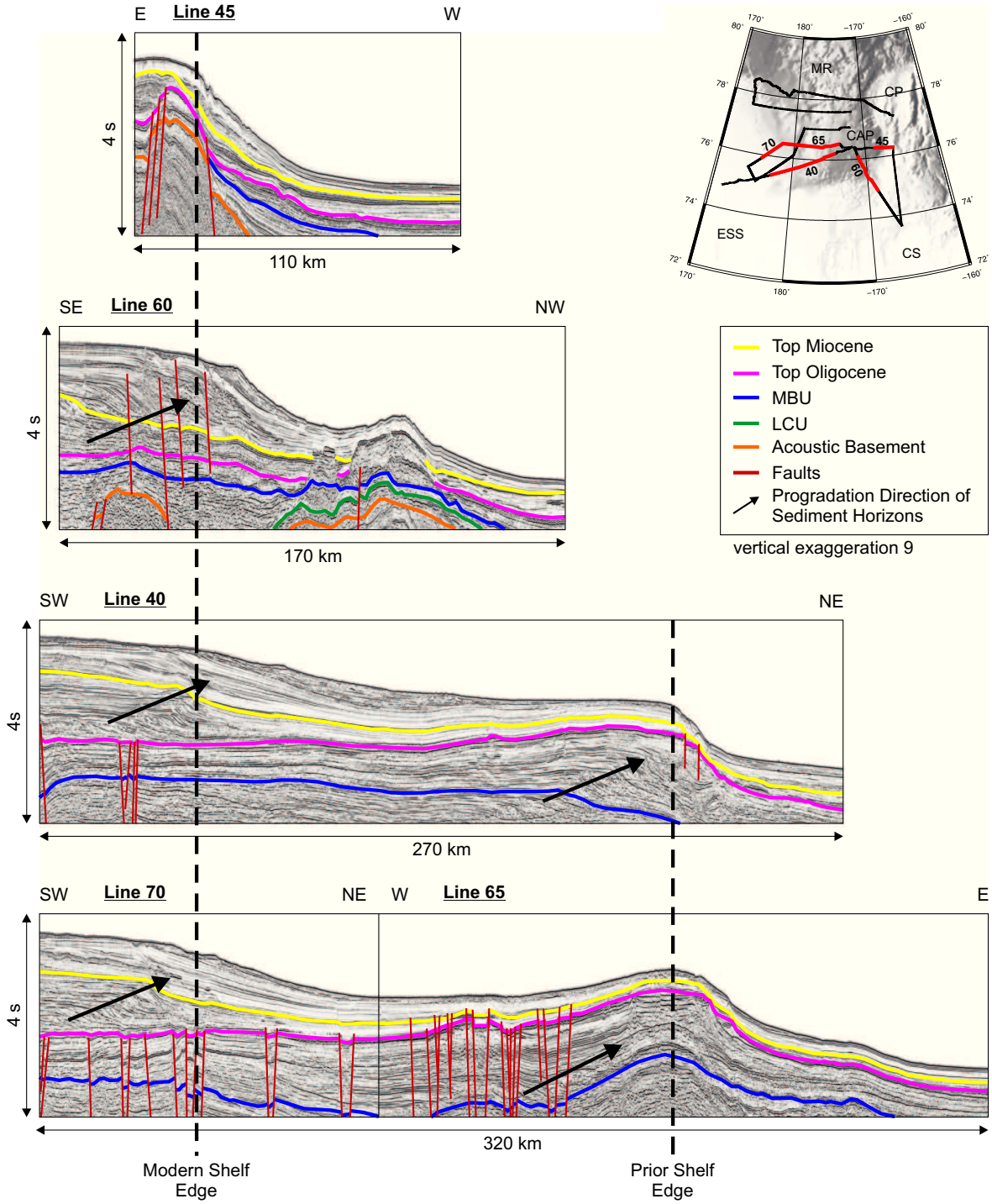

Figure 3.21: Five interpreted AWI MCS lines across the Chukchi Shelf margin showing the variation of the slope shape from the Chukchi Plateau to the Mendeleev Ridge. The age control for the sediment horizons is described in Chapter 3.1.2.

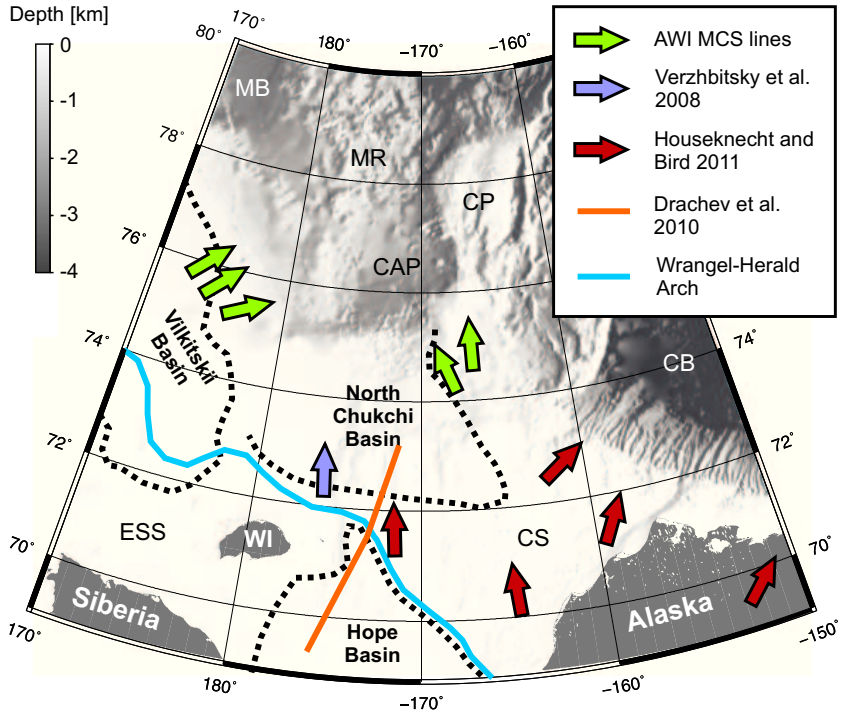

Figure 3.22: Bathymetric map (IBCAO, Jakobsson et al. 2008a) showing the directions (arrows) of the Tertiary prograding sediment horizons in the seismic lines on the Chukchi Shelf. The orange line marks the location of the modelled section across the Wrangel-Herald Arch after Drachev et al. (2010).

3.5 Relative Sea Level Variations

The subsequent results including the relative sea level (RSL) variations in the Chukchi region, its interpretation for the Arctic Ocean and the comparison with the global RSL curve are published by Hegewald & Jokat (2012).

Since the opening of the Amerasian Basin (Arctic Ocean) in Jurassic to Early Cretaceous time (Grantz & May 1982), several seaways connected the Arctic Ocean with the global oceans. In the Eocene, the Turgai Strait (located between Europe and Asia) formed a seaway between the Arctic and the Tethys Ocean, and was closed by marine regression in Late Eocene or Oligocene time (Marincovich et al. 1990). The marine regression is supposed to be the result of a significant reorientation of relative plate motions, which occurred in the circum Arctic Ocean when seafloor spreading

in the Labrador Sea terminated and the separation of NE Greenland from Svalbard began (Chalmers et al. 1993). About 15 Ma later, the Fram Strait opened in the Early Miocene and recently represents the only deep-water connection between the Arctic and Atlantic Ocean (Engen et al. 2008). The youngest shallow seaway, the Bering Strait, connects the Arctic with the Pacific Ocean and opened near the end of the Miocene (Gladenkov et al. 2002). For the Late Eocene to the Early Miocene, nothing is known about the existence of seaways to the Arctic Ocean or about the RSL variations in the High Arctic.

Based on the prograding sediment sequences in the upper 3 s TWT (equates to 4 km depth) of five AWI MCS lines on the Chukchi and East Siberian Shelf (Fig. 3.23) and the method of seismic sequence stratigraphy (Catuneanu 2006), we were able to calculate the first RSL curve for the Chukchi region, beginning in the Late Eocene (40 Ma). In general, RSL variations are a result of tectonic activity, changing of the water volume of ocean basins (e.g. due to increasing/decreasing of ice volume, evaporation) and variations in the regional to global climate which influences erosional processes and material transport.

3.5.1 Seismic Sequence Stratigraphy

The method of seismic sequence stratigraphy is described in detail by Catuneanu (2006) and provides the basis for the subsequent investigations. This method bases on the identification of three structural elements in the seismic data: (1) stratal termination, (2) stratigraphic surfaces, (3) systems tracts and sequences. Figure 3.24a shows the types of stratal termination. These include information about the direction and type of shoreline shift, erosion events and depositional trends. For example, downlap is indicating progradational depositional trends. In contrast, onlap is indicating mainly vertical aggradational trends. Furthermore, each seismic sequence consists of three stratigraphic surfaces (Fig. 3.24b, upper labelling). Most of these surfaces provide the closest approximation to time lines. Moreover, the seismic sequences are divided into four systems tracts which are bounded by these stratigraphic surfaces (Fig. 3.24c).

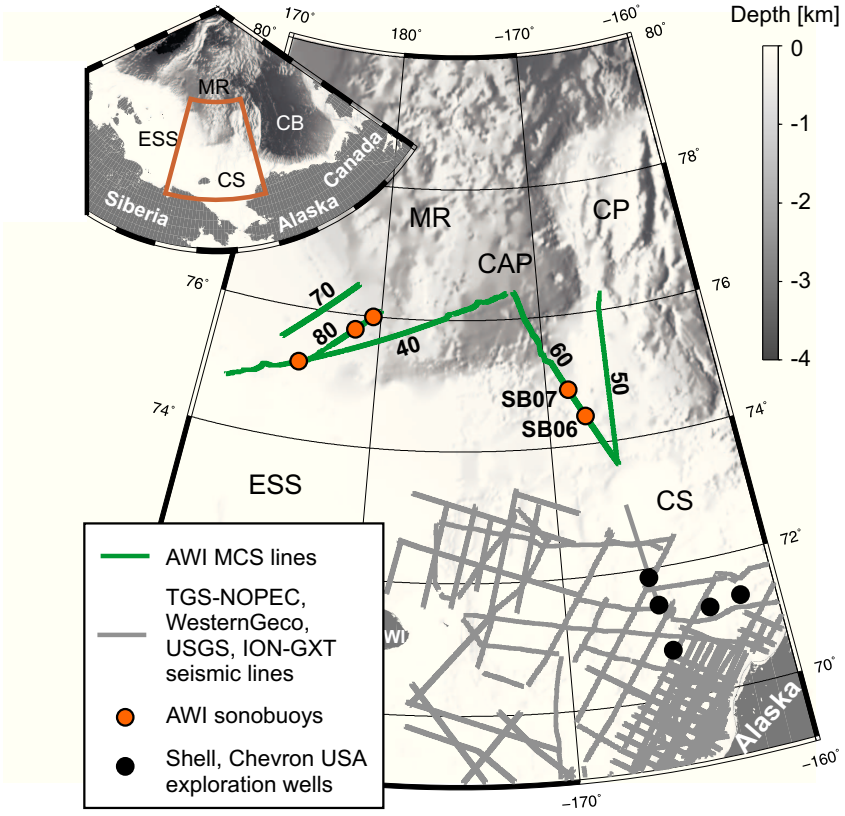

Figure 3.23: Bathymetric map (IBCAO, Jakobsson et al. 2008a) showing the five AWI MCS lines on the Chukchi and East Siberian Shelf (green lines) which include prograding sequences in the upper 3 s TWT; modified after Hegewald & Jokat (2012).

Focusing on the interpretation, each seismic sequence represents one flooding event, consisting of four systems tracts (Fig. 3.24c): falling stage systems tract (FSST), lowstand systems tract (LST), transgressive systems tract (TST) and highstand systems tract (HST). The basis of each seismic sequence is defined by a fast basinward progradation of the deposition area. Mostly, the boundary is an erosional surface (unconformity) on the outer shelf and upper slope, and can be correlated to its marine conformity (regressive surface). The FSST represents the lowstand submarine fan complex with onlapping horizons in the margin area and is mostly interpreted as part of the LST. The horizons in the LST show onlapping at the mid-slope and offlapping on the shelf. The top of the lowstand system is marked by the maximum regressive surface (MRS), which is also the basis of the TST (Fig. 3.24b). In the transgressive system, the horizons onlap the

geologically older sediments at the slope and prograde towards the shelf. Top of the transgressive system is the maximum flooding surface (MFS), which is also the basis of the HST (Fig. 3.24b). The highstand system is presented by thick topset strata of mainly vertical aggradation on the shelf and some basinward progradation of the shelf edge. The top of the highstand system is mostly characterised by an unconformity, which marks the beginning of the next stratigraphical younger seismic sequence.

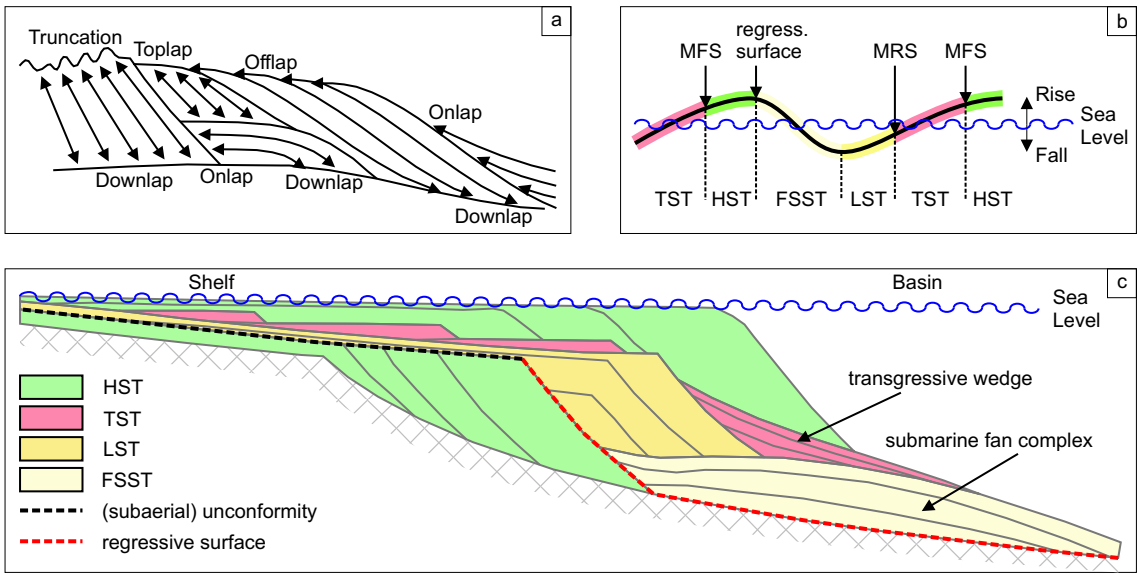

Figure 3.24: Method of seismic sequence stratigraphy modified after Catuneanu (2006). (a) Types of stratal terminations. (b) Systems tracts and stratigraphic surfaces in one sequence which consists of FSST, LST, TST and HST. (c) Systems tracts shown in a cross-section.

The application of the seismic sequence stratigraphy on the AWI MCS data (Fig. 3.23) concluded ten prograding sequences next to the Chukchi Plateau which reach back to the Late Eocene (Figs. 3.25a-b). In contrast, next to the Mendeleev Ridge only four sequences dated between Top Oligocene and Top Miocene could be observed. However, geologically older sequences could not be identified due to many faults below the Top Oligocene horizon (Figs. 3.25c-d). All these prograding sequences show different horizontal and vertical dimensions which were caused by the Cenozoic RSL variations.

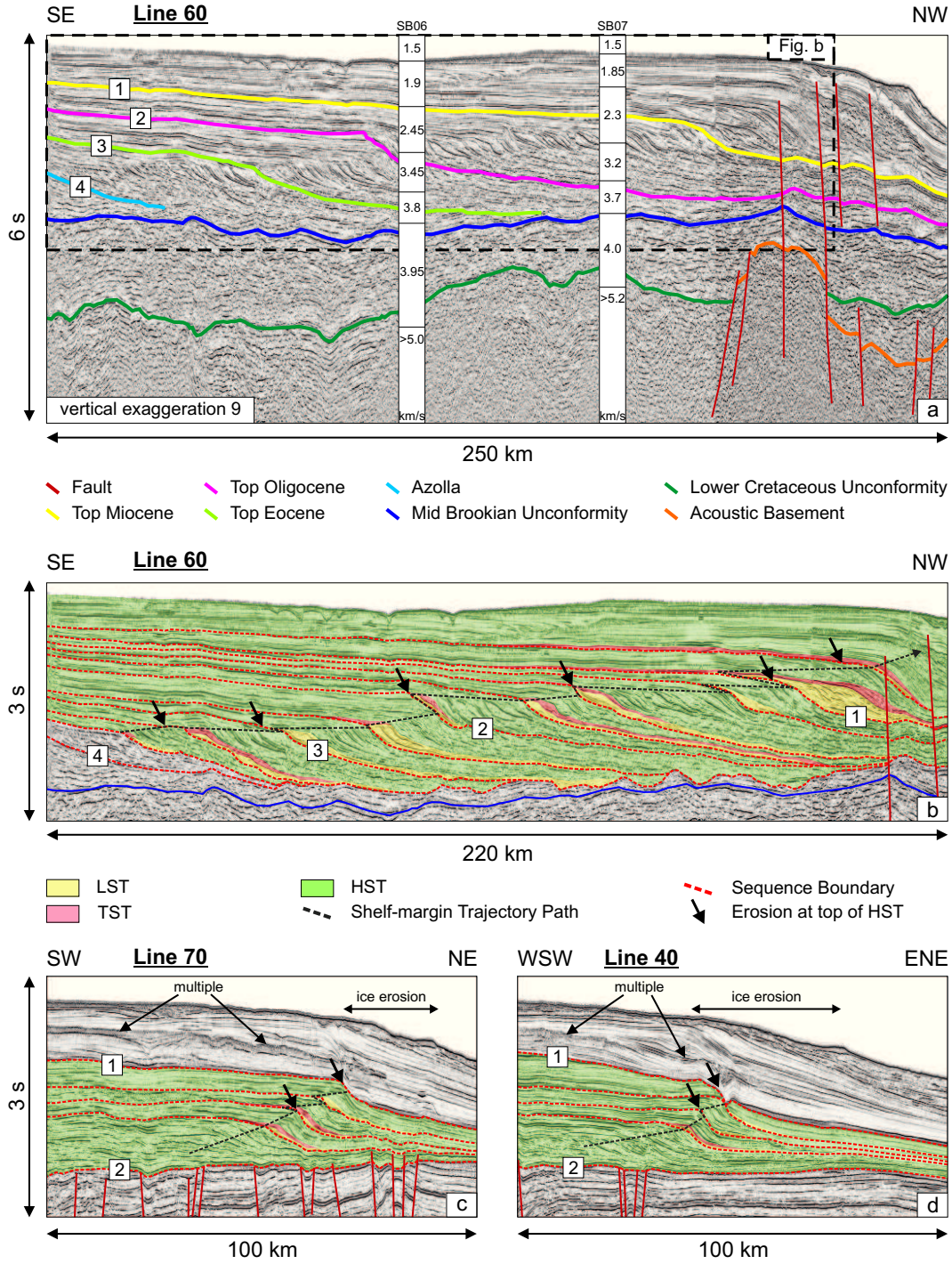

Figure 3.25: Three interpreted AWI MCS lines located on the Chukchi Shelf (Fig. 3.23); modified after Hegewald & Jokat (2012). (a) Shelf part of line 60 with six dated horizons and interval velocities of two sonobuoys. (b) Upper 3 s TWT of line 60 showing ten prograding sequences. (c) Shelf part of line 70 showing four prograding sequences. (d) Shelf part of line 40 showing the same four prograding sequences like line 70.

3.5.2 Relative Sea Level Variations in the Chukchi Region

The reconstruction of the RSL variations in the Chukchi region bases on the detection of costal onlaps of seismic reflectors in the margin area (Vail et al. 1977a). Using our prior calculated TWT-depth relation (Fig. 3.10), the positions of the costal onlaps were converted from time to depth values. Based on the dated horizons in the AWI MCS lines (Fig. 3.25a), an age was assigned to each onlapping horizon. Afterwards, these horizon ages were plotted over the depth values of the onlapping positions. Finally, the RSL variations result after subtraction of a linear trend (Fig. 3.26). This trend represents in a first approximation a constant subsidence, driven by the weight of the deposited sediments and the resulting compaction of the lower layers.

Furthermore, using the known thickness of the shelf sediments between two horizons with known ages we could calculate the minimum sedimentation rates for the northern Chukchi Shelf since the Late Eocene (Fig. 3.26). The minimum sedimentation rates are without consideration of sediment compaction. These resulting minimum sedimentation rates are between 2 cm/ky and 10 cm/ky. The comparison with sedimentation rates from other shelf areas, e.g. the sedimentation rate on the New Jersey continental margin during the Oligocene and the Pliocene was >30 cm/ky (Steckler et al. 1999), shows that the minimum sedimentation rates in the northern part of the Chukchi Shelf are unusually low. This might be the result of the long distance of sediment transport from the sediment source area to the deposition area of more than 400 km (Chapter 3.4).

Focusing on our interpretation, the resulting RSL curve for the Chukchi region starts in the Late Eocene (Fig. 3.26). To make quantitative statements about the RSL variations, the Chukchi curve was compared with the global RSL curve (Fig. 3.26, Vail et al. 1977b). We decided to compare our data with the 1977 curve because newer global RSL curves have a higher resolution (Miller et al. 2005) caused by additional information from analysed sediment cores, drill holes and outcrops on land. However, the trends as detected in the 1977 curve as well as in the newer global curves remain similar.

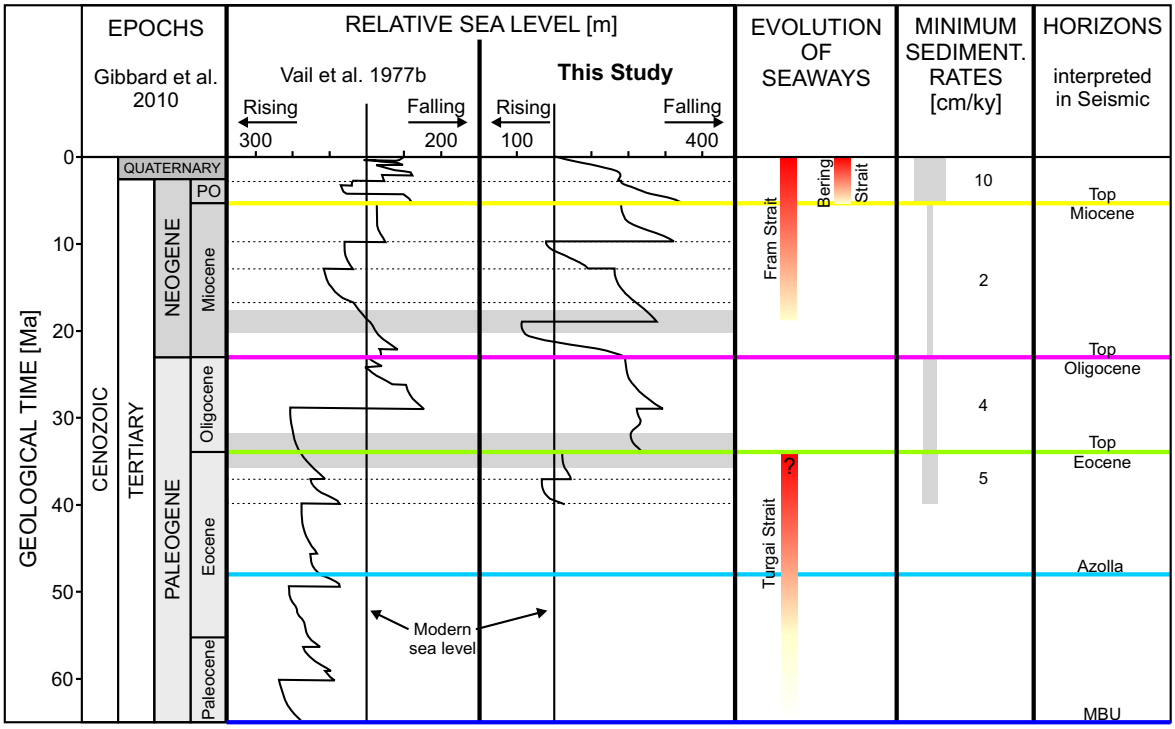

Figure 3.26: Comparison of the two Cenozoic RSL variation curves from the Chukchi region and the other global oceans; modified after Hegewald & Jokat (2012). Left graph: global RSL variation curve (Vail et al. 1977b). Right graph: RSL variation curve from the Chukchi region (this study). Dashed lines: RSL lowering events observed in both curves. Grey areas: two major lowering events observed in the RSL curve from the Chukchi region, but not observed in the global curve.

For both, the global and the Chukchi curve, the maximum RSL variations were about 400 m between the Late Eocene and the present day (Fig. 3.26). From the Late Eocene to the Eocene/Oligocene boundary the Chukchi and the global RSL are similar. In the Late Eocene a small relative marine regression of less then 100 m can be observed in both curves (Fig. 3.26). In this period (Late Eocene-Eocene/Oligocene), the first large ice sheets appeared in Antarctica, and isolated glaciers evolved on East Greenland (Eldrett et al. 2007), indicating a cooling of the global climate (Zachos et al. 2001). Until the Eocene/Oligocene boundary, the Turgai Strait connected the Arctic Ocean with the Tethys (Marincovich et al. 1990). On the Chukchi Shelf, the sediments of

the highstand systems tract were eroded (Fig. 3.25b, above horizon 4) and the minimum sedimentation rate was 5 cm/ky. At the Eocene/Oligocene boundary, the large Chukchi RSL lowering event of more than 200 m was not observed in the global curve (Fig. 3.26). In this phase of the relative marine regression, the Chukchi Shelf area was considerably eroded (Fig. 3.25b, below horizon 3). The Turgai Strait fell dry and opened up a continental pathway between Europe and Asia (Hou et al. 2011). At this time, a significant reorientation of relative plate motions occurred in the circum Arctic Ocean, when the seafloor spreading in the Labrador Sea ended and the separation of NE Greenland from Svalbard was initiated (Chalmers et al. 1993). Above all, the global temperature decreased by 4 degrees Celsius and the climate changed from global greenhouse to icehouse conditions (Zachos et al. 2001).

In the following 15 Ma (Eocene/Oligocene - Early Miocene), the Chukchi RSL variations are different in amplitudes and the temporal occurrence of lowering events compared with the global curve (Fig. 3.26). From the Eocene/Oligocene boundary to the Mid Oligocene the Chukchi RSL variations were minor, whereas the global curve shows a pronounced relative marine transgression for the entire time period (Fig. 3.26). Since the Upper Oligocene, the Chukchi RSL rose about 100 m and increased for further 300 m in the Early Miocene (Fig. 3.26). In the Mid Oligocene, the global RSL fell more than 350 m, and varied in short regression and transgression episodes with a total rise of about 150 m until the Early Miocene (Fig. 3.26). During most of the Oligocene, the global climate was constant and cooler than in the Eocene (Zachos et al. 2001). The consequences for the Chukchi Shelf were a low sediment influx with a minimum sedimentation rate of 4 cm/ky, and a continuous progradation of the Chukchi Shelf margin with no erosion of the shelf sediments until the Oligocene/Miocene boundary (Fig. 3.25b, between horizon 2 and 3). From the Late Oligocene to the Early Miocene, the temperatures decreased by about 2 degrees Celsius (Zachos et al. 2001). The Chukchi RSL increased considerably in contrast to the minor rise observed globally (less than 50 m, Fig. 3.26). This large Chukchi relative marine transgression in the Early Miocene produced a pronounced erosion of the palaeo-shelf edge, and a large

vertical offset in the shelf-margin trajectory path (Fig. 3.25b, across horizon 2). With the opening of the Fram Strait in the Early Miocene (Engen et al. 2008), the Chukchi RSL fell dramatically by approximately 400 m (Fig. 3.26) and reconnected the Arctic Ocean to the global oceans, in particular, the Atlantic Ocean. In this period, the global RSL curve shows a slow and continuous increase (Fig. 3.26).

The Chukchi RSL variations can be generalised for the entire Arctic Ocean, because Eocene-Oligocene age unconformities reported in sediments on the East Siberian Shelf (Sekretov 2001), the Laptev Shelf (Franke & Hinz 2005) and the Mackenzie Delta (Dixon et al. 1992), correlate with the RSL lowering events observed in the Chukchi curve. Moreover, no local tectonic events are known in the Chukchi region since the Late Eocene, and the sediment influx was not influenced by e.g. large river systems, based on the low minimum sedimentation rates between 2 cm/ky and 5 cm/ky. Finally, geochemical analyses at the IODP core from the ACEX expedition 302 to the central Lomonosov Ridge (Jakobsson et al. 2007) lead to the interpretation that the Arctic Ocean was predominantly isolated after the closure of gateways in the Eocene until the opening of the Fram Strait in the Early Miocene (O'Regan et al. 2008). In this period, large volumes of fresh water were discharged from Canadian, Alaskan and Siberian rivers into the landlocked Arctic Ocean, which reduced the salinity of the Arctic surface water (Jakobsson et al. 2007). In the Early Miocene, the sediments on the central Lomonosov Ridge show erosion, redeposition of older sediment, and deposition of new sediment in a shallow water regime (März et al. 2011, Jakobsson et al. 2007), which correlates with our considerable RSL lowering at this time. Based on these facts, we applied our Chukchi RSL curve for the Arctic Ocean. Therefore, we suggest an isolated Arctic Ocean from the Eocene/Oligocene boundary to the Early Miocene (Fig. 3.26). Our observed RSL fall of 400 m in the Early Miocene leads to the interpretation that the RSL in the isolated Arctic basin was higher than in the global oceans. With the opening of the Fram Strait, the Arctic Ocean water flowed into the Atlantic Ocean. On the New Jersey Costal Plain (northeast coast of the USA), an absolute sea level increase of about 15 m was observed in the Early Miocene (Kominz et al. 2008). Hy-

pothetically, an absolute sea level fall of about 400 m in the Arctic Ocean (total area of 14 million km^2) would produce an absolute sea level increase of 15 m in the global oceans (total area 360 million km^2).

During Miocene times, when the Fram Strait deepened through seafloor spreading, the Arctic Ocean became a well-ventilated saline ocean because of the inflow of saline North Atlantic water (Jakobsson et al. 2007). Since the opening of the Fram Strait, the variations of the Chukchi and global RSL show the same trend (Fig. 3.26). From Early to Mid Miocene, the RSL increased in total about 150 m to 200 m (Fig. 3.26) and the Chukchi Shelf edge prograded continuously (Figs. 3.25b-d, above horizon 2), with a minimum sedimentation rate of 2 cm/ky. In this period the global temperatures increased until the Mid Miocene climate optimum (Zachos et al. 2001). Since the Mid Miocene, both curves show a general lowering trend, which correlates with the onset of global cooling and the evolution of partial and ephemeral ice sheets on the Northern Hemisphere (Fig. 3.26). At the Miocene/Pliocene boundary, the global and the Chukchi RSL fell about 100 m to 150 m (Fig. 3.26), and the Chukchi Shelf sediments were eroded (Figs. 3.25b-d, below horizon 1). In the Pliocene, the minimum sedimentation rate increased significantly to 10 cm/ky , which presents a 5-fold increase relative to the Miocene. Corresponding results are reported from the Beaufort-Mackenzie area (McNeil et al. 2001): a regional uplift across the cratonic margin in the Late Miocene, combined with eustatic lowstand, and followed by tectonic quiescence and dry cool climatic conditions in the Early Pliocene produced widespread erosion and a 23-fold increase in the sedimentation rate relative to the Early and Middle Miocene. Furthermore, the Bering Strait between Alaska and Siberia opened and connected the Arctic Ocean with the Pacific Ocean (Gladenkov et al. 2002, Fig. 3.26). Since the Pliocene, larger and permanent ice sheets covered the Arctic Ocean (Eldrett et al. 2007) and eroded the Chukchi Shelf sediments (Figs. 3.25c-d, below the ocean bottom).

Summarising the above, we calculated the first RSL curve for the Chukchi region, based on interpreted AWI MCS data from the Chukchi Shelf. We showed that our Chukchi RSL curve is representative for the Arctic Ocean. Comparing the Chukchi RSL with

the global RSL curve, we suggest that the Arctic Ocean was an isolated basin from the Eocene/Oligocene boundary to the opening of the Fram Strait in the Early Miocene (Engen et al. 2008). The opening of the Fram Strait might has caused a global RSL rise, consequently led to a significant fresh water input into the North Atlantic Ocean. Hence, our investigations conclude that the RSL in the isolated Arctic Ocean was higher than in the global ocean.

4 Gravity Data

Based on the public-domain Arctic Gravity Project (ArcGP, Kenyon et al. 2008) grid we developed a 3D gravity model of the Chukchi region and the southern part of the Mendeleev Ridge. As boundary conditions for the 3D modelling, the sediment thickness, the basement depth and the Moho depth were calculated using the interpreted seismic data (Chapter 3). Furthermore, the sediment densities are based on the bulk density logs of the five exploration wells, drilled on the Chukchi Shelf near the coast of Alaska (Chapter 3.1.2, Fig. 3.3; Sherwood et al. 2002). The maximum drilling depth varys between 2000 m and 3600 m.

4.1 The Arctic Gravity Project (ArcGP)

The ArcGP has compiled a gravity field on a 5' x 5' grid of the entire Arctic region north of 64°N (Fig. 4.1, Kenyon et al. 2008). The project incorporated data measured from different platforms: airborne (Brozena et al. 1997, Forsberg et al. 2002), surface, submarine (Edwards & Coakley 2003), ice breaker and satellite (Laxon & McAdoo 1994, Forsberg & Skourup 2005). Following Forsberg et al. (2004), the public-domain gravity grid (ArcGP) includes atmospheric corrected free-air gravity anomalies with reference to the World Geodetic System from 1984 (WGS84). Subsequent investigations are based on the last ArcGP grid version (updated: March 19^{th}, 2008).

4.2 Sedimentary Thickness and Basement Depth

Based on several seismic reflection lines and published basement depth values (Fig. 4.2) we were able to calculate the sedimentary thickness and the basement depth of the Chukchi region and adjacent areas. Therefore, existing basement depth values from the Canada Basin (Jackson et al. 1990) and the Chukchi and East Siberian Shelf (Drachev et al. 2010) were combined with the interpreted basement in the seismic reflection lines from the Chukchi Borderland and the southern part of the Mendeleev Ridge (Fig. 4.2, black lines; Chapter 3.1.2, Fig. 3.3).

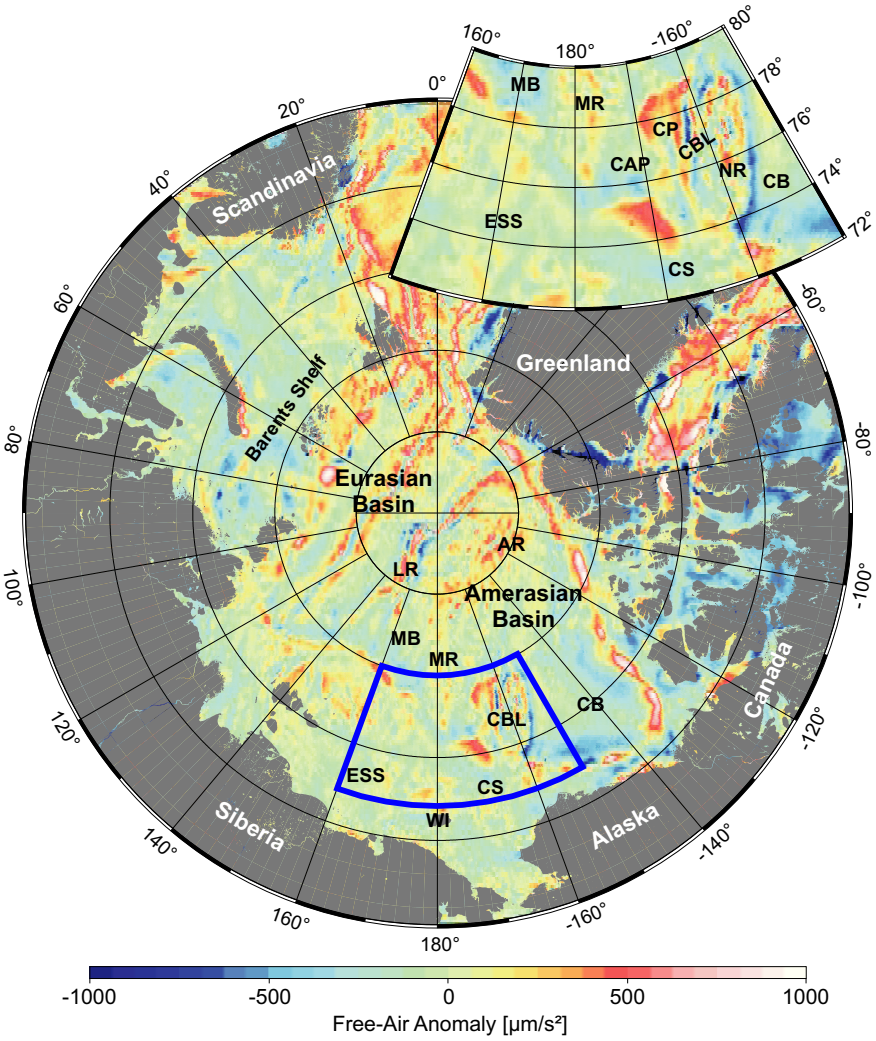

Figure 4.1: Free-air anomaly map of the entire Arctic region north of 64°N with a resolution of 5' x 5' (ArcGP, Kenyon et al. 2008). The blue frame and the small map show the free-air anomalies of the Chukchi region and the southern part of the Mendeleev Ridge.

The combination of our interpreted basement TWT values and the basement depth values published by Jackson et al. (1990) and Drachev et al. (2010) requires the transformation of the TWT values into depth values, using the prior calculated TWT-depth relation for the Chukchi region (Fig. 3.10, Eq. 3.1). Afterwards, the basement depth values were gridded with a resolution of 5' x 5' for the Chukchi region and adjacent areas (Fig. 4.3). Finally, the sedimentary thickness was calculated by subtraction of the bathymetry (IBCAO, Jakobsson et al. 2008a) from the basement depth (Fig. 4.4).

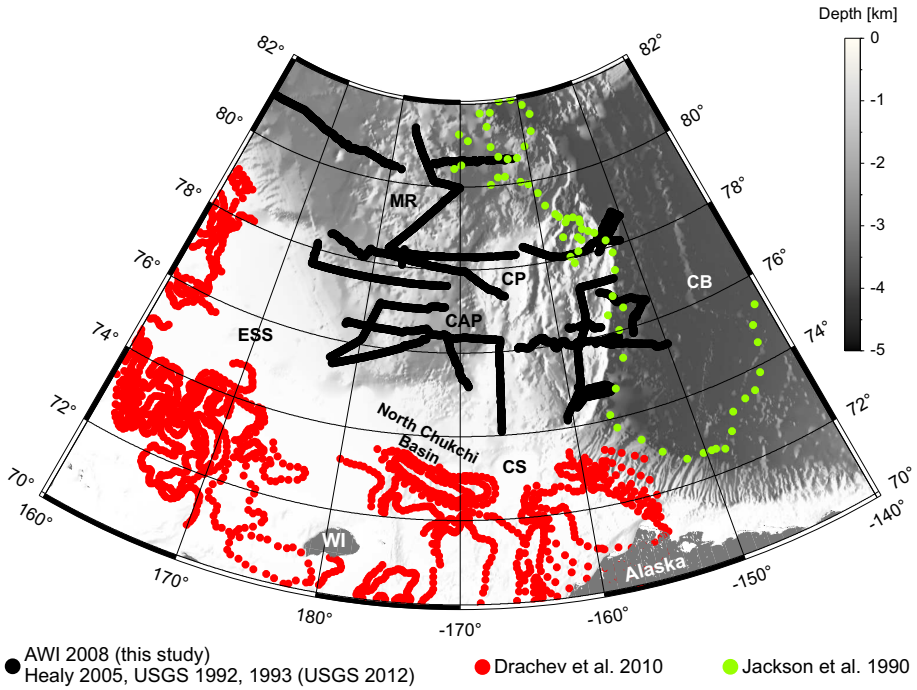

Figure 4.2: Data sets for the calculation of the basement depth. The black dots show the location of our interpreted basement in the seismic reflection lines from the AWI 2008 expedition (Jokat et al. 2009) and from public-domain data (USGS 2012; Chapter 3.1.2, Fig. 3.3), acquired by the USGS in 1992, 1993 (Grantz et al. 2004) and on the Healy expedition in 2005 (Darby et al. 2005).

The basement depth (Fig. 4.3) in the Chukchi region and adjacent areas range between 100 m and 18 km below sea level. In the North Chukchi Basin, the sediment thickness reaches the highest values of about 18 km (Fig. 4.4, Drachev et al. 2010). In contrast, the basement depth of the Chukchi Borderland, the southern part of the Mendeleev Ridge as well as the biggest part of the Chukchi and East Siberian Shelf is less than 4 km. These areas are covered by about 500 m, 1 km, 3 km and 2 km thick sediments, respectively. In the Canada Basin, the average basement depth is approximately 8 km with a sediment cover of about 4 km in thickness (Jackson et al. 1990). Based on the AWI MCS data, acquired during the 2008 expedition, the average basement depth for the Chukchi Plateau is 2 km, covered by 1 km thick sediments. Furthermore, the Chukchi Abyssal Plain is covered by about 4 - 5 km thick sediments and has an

average basement depth of 8 km. Finally, the basement depth of the southern part of the Mendeleev Ridge is about 4 km, covered by 1 - 2 km thick sediments.

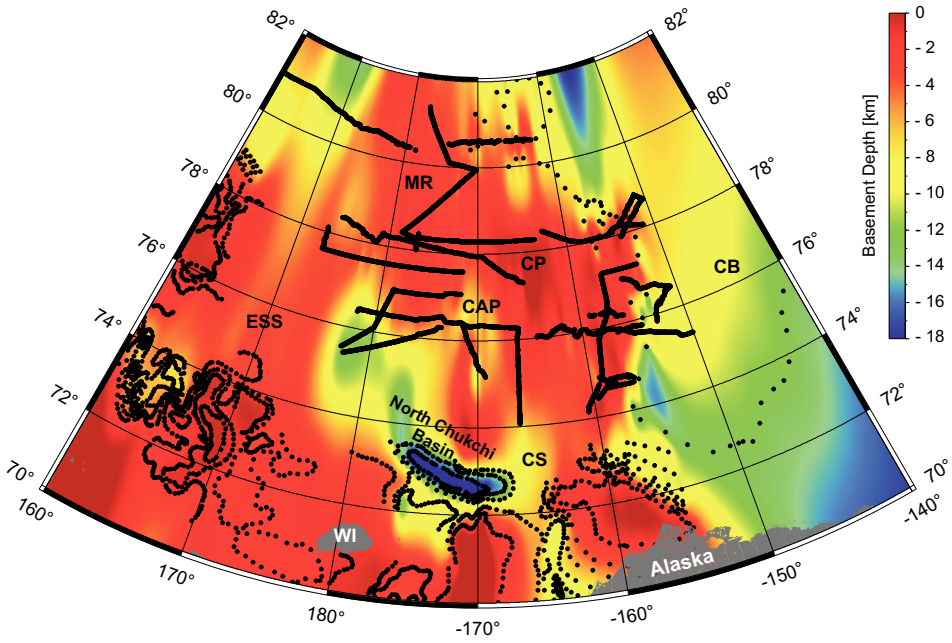

Figure 4.3: Basement depth resulting from the combination of different data sets (Fig. 4.2).

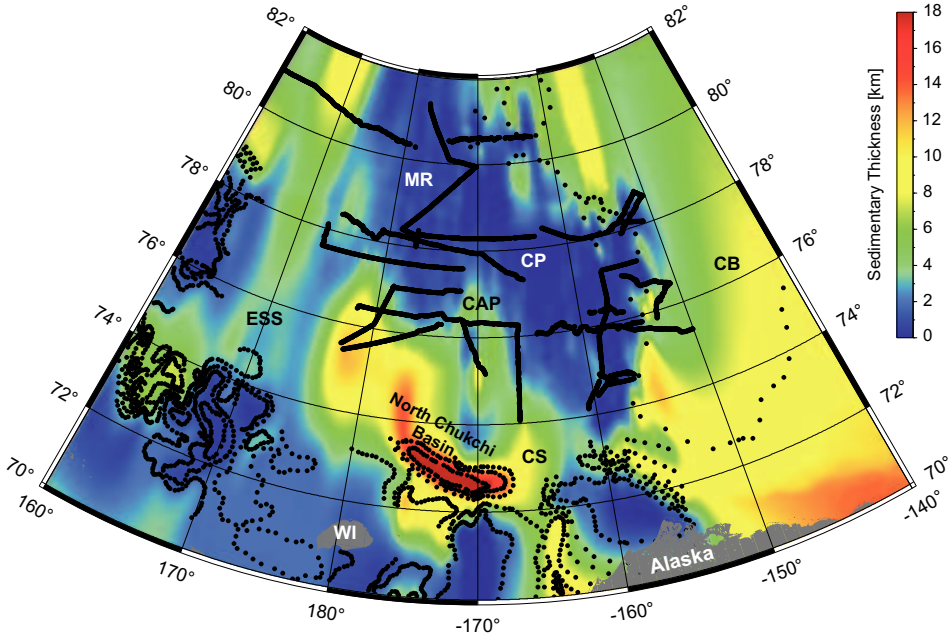

Figure 4.4: Sedimentary thickness resulting from the subtraction of the bathymetry (IBCAO Jakobsson et al. 2008a) from the basement depth (Fig. 4.3).

4.3 Calculation of Moho Depth

For the calculation of the Moho depth we used three data sets: (1) the free-air anomalies (ArcGP, Kenyon et al. 2008), (2) the bathymetry (IBCAO, Jakobsson et al. 2008a), and (3) the sedimentary thickness (Chapter 4.2). The calculation was done with the software package LithoFLEX (Wienecke et al. 2008) which is based on gravity inversion using the Parker-Oldenburg algorithm (Parker 1972, Oldenburg 1974). This method was successfully tested in other investigation areas, e.g. the Tibetan Plateau (Braitenberg et al. 2000a, Braitenberg et al. 2000b), the Barents Sea (Ebbing et al. 2007) and the Tien Shan (Steffen et al. 2011). The dimension of the area which we used for LithoFLEX is 1443 km x 1209 km. This area is enlarged by 200 km to each side compared with the 3D gravity model area (Fig. 4.5; Chapter 4.4), to avoid boundary effects in the calculated Moho depth values within the region of the 3D model. Later on, we are using the Moho depth as boundary condition for the crust-mantle discontinuity in the 3D gravity model (Chapter 4.4).

Before calculating the Moho depth, two important input parameters for LithoFLEX are necessary: a reference level and a cut-off wavelength. The reference level is a rough estimation of the mean crustal thickness with a tendency to lower values. The cut-off wavelength is used for the low pass filtering process to eliminate free-air anomalies with short wavelengths, that are generated by shallow crustal bodies with different densities. Theoretically, small wavelength anomalies in the observed gravity field correspond to the sediments and intra crustal density inhomogeneities, while the long wavelength information corresponds to the crust/mantle density contrast. On the other hand, according to the principles of equivalence, large sediment basins would also produce long wavelength in the observed gravity field. Therefore, we made a spectral analysis of the free-air anomalies and plotted the results against the wavenumber and wavelength (Figs. 4.6).

However, the calculation of the Moho depth consists of several steps. Based on the bathymetry (IBCAO, Jakobsson et al. 2008a) and the sedimentary thickness, the grav-

ity effect of the sediments can be calculated. Therefore, a function which describes the density increase of the sediment cover with depth was applied. The used density-depth relation was approximated by a linear function with 2200 kg/m^3 at the seafloor surface and 2550 kg/m^3 at the sediment-basement boundary. Afterwards, the gravity effect of the sediments was subtracted from the free-air anomalies (ArcGP, Kenyon et al. 2008). Furthermore, several reference levels have to be tested and the results of the Moho depth have to be compared to published depth values resulting from other methods, e.g. seismic refraction or gravity models. The best fit between our calculated Moho depth (Fig. 4.7) and published values (Tab. 4.1) are based on a reference level of 30.4 km (Fig. 4.6a) and a cut-off wavelength of 372 km (Fig. 4.6b). Finally, using these two values and a density contrast at the crust-mantle discontinuity of -350 kg/m^3, the Moho depth (Fig. 4.7) was calculated by gravity inversion. The accuracy of the Moho depth is difficult to estimate, but it can be improved by elimination of errors such as heterogeneities in the crust, approximation of the sediment densities, and the interpolated sedimentary thickness in the study area which is based on few seismic and gravity data (Chapter 4.2).

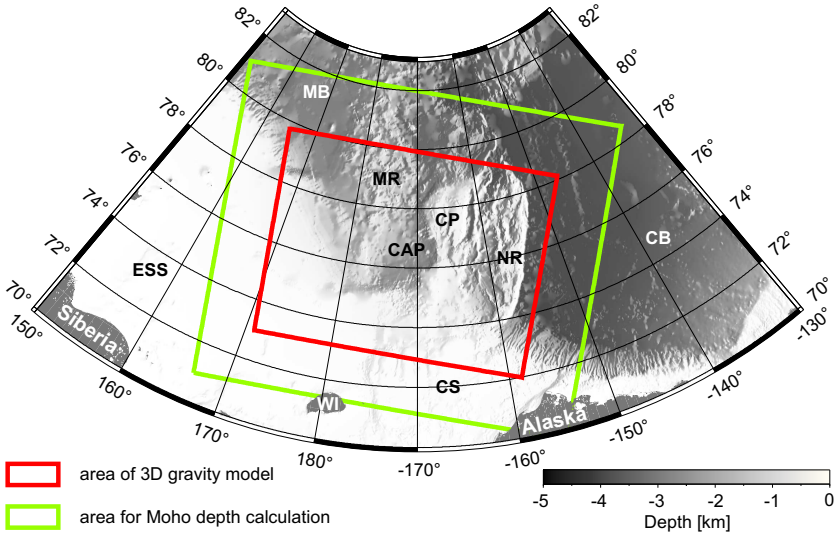

Figure 4.5: Green box: area for the calculation of the Moho depth. Red box: area of the 3D gravity model. To avoid boundary effects in the Moho depth within the region of the 3D model, the green area is extended to each side by 200 km.

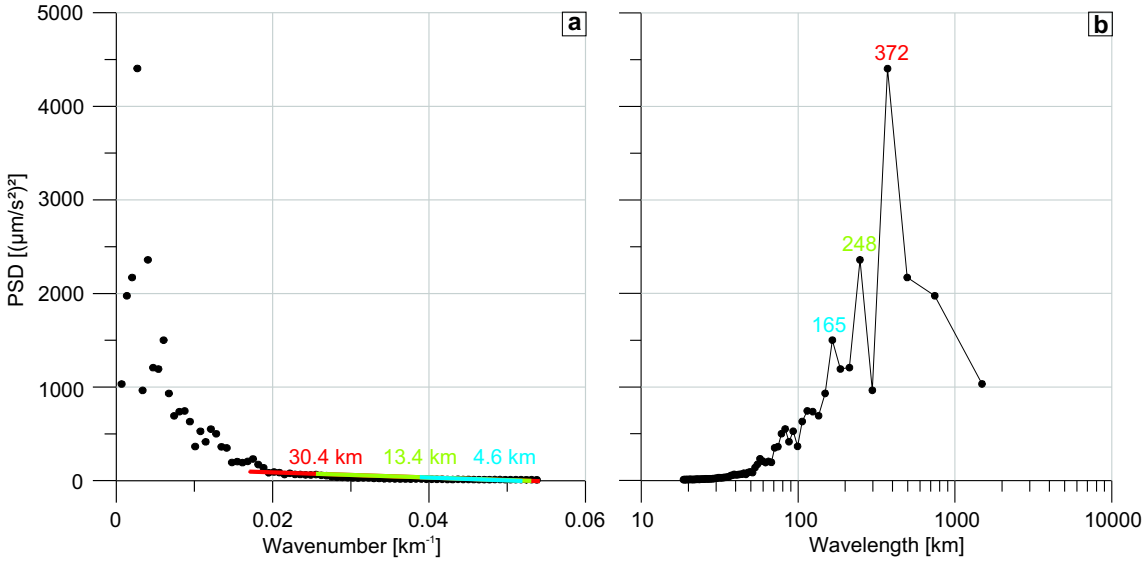

Figure 4.6: Power spectral density (PSD) of the free-air anomaly of the Chukchi region and the southern part of the Mendeleev Ridge (Fig. 4.5, green box) against (a) the wavenumber and (b) the wavelength. The used reference level is indicated with 30.4 km (red), which corresponds to the slope of the regression line, and the cut-off wavelength with 372 km (red). The green and blue coloured values mark the other tested reference levels (Tab. 4.1).

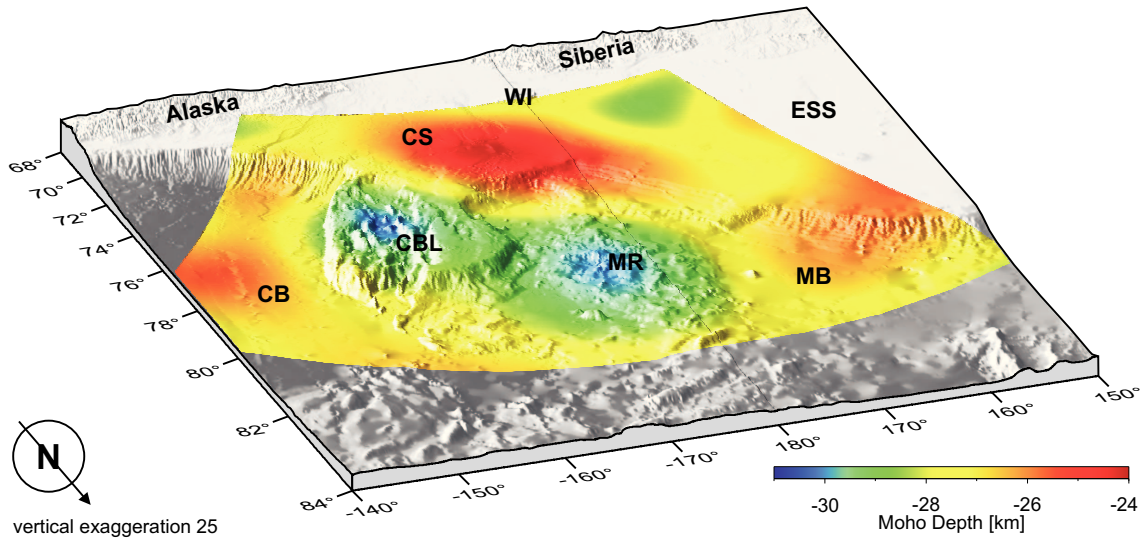

Figure 4.7: Bathymetric map (IBCAO, Jakobsson et al. 2008a) showing the estimated Moho depth.

Table 4.1: Moho depths [km] resulting from our calculations, using different reference levels (Fig. 4.6a) as input parameters for LithoFLEX (Wienecke et al. 2008). Moho depth values [km] based on gravity models published by: (A) Shaver & Hunkins (1964), (B) Hall (1990), (C) Alvey et al. (2008). The calculated Moho depth, based on the reference level of 30.4 km, corresponds most closely to the published values.

Geological Region	Reference Level			(A)	(B)	(C)
	30.4 km	13.4 km	4.6 km			
Chukchi Shelf	25 - 28	8 - 10	0 - 2	-	-	40
Chukchi Abyssal Plain	28 - 29	10 - 11	1 - 2	21	13	22
Canada Basin	26 - 28	9 - 10	0 - 2	-	21	18
Mendeleev Ridge	29 - 31	11 - 14	3 - 5	-	-	38
Chukchi Borderland	29 - 30	11 - 14	3 - 5	32	28	35

4.4 Gravimetric 3D Modelling

Using seismic reflection data, the sediment structures and the topography of the acoustic basement can be displayed (Chapter 3.3). On the other hand, to gain more information about crustal structures and the topography of the Moho, gravimetric modelling is necessary. Therefore, a complex 3D gravity model of the Chukchi region and the southern part of the Mendeleev Ridge was calculated, using the software package IGMAS+ (Interactive Gravity and Magnetic Assistant System; Götze 1978, Götze & Lahmeyer 1988, Schmidt & Götze 1999, Schmidt 2004).

Based on the ArcGP grid (Kenyon et al. 2008, Chapter 4.1) a 3D gravity model of 1036 km x 780 km x 50 km, consisting of 21 sections, was developed. The outer borders of the entire model are 3000 km x 3000 km in dimension to avoid boundary effects in the main 3D model area. The sections are oriented in east-west direction, to cross the main geological provinces perpendicular (Figs. 4.8 and 4.9). The distance between each section is 39 km and the station spacing along each section is 10 km. Therefore, to

avoid alias effects, the modelling of gravity anomalies with wavelength > 20 km along the sections is possible. Concerning the free-air anomalies of the modelling area, the main wavelengths are between 100 km and 400 km (Fig. 4.6b).

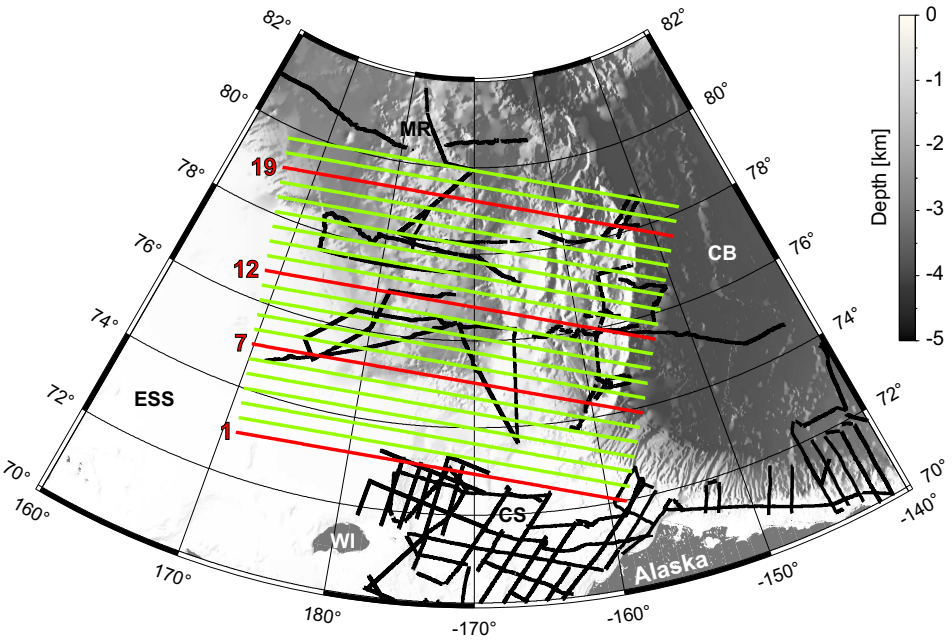

Figure 4.8: Bathymetric map (IBCAO, Jakobsson et al. 2008a) showing the locations of the 21 sections, used for the 3D gravity model. The four annotated red sections are shown in Chapter 4.4.2; black lines - seismic reflection data (Chapter 3.1.2, Fig. 3.3).

4.4.1 Boundary Conditions

Boundary conditions are necessary to reduce the ambiguity, associated with potential methods. These additional information can be geological, tectonic, well logs and further geophysical data sets for the modelling area.

The results of our calculated basement depth (Chapter 4.2) and Moho depth (Chapter 4.3) were directly used for the 3D gravity model. Furthermore, the sediment densities we received from the bulk density logs of the five exploration wells, drilled on the Chukchi Shelf near the coast of Alaska (Sherwood et al. 2002, Chapter 3.1.2). Based on the logging information, we divided the sediment cover of the study area into three layers (Tab. 4.2).

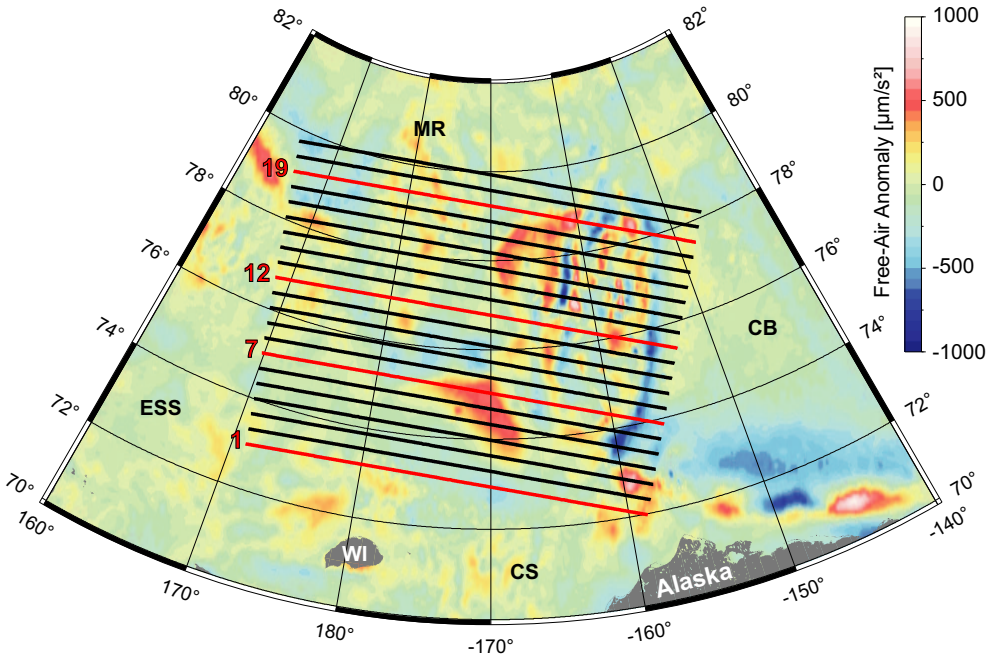

Figure 4.9: Free-air anomaly map (ArcGP, Kenyon et al. 2008) showing the locations of the 21 sections (section length 1036 km, distance between each section 39 km), used for the 3D gravity model. The four annotated red sections are shown in Chapter 4.4.2.

Table 4.2: Sediment densities received from the bulk density logs of the five exploration wells, drilled on the Chukchi Shelf near the coast of Alaska (Sherwood et al. 2002). Based on the bulk density logs the sediment cover in the Chukchi region was divided into three layers.

Sediment Layer	Density [kg/m^3]
Upper Sediments	2000
Middle Sediments	2200
Lower Sediments	2550

The crust of the modelling area was divided into five model bodies, derived from the five existing geological provinces (Fig. 4.10). Hence, the Canada Basin and the Makarov Basin were characterised with an oceanic crust (2900 kg/m^3), like published by Baggeroer & Falconer (1982) and Sorokin et al. (1999). In contrast, the Chukchi Shelf

and the Chukchi Borderland were characterised with a continental crust (2670 kg/m^3), like published by Dinkelman et al. (2008) and Grantz et al. (1998). In addition, the Chukchi Shelf crust was divided into an upper and a lower crust (2900 kg/m^3). The origin of the Mendeleev Ridge remains controversial (Dove et al. 2010). However, we selected a density of 2850 kg/m^3 for the crust of the Mendeleev Ridge like already suggested by Dove et al. (2010).

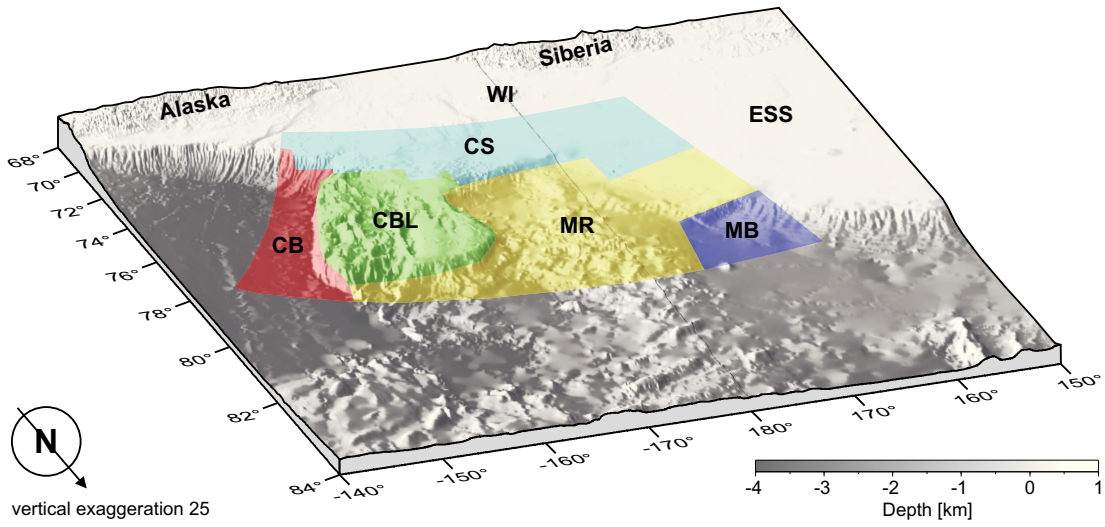

Figure 4.10: Bathymetric map (IBCAO, Jakobsson et al. 2008a) showing the five crustal model bodies, derived from the five existing geological provinces in the main study area.

4.4.2 The 3D Model

Following our results, the 3D gravity model consists of 21 sections (Figs. 4.8 and 4.9) and 11 geological model bodies which include the ocean water, the sediments, the crust and the mantle. The densities of these geological model bodies are listed in Table 4.3. Four sections of the final 3D gravity model are shown exemplary in the following: section 1 (Fig. 4.11), section 7 (Fig. 4.12), section 12 (Fig. 4.13) and section 19 (Fig. 4.14).

Section 1 is located on the Chukchi Shelf and shows the North Chukchi Basin (Fig. 4.11) which is filled with up to 10 km of sediments. The thickness of the continental crust of the Chukchi Shelf is between 20 km (below the North Chukchi Basin) and 33 km.

The Moho depth varies from 30 km (below the North Chukchi Basin) to 35 km. This modelled Moho depth is about 5 km deeper than the prior calculated Moho depth using gravity inversion (Fig. 4.11, pink line; Chapter 4.3).

Table 4.3: Densities of the 11 geological model bodies which build the 3D gravity model. The reference body surrounds the entire 3D model.

Model Body	Density [kg/m^3]
Water	1030
Upper Sediments	2000
Middle Sediments	2200
Lower Sediments	2550
Upper Crust - Chukchi Shelf	2670
Lower Crust - Chukchi Shelf	2900
Crust - Chukchi Borderland	2670
Crust - Mendeleev Ridge	2850
Crust - Canada Basin	2900
Crust - Makarov Basin	2900
Mantle	3200
Reference	2670

Section 7 crosses the Chukchi Shelf, the Chukchi Borderland and the Canada Basin (Fig. 4.12). The thickness of the sediment cover ranges from 1 km to 8 km. Furthermore, below the Chukchi Shelf the modelled Moho depth is 28 km to 32 km, which is about 3 km deeper than the prior calculated Moho depth (Fig. 4.12, pink line; Chapter 4.3). In contrast, the average continental crust of the Chukchi Borderland is 22 km thick and the oceanic crust of the Canada Basin is 18 km thick. However, the calculated Moho depth below the Chukchi Borderland and the Canada Basin is shallower than the prior calculated Moho depth (Fig. 4.12, pink line; Chapter 4.3).

Section 12 crosses the Mendeleev Ridge, the Chukchi Borderland and the Canada Basin (Fig. 4.13). The thickness of the sediment cover ranges between 1 km (on the Chukchi Borderland) and 6 km (in the Chukchi Abyssal Plain). Furthermore, the crustal thickness of the Mendeleev Ridge is up to 32 km. On the other hand, the crustal thickness of the Chukchi Abyssal Plain is only 12 km. The continental crust of the Chukchi Borderland clearly shows the separation of the Chukchi Plateau and the Northwind Ridge by the graben system inbetween. The crustal thickness below this graben system is approximately 6 km thinner compared with the crustal thickness of the Chukchi Plateau and the Northwind Ridge (Fig. 4.13).

Section 19 crosses the Makarov Basin, the Mendeleev Ridge, the Chukchi Borderland and the Canada Basin (Fig. 4.14). The sediment cover becomes thinner compared with the other sections (Figs. 4.11 - 4.13) and ranges between 1 km and 2 km on the Chukchi Borderland and the Mendeleev Ridge. In the Canada Basin and the Makarov Basin the sedimentary thickness is 4 km to 8 km. Furthermore, the modelled Moho depth becomes significantly lower compared with the prior calculated Moho depth (Fig. 4.14, pink line; Chapter 4.3). The modelled Moho depth below the Canada Basin is about 18 km, below the Chukchi Borderland between 18 km and 22 km, below the Chukchi Abyssal Plain about 21 km, below the Mendeleev Ridge between 25 km and 32 km, and below the Makarov Basin about 22 km.

Table 4.4 shows the Moho depth resulting from our calculation using gravity inversion (Chapter 4.3), from the 3D gravity modelling, and from four gravity models published by Shaver & Hunkins (1964), Hall (1990), Sorokin et al. (1999) and Alvey et al. (2008). The comparison of all values shows that the modelled Moho depth fits much better to the published values than the calculated Moho depth. However, the calculated Moho depth is a sufficient estimation which can be calculated really fast, compared with the time proven gravity modelling.

Based on the final 3D gravity model, the gravity effects of the sediments, the crust and the mantle can be calculated. Therefore, we replaced the densities of the model bodies by the reference density of 2670 kg/m^3, excluding the model bodies from which the

gravity effect has to be calculated. The results are shown in Figure 4.15. Hence, the gravity effect of the sediments ranges between -1000 μm/s^2 and 500 μm/s^2 (Fig. 4.15A). The areas showing positive gravity values are covered by a thin sediment layer (e.g. Chukchi Plateau, Mendeleev Ridge), whereas the areas showing negative gravity values are covered by thick sediments (e.g. Chukchi Shelf). Furthermore, the gravity effect of the crust ranges between -1000 μm/s^2 and 1000 μm/s^2 (Fig. 4.15B). The areas showing positive gravity values were modelled with a denser and thicker crust (e.g. Mendeleev Ridge) than areas showing negative gravity values (e.g. Chukchi Borderland). In contrast, the gravity effect of the mantle varies between -1700 μm/s^2 and 2000 μm/s^2 (Fig. 4.15C). The areas showing positive gravity values are dominated by a shallow Moho depth (e.g. Chukchi Abyssal Plain), and areas showing negative gravity values are dominated by a great Moho depth (e.g. Chukchi Shelf, Mendeleev Ridge).

Summarising our results, the 3D gravity model shows the crustal and mantle structures of the Chukchi region and adjacent areas in addition to the sedimentary structures resulting from the interpreted seismic reflection lines (Chapter 3.3). Regarding the densities of the different crustal model bodies, the Chukchi Shelf and the Chukchi Borderland consist of continental crust. In contrast, the Canada Basin and the Makarov Basin consist of oceanic crust. The crust of the Mendeleev Ridge was modelled with a density of 2850 kg/m^3, which ranges between the typical densities for a continental (2670 kg/m^3) and for an oceanic crust (2900 kg/m^3). Despite the basement interval velocities (from sonobuoy data), the observed subbasement seismic reflectors (Chapter 3.3.3) and the high magnetic anomalies (Chapter 2.1, Fig. 2.2C), a clear identification of the Mendeleev Ridge as an oceanic plateau (Hall 1970) or a rifted volcanic continental margin (Lebedeva-Ivanova et al. 2006) is not possible. Furthermore, the Chukchi Abyssal Plain seems to be underlain by a thinner extremity of the Mendeleev Ridge crust. Concerning the Chukchi Borderland, the continental crust of the graben system, inbetween the Chukchi Plateau and the Northwind Ridge, is much thinner than of its surrounding provinces. This thinned crust might be the result of the evolution of the Chukchi Borderland in an E-W directed extensional regime.

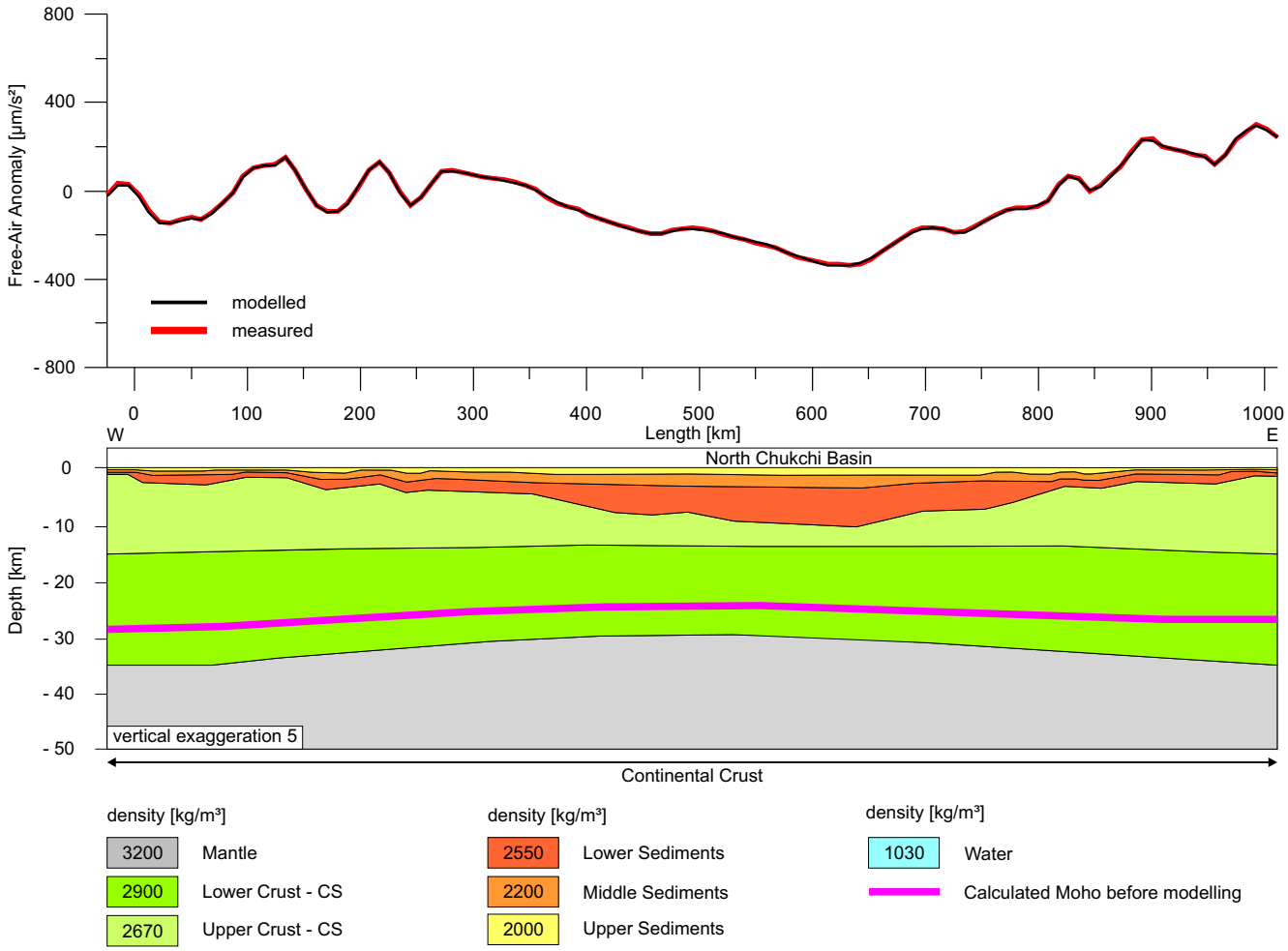

Figure 4.11: Section 1 crosses the Chukchi Shelf with the North Chukchi Basin. The calculated Moho depth (pink line) was evaluated before modelling (Chapter 4.3). For the location of this section see Figures 4.8 and 4.9. The accuracy of the modelling is shown in Figure 4.16C.

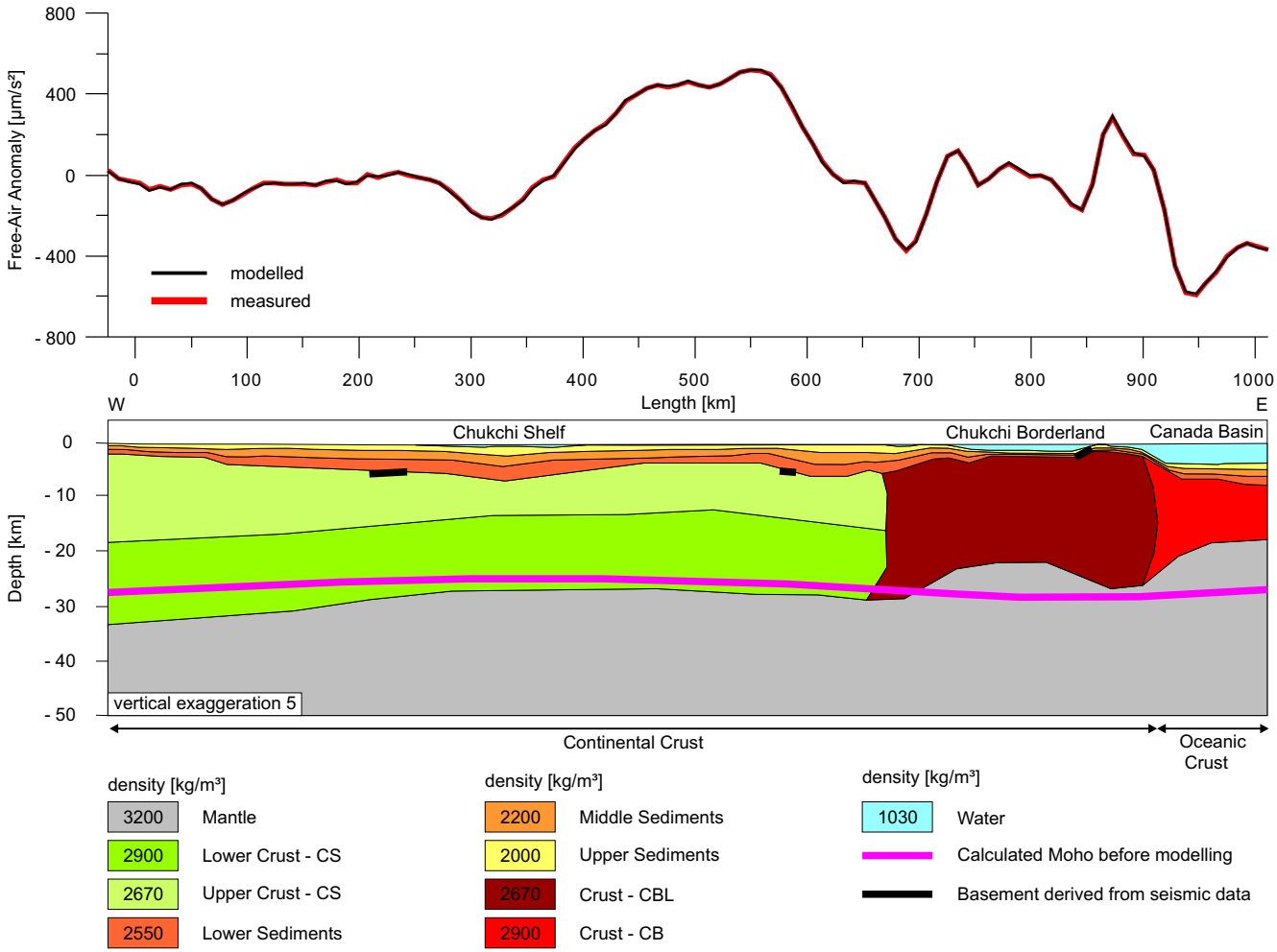

Figure 4.12: Section 7 crosses the Chukchi Shelf, the Chukchi Borderland and the Canada Basin. The calculated Moho depth (pink line) was evaluated before modelling (Chapter 4.3). The black lines show the locations of the basement, derived from the interpreted seismic reflection lines (Chapter 3.1.2, Fig. 3.3). For the location of this section see Figures 4.8 and 4.9. The accuracy of the modelling is shown in Figure 4.16C.

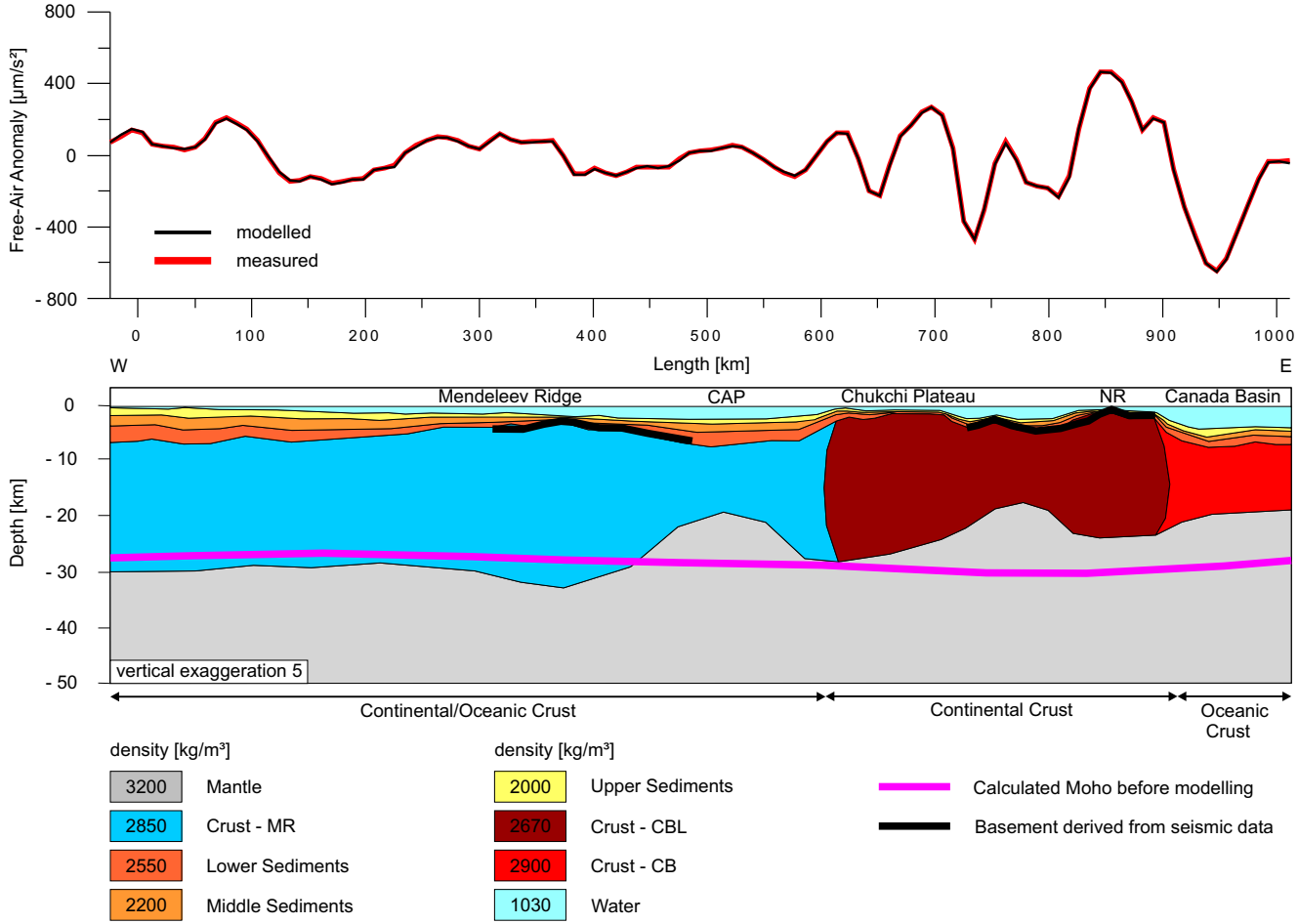

Figure 4.13: Section 12 crosses the Mendeleev Ridge, the Chukchi Borderland and the Canada Basin. The calculated Moho depth (pink line) was evaluated before modelling (Chapter 4.3). The black lines show the locations of the basement, derived from the interpreted seismic reflection lines (Chapter 3.1.2, Fig. 3.3). For the location of this section see Figures 4.8 and 4.9. The accuracy of the modelling is shown in Figure 4.16C.

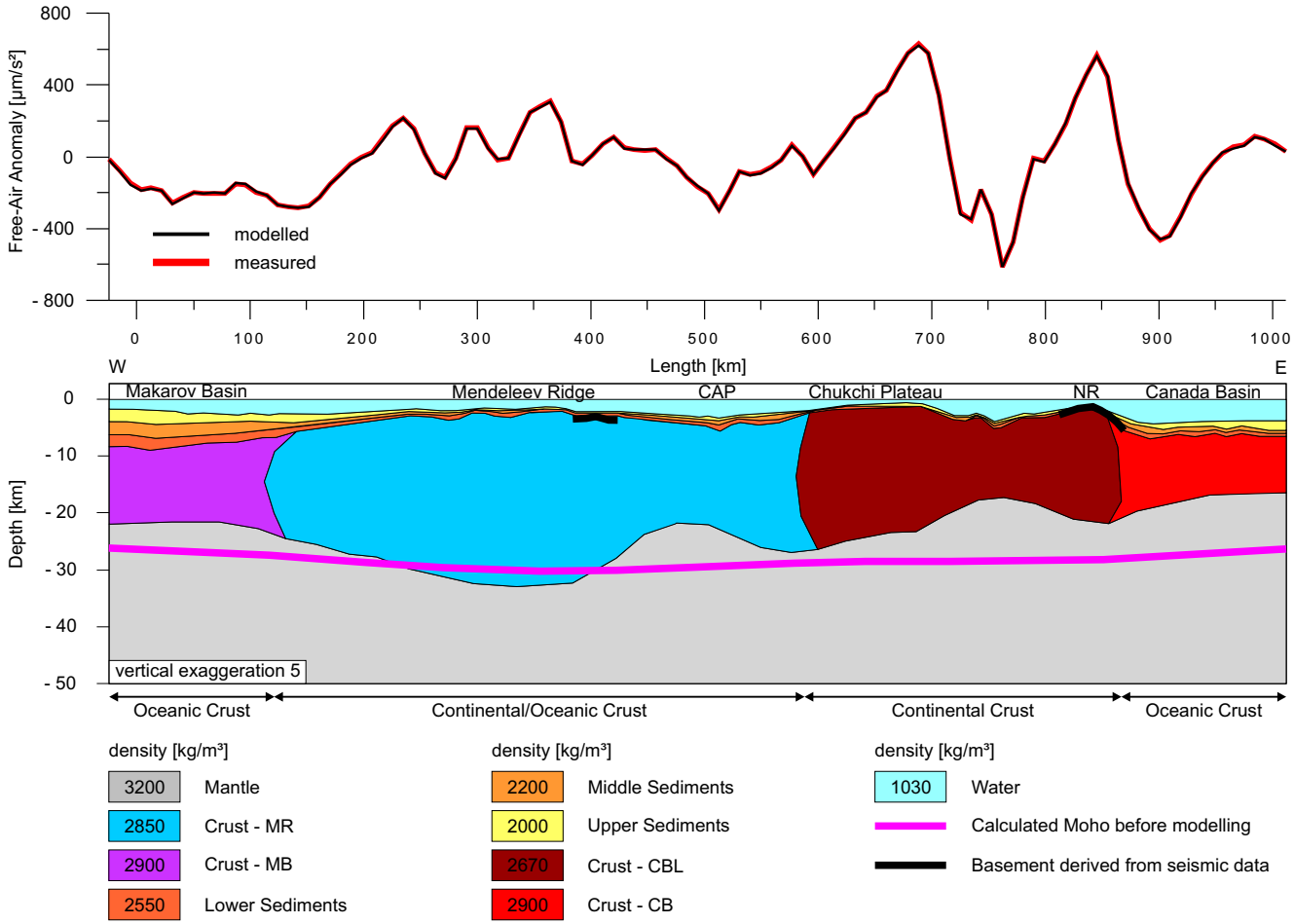

Figure 4.14: Section 19 crosses the Makarov Basin, the Mendeleev Ridge, the Chukchi Borderland and the Canada Basin. The calculated Moho depth (pink line) was evaluated before modelling (Chapter 4.3). The black lines show the locations of the basement, derived from the interpreted seismic reflection lines (Chapter 3.1.2, Fig. 3.3). For the location of this section see Figures 4.8 and 4.9. The accuracy of the modelling is shown in Figure 4.16C.

Table 4.4: Moho depths [km] resulting from the calculation using gravity inversion (Chapter 4.3), from the 3D gravity model (this Chapter) and from four gravity models published by: (A) Shaver & Hunkins (1964), (B) Hall (1990), (C) Sorokin et al. (1999), and (D) Alvey et al. (2008).

Geological Region	This Study		(A)	(B)	(C)	(D)
	calculated	modelled				
Chukchi Shelf	25 - 28	28 - 35	-	-	-	40
North Chukchi Basin	24 - 25	27 - 30	-	-	-	-
Canada Basin	26 - 28	15 - 18	-	13	-	18
Mendeleev Ridge	29 - 31	30 - 35	-	-	-	38
Makarov Basin	27 - 28	20 - 23	-	-	21 - 25	18
Chukchi Abyssal Plain	28 - 29	18 - 22	21	21	-	22
Chukchi Borderland	29 - 30	18 - 25	32	23 - 28	-	35

4.4.3 Residuals

Based on the measured free-air anomaly (ArcGP, Kenyon et al. 2008) and our modelled free-air anomaly, resulting from the 3D model, the residuals could be calculated. Therefore, the measured gravity values (Fig. 4.16A) were subtracted from the modelled gravity values (Fig. 4.16B). The residuals (Fig. 4.16C) range between -30 μm/s^2 and 30 μm/s^2, which is an excellent result relative to the size of the modelling area. However, in most regions of the gravity model the residuals are about $\pm$ 5 μm/s^2. The big discrepancies between the measured and the modelled free-air anomalies are concentrated at the eastern and western boundary of the model area (Fig. 4.16C). Therefore, these discrepancies might be boundary effects, resulting from the homogeneous model structure which surrounds the main model area. The well adaptation of the modelled gravity to the ArcGP data was possible because of less boundary conditions, consisting of our interpreted seismic reflection data as well as published values of the Moho depth,

the sedimentary and the crustal thickness (Chapters 4.2 and 4.3).
Furthermore, we calculated the discrepancies between the calculated (Fig. 4.17A; Chapter 4.2) and modelled basement depths (Fig. 4.17B). These residuals (Fig. 4.17C) vary between -5 km and 10 km. The biggest discrepancies are in the North Chukchi Basin and along the continental margin at the Makarov Basin. In the area of the North Chukchi Basin, the calculated basement depth is 10 km deeper than the modelled basement depth. Reason for this might be the unknown sediment densities in this deep basin. Therefore, our used sediment densities are eventually to low, which result in a more shallow modelled basement. However, the used input data for the calculation of the basement depth of the North Chukchi Basin were published by Drachev et al. (2010). These published depth values are only based on one cross-section derived from seismic reflection data and ERS-2 satellite gravity data. This one cross-section, however, is not representative for the entire North Chukchi Basin. Moreover, there are no further elaborations about the uncertainties regarding the modelled basement depth following Drachev et al. (2010).
Finally, the discrepancies between the calculated (Fig. 4.18A; Chapter 4.3) and modelled Moho depths (Fig. 4.18B) are shown in Figure 4.18C. These residuals vary between -8 km and 10 km. Especially for the Canada Basin, the Chukchi Borderland, the Chukchi Abyssal Plain and the Makarov Basin the modelled Moho depth is about 5 km to 10 km above the prior calculated Moho depth. Whereas, the modelled Moho depth of the Mendeleev Ridge and Chukchi Shelf is about 5 km below the calculated Moho depth. Reasons for these differences between the modelled and calculated Moho depths are the unknown accuracy of the calculated Moho depth (Chapter 4.3), and the existence of only a few published average Moho depth values for the study area, which were used as boundary conditions for the 3D modelling (Tab. 4.4).

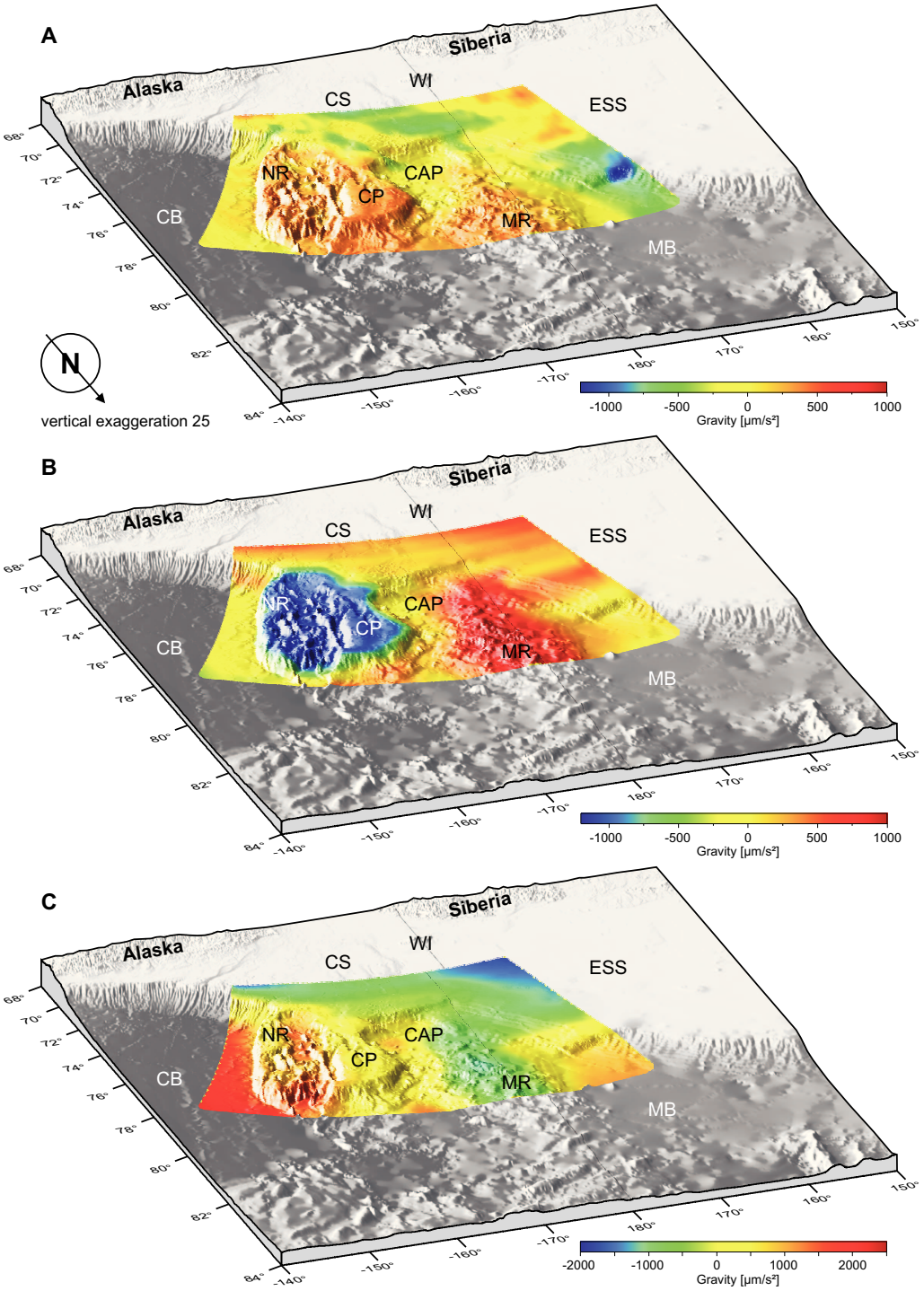

Figure 4.15: Bathymetric map (IBCAO, Jakobsson et al. 2008a) showing the gravity effects of (A) the sediments, (B) the crust, and (C) the mantle. The scales of Figure (A) and (B) are different from Figure (C).

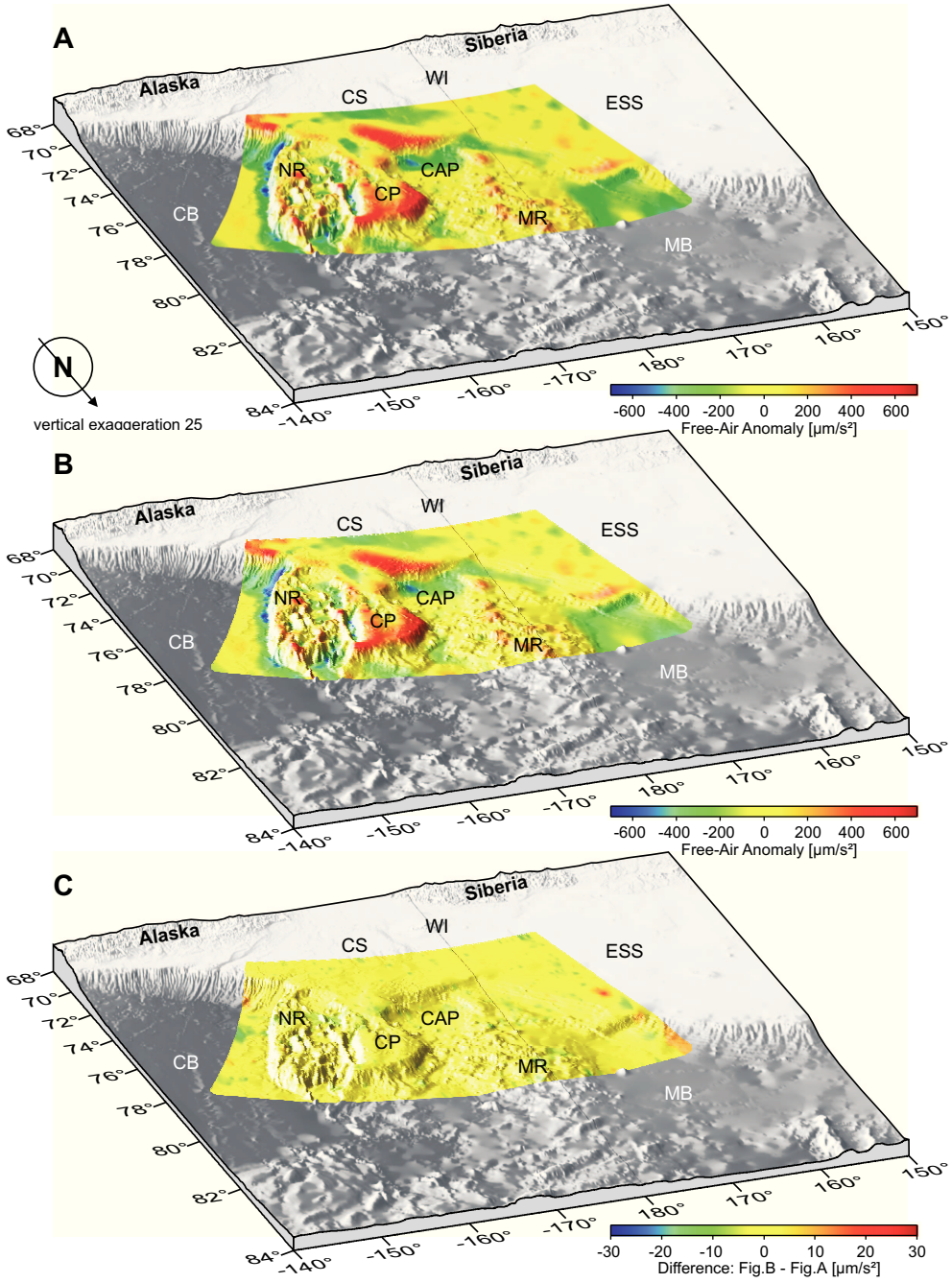

Figure 4.16: Bathymetric map (IBCAO, Jakobsson et al. 2008a) showing the free-air anomalies and the residuals. (A) The measured free-air anomaly of the ArcGP, (B) the modelled free-air anomaly resulting from the 3D gravity model, and (C) the residuals of the 3D gravity model (Fig.(B) - Fig.(A)). The scales of Figure (A) and (B) are different from Figure (C).

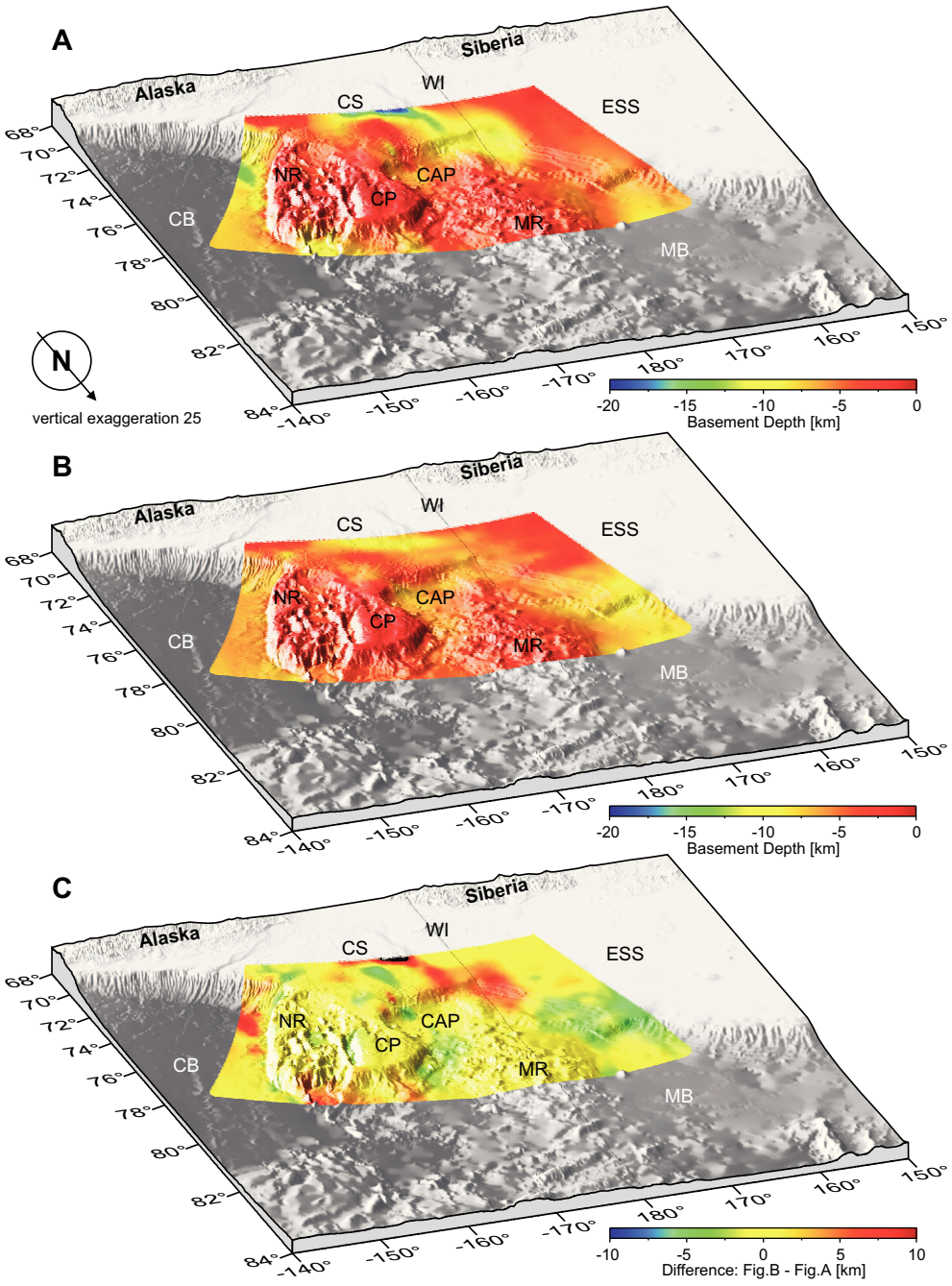

Figure 4.17: Bathymetric map (IBCAO, Jakobsson et al. 2008a) showing the basement depths and the residuals. (A) The calculated basement depth resulting from interpreted seismic reflection data (Chapter 4.2), (B) the modelled basement depth resulting from the 3D gravity model, and (C) the residuals between the modelled and the calculated basement depth (Fig.(B) - Fig.(A)). The scales of Figure (A) and (B) are different from Figure (C).

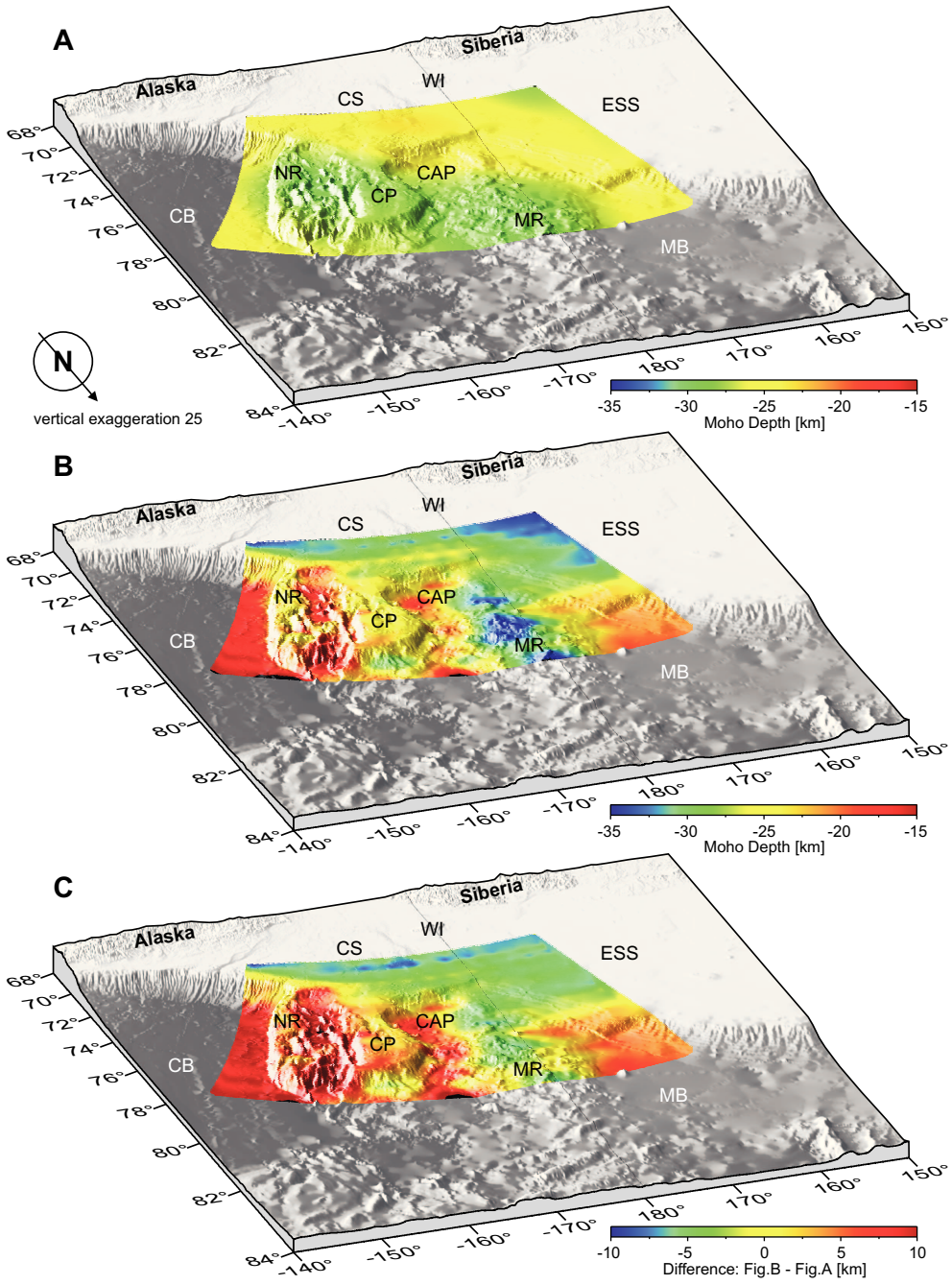

Figure 4.18: Bathymetric map (IBCAO, Jakobsson et al. 2008a) showing the Moho depths and the residuals. (A) Calculated Moho depth using gravity inversion (Chapter 4.3), (B) modelled Moho depth resulting from the 3D gravity model, and (C) residuals between the modelled and the calculated Moho depth (Fig.(B) - Fig.(A)). The scales of Figure (A) and (B) are different from Figure (C).

5 Models for the Origin of the Chukchi Region

The opening of the Arctic Ocean, especially the geologically older Amerasian Basin, remains controversial (Lawver & Scotese 1990, Lane 1997). This deep basin is almost certainly made of oceanic crust and is most likely Jurassic to Early Cretaceous in age (Baggeroer & Falconer 1982, Grantz & May 1982, Grantz et al. 1990). Four main oceanic rift models for the opening of the Amerasian Basin exist (Chapter 2.2, Figs. 2.3): (A) the counterclockwise rotation of the AACM from the Arctic Canada where the pole of rotation is located in the Mackenzie Delta (Grantz et al. 1979), (B) the simultaneously rotation of the AACM from the Arctic Canada and the Barents Shelf where two poles of rotation are located in the Mackenzie Delta and in the Laptev Sea (Miller et al. 2006), (C) the strike-slip model where the Lomonosov Ridge is an early spreading centre (Dutro 1981 and Miller & Verzhbitsky 2009), and (D) the strike-slip model where the AACM moved off the Arctic Canada (Herron et al. 1974). The Chukchi Borderland, however, is difficult to place in all these models. Following Grantz et al. (1998), the continental basement of the Chukchi Borderland is of Phanerozoic age, and the earliest syn-rift sediments recovered from the Northwind Ridge are of Early Jurassic time which correlates with the beginning of rifting in the Amerasian Basin (Chapter 2.2).

Focusing on our results from the interpreted seismic reflection data (Chapter 3.3) and the gravity modelling (Chapter 4.4.2), new statements can be made about the geological evolution of the Chukchi region and the southern part of the Mendeleev Ridge. The Chukchi Plateau evolved in an E-W directed extensional regime (Chapter 3.3.1) as well as the Chukchi Abyssal Plain (Chapter 3.3.2), the Northwind Ridge (Arrigoni 2008) and the Mendeleev Ridge (Chapter 3.3.3; Dove et al. 2010). Furthermore, the Chukchi Borderland consists of thinned continental crust (thickness of 20 km - 25 km) compared with the continental crust of the Chukchi Shelf (thickness 28 km - 35 km; Chapter 4.4.2, Fig. 4.12). Especially the continental crust of the graben system, in-between the Chukchi Plateau and the Northwind Ridge, has an average thickness of 18 km (Chapter 4.4.2, Fig. 4.13). The thinned crust might be the result of the men-

tioned E-W directed extension. In contrast, the Chukchi Abyssal Plain is underlain by an oceanic crust or a thinner extremity of the Mendeleev Ridge crust (Chapter 3.3.2 and Chapter 4.4.2, Fig. 4.13). However, based on our results (Chapters 3.3.3 and 4.4.2), a clear identification of the Mendeleev Ridge as an oceanic plateau (Fig. 5.1A), like firstly described by Hall (1970), or as a rifted volcanic continental margin (Fig. 5.1B), as suggested by Lebedeva-Ivanova et al. (2006), is not possible.

Regarding the sediment cover in the study area and our dated sediment horizons (Chapter 2.3, Fig. 2.5), the ages of the geological provinces and their tectonic active period can be estimated. Therefore, the Chukchi Abyssal Plain is covered by Cretaceous and Cenozoic sediments. The geologically oldest horizon which could be dated is the Lower Cretaceous unconformity (LCU; Chapter 3.3.2, Fig. 3.14). Based on the LCU horizon, we suggest that the Chukchi Abyssal Plain evolved while the deposition of this horizon. Furthermore, the eastern part of the Chukchi Abyssal Plain, next to the Chukchi Plateau, is the geologically oldest part, since the LCU is not effected by basement faulting (Chapter 3.3.2, Fig. 3.14). In west direction, next to the Mendeleev Ridge, the Chukchi Abyssal Plain becomes younger, because the LCU is effected by basement faulting. The abyssal gap, northern part of the Chukchi Abyssal Plain, is the geologically youngest part of this province, because the LCU does not exist and the Mid Brookian unconformity is effected by basement faulting. The observations indicate that the Chukchi Plateau moved to its recent position during the opening of the Amerasian Basin. For this movement two possibilities exist: (1) the clockwise rotation of the Chukchi Borderland from the Eurasian continental margin (Fig. 5.1C), firstly described by Grantz & Hart (2006), or (2) the movement from west to east (Fig. 5.1D), like suggested by Miller & Verzhbitsky (2009). Furthermore, the Chukchi Plateau and the Mendeleev Ridge are covered by Cenozoic sediments (Chapter 3.3.1, Fig. 3.11 and Chapter 3.3.3, Fig. 3.17). In both provinces, the Mid Brookian unconformity is the geologically oldest horizon. On the Mendeleev Ridge, the Mid Brookian unconformity is highly faulted with the basement (Chapter 3.3.3, Fig. 3.17). This leads to the conclusion that the Mendeleev Ridge evolved in the Late Cretaceous, like proposed by

Weber & Sweeney (1990), Jokat (2003) and Verzhbitsky et al. (2011), and was still tectonically active until the Early Tertiary. Finally, the absence of older sediments on the Chukchi Plateau must be the result of heavy erosion of the Cretaceous sediments in this province (Chapter 3.3.1, Fig. 3.11).

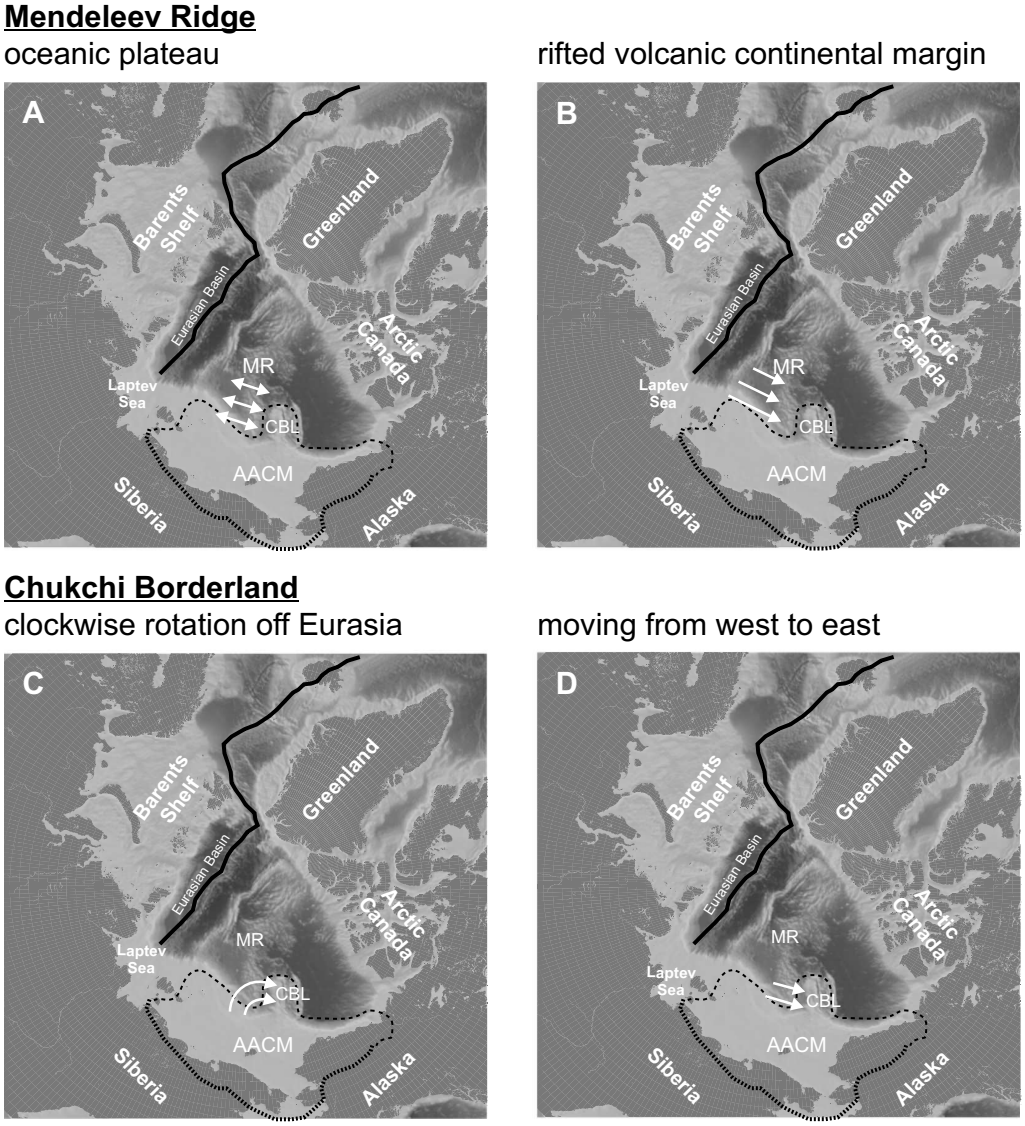

Figure 5.1: Bathymetric map (IBCAO, Jakobsson et al. 2008a) showing the two evolution models for the Mendeleev Ridge and the Chukchi Borderland, based on our results and published interpretations proposed by different authors (for further information see text; modified after Miller et al. 2010). The black line marks the recent oceanic spreading centre of the North Atlantic mid-ocean ridge and the Gakkel Ridge in the Eurasian Basin.

Discussing the probability of the four main oceanic rift models for the opening of the Amerasian Basin (Chapter 2.2, Figs. 2.3A-D), based on our results and the mentioned publications above, only two of these models are possible (models A and C; Chapter 2.2, Figs. 2.3A, C). The models B and D (Chapter 2.2, Figs. 2.3B, D) do not work in combination with our interpretations, since these models can not explain the E-W directed extension, which was identified in the Chukchi Borderland, the Chukchi Abyssal Plain and the Mendeleev Ridge. In this regard, models A and C work within some limitations. Model A (Chapter 2.2, Fig. 2.3A; Grantz et al. 1979): during the counterclockwise rotation of the AACM from the Arctic Canada, the Chukchi Borderland rotated clockwise or moved from west to east to its recent position. But, based on these movements we would expect a compression front in east direction of the Northwind Ridge. No signs of tectonic inversion have been reported in this area of the Canada Basin (Hutchinson et al. 2009). However, the opening of the Amerasian basin is probably more complex and still not well understood. Model C (Chapter 2.2, Fig. 2.3C; Dutro 1981 and Miller & Verzhbitsky 2009): this strike-slip model shows a NW-SE directed extensional regime during the opening of the Amerasian Basin. If the transform fault along the south-western boundary of the AACM would be more located in E-W direction, the model would work well with the E-W directed extension which was observed in the Chukchi Borderland, the Chukchi Abyssal Plain and the Mendeleev Ridge. In both models, the Mendeleev Ridge would evolve after the opening of the Amerasian Basin (Weber & Sweeney 1990, Jokat 2003 and Verzhbitsky et al. 2011) as an oceanic plateau (Hall 1970) or as a rifted volcanic continental margin (Lebedeva-Ivanova et al. 2006).

In addition, based on our investigations new statements can also be made about the geologically younger evolution of the Arctic Ocean. In the period ranging from the Eocene/Oligocene boundary to the opening of the Fram Strait in the Early Miocene (Engen et al. 2008), the Arctic Ocean was an isolated basin with a higher relative sea level compared with the global oceans at that time (Chapter 3.5.2, Fig. 3.26). Furthermore, the sediments on the Chukchi Plateau are effected by basement faulting

at least until the Pliocene which shows a more or less recent tectonic activity in this region (Chapter 3.3.1, Fig. 3.12). More recently, various indications for glaciation on the Chukchi Plateau are corresponding to published data about an ice covered Chukchi Borderland in the Quaternary by Jakobsson et al. (2008b).

6 Conclusion and Discussion

The main focus of this thesis was the processing and interpretation of the multi channel seismic lines as well as the wide-angle reflection and refraction data from the Chukchi region and the southern part of the Mendeleev Ridge, Arctic Ocean. The used data were acquired by the Alfred Wegener Institute (AWI) during the ARK-XXIII/3 expedition in 2008 (Jokat et al. 2009). In addition, three other data sets were available and important for the final interpretation: (1) a considerable amount of seismic reflection lines from the Chukchi Shelf, the Northwind Ridge and the northern part of the Mendeleev Ridge, acquired from different institutes and companies (Chapter 3.1.2, Fig. 3.3), (2) various logging information from five exploration wells, drilled on the Chukchi Shelf near the coast of Alaska (Chapter 3.1.2, Fig. 3.3; Sherwood et al. 2002), and (3) public-domain gravity data (ArcGP) of the entire Arctic Ocean (Chapter 4.1, Fig. 4.1; Kenyon et al. 2008).

Summarising our results, the dating of sediment horizons in the Chukchi region was possible, using the age information from five exploration wells (Chapter 3.1.2, Fig. 3.5; Sherwood et al. 2002). The interpretation of the seismic lines gave an overview about the tectonic activity and the age of evolution of the three provinces in the study area (Chukchi Plateau, Chukchi Abyssal Plain, Mendeleev Ridge; Chapter 3.3). Furthermore, the interpretation of the prograding sediment horizons on the Chukchi Shelf made it possible to reconstruct the relative sea level variations in the Chukchi region since the Late Eocene (Chapter 3.5.2, Fig. 3.26). On the other hand, to gain more information about the crustal structures and the topography of the Moho, a complex 3D gravity model of the Chukchi region and adjacent areas was developed. Using all results, two tectonic models for the origin of the Chukchi Borderland and the Mendeleev Ridge were presented (Chapter 5, Fig. 5.1). Finally, these models led to the conclusion about the tectonic evolution of the Amerasian Basin, Arctic Ocean (Chapter 5).

The following discussion focuses on the key statements concerning our results from the Chukchi region and the Mendeleev Ridge, presented in this thesis.

Are the sediment horizon ages from the five exploration wells representative for the study area?

The five exploration wells, drilled on the Chukchi Shelf near the coast of Alaska, are located more than 200 km southeast of the AWI MCS lines (Chapter 3.1.2, Fig. 3.5; Sherwood et al. 2002). Furthermore, between the southern seismic network, consisting of a large amount of additional seismic reflection lines, and the AWI seismic network a "data gap" of about 70 km exists (Chapter 3.1.2, Fig. 3.5). However, as shown in Chapter 3.4, Figure 3.22, the sediments which cover the Chukchi Shelf and the northern Chukchi region originated from the north-western Alaska and north-eastern Siberia hinterland as well as from the region of the Bering Strait before its opening at the end of the Miocene (Gladenkov et al. 2002). Therefore, the sediments were transported from the source area to the northern Chukchi region over a distance of more than 400 km (Chapter 3.4, Fig. 3.22). Concerning the seismic data, the dated marker horizons were followed trough the southern seismic network up to the north. Based on the multiple crossing points of the seismic reflection lines it was possible to identify the marker horizons with a high accuracy in the southern seismic network. Over the "data gap" of about 70 km, the marker horizons were extrapolated from the southern network into the AWI MCS lines, using seismic interval velocities of the sediments as well as reflection characteristics of the seismic reflectors (Chapter 3.1.2, Fig. 3.4). The identification of the marker horizons in the AWI MCS lines were done with the help of the seismic interval velocities (Chapter 3.2, Fig. 3.9), the interpreted prograding sequences on the northern Chukchi Shelf (Chapter 3.5.1, Fig. 3.25) and the reflection characteristics of the seismic reflectors (Chapter 3.3). Finally, our resulting interpretations, concerning the ages of tectonic events and the ages of the evolution of the Chukchi Borderland and the Mendeleev Ridge correspond to published data assumed by different authors (Chapter 5). Therefore, we propose that the dated horizons - using the logging information from the five exploration wells - present the best age control for the sediments in the northern Chukchi region and the southern part of the Mendeleev Ridge.

Can our reconstructed relative sea level variations of the Chukchi region since the Late Eocene be assigned for the entire Arctic Ocean?

The relative sea level variations (RSL) in the Chukchi region were reconstructed by means of interpreting the prograding sediment horizons on the northern Chukchi Shelf (Chapter 3.5.2, Fig. 3.26). These Chukchi RSL variations can be generalised for the entire Arctic Ocean, since Eocene-Oligocene age unconformities reported in sediments on the East Siberian Shelf (Sekretov 2001), the Laptev Shelf (Franke & Hinz 2005) and the Mackenzie Delta (Dixon et al. 1992) correlate with the RSL lowering events observed in the Chukchi curve. Moreover, no local tectonic events are known in the Chukchi region since the Late Eocene, and the sediment influx was not influenced by e.g. large river systems, based on the low minimum sedimentation rates between 2 cm/ky and 5 cm/ky (Chapter 3.5.2, Fig. 3.26). Finally, geochemical analyses at the IODP core from the ACEX expedition 302 to the central Lomonosov Ridge (Jakobsson et al. 2007) led to the interpretation that the Arctic Ocean was predominantly isolated after the closure of gateways in the Eocene until the opening of the Fram Strait in the Early Miocene (O'Regan et al. 2008). In this period, large volumes of fresh water were discharged from Canadian, Alaskan and Siberian rivers into the landlocked Arctic Ocean, which reduced the salinity of the Arctic surface water masses (Jakobsson et al. 2007). In the Early Miocene, the sediments accumulated on the central Lomonosov Ridge show erosion, redeposition of older sediment, and deposition of new sediment in a shallow water regime (März et al. 2011, Jakobsson et al. 2007) which correlates with our considerable RSL lowering at this time. Based on these facts, we applied our Chukchi RSL curve for the Arctic Ocean. Therefore, we suggest an isolated Arctic Ocean from the Eocene/Oligocene boundary to the Early Miocene (Chapter 3.5.2, Fig. 3.26). In addition, we conclude that the RSL in the isolated Arctic basin was higher than in the global oceans. With the opening of the Fram Strait, the Arctic Ocean water flowed into the Atlantic Ocean, and increased the absolute sea level, observed on the New Jersey Costal Plain (Kominz et al. 2008).

Are the results of the 3D gravity model a sufficient estimation for the crustal and mantle parameters in the study area due to the ambiguity of this method?

The modelling of potential field data (e.g. gravity, magnetics) bases on the principles of equivalence. Therefore, measured potential field data can be explained by multiple underground models. In our modelling area - Chukchi region and southern part of the Mendeleev Ridge - several boundary conditions exist which reduce the ambiguity of our 3D gravity model. Using our interpreted seismic reflection data and basement depth values published by Jackson et al. (1990) and Drachev et al. (2010), the basement depth as well as the sedimentary thickness could be calculated for the study area (Chapter 4.2, Figs. 4.3 and 4.4). Furthermore, the Moho depth was calculated (Chapter 4.3, Fig. 4.7) and verified with Moho depth values published by Shaver & Hunkins (1964), Hall (1990), Sorokin et al. (1999) and Alvey et al. (2008). Finally, the sediment densities were received from the bulk density logs of the five exploration wells (Chapter 4.4.1, Tab. 4.2). Based on all the boundary conditions we propose that our 3D gravity model is a sufficient estimation for the crustal and mantle parameters in the modelling area.

The suggested tectonic models, describing the origin of the Chukchi Borderland and the Mendeleev Ridge, are they realistic?

The results of the seismic data interpretation and the gravity data modelling support two tectonic models for the origin of the Chukchi Borderland and the Mendeleev Ridge. Therefore, the Chukchi Borderland rotated clockwise from the Eurasian continental margin (Chapter 5, Fig. 5.1C; Grantz & Hart 2006) or moved from west to east to its recent position (Chapter 5, Fig. 5.1D; Miller & Verzhbitsky 2009). The Mendeleev Ridge evolved as an oceanic plateau (Chapter 5, Fig. 5.1A; Hall 1970) or as a rifted volcanic continental margin (Chapter 5, Fig. 5.1B; Lebedeva-Ivanova et al.

2006). These models correspond to our observations and interpretations of the seismic and gravity data. Therefore, we propose that the tectonic models are still the best description for the origin of the Chukchi Borderland and the Mendeleev Ridge. Concerning the opening of the Amerasian Basin, two already existing oceanic rift models are matching our results within some limitations (Chapter 2.2, Figs. 2.3A, C): (1) the counterclockwise rotation of the AACM from the Arctic Canada where the pole of rotation is located in the Mackenzie Delta (Grantz et al. 1979) and a clockwise rotation or a W-E movement of the Chukchi Borderland occurred at the same time, and (2) the strike-slip model with the Lomonosov Ridge as an early spreading centre (Dutro 1981, Miller & Verzhbitsky 2009) where the NW-SE strike-slip direction has to change to an E-W direction (Chapter 5). However, no seismic data were available from the Canada Basin or the Makarov Basin for this thesis to further include this areas into our interpretations. Therefore, our proposed changes in the two already existing oceanic rift models remain theoretical.

7 Outlook

This thesis includes the interpretations of the first seismic reflection data and 3D gravity model from the Chukchi Plateau, the Chukchi Abyssal Plain, the northern Chukchi Shelf as well as the southern part of the Mendeleev Ridge. Based on our results many questions, concerning the local to global scale, remain open and offering potential for further investigations.

Within local scale, the cause for the tectonic activity of the Mendeleev Ridge until the Top Oligocene, shown by many faults in the sediment cover above the ridge (Chapter 3.3.4, Fig. 3.21), is still unknown as well as the significant relocation of the Chukchi Shelf margin next to the Mendeleev Ridge in the Late Oligocene. Therefore, the interpretation of further seismic reflection data from the Makarov Basin and the East Siberian Shelf (acquired by several Russian cruises, WesternGeco, TGS-NOPEC and BGR) might provide further information about the extension and the cause of the tectonic event in the Late Oligocene.

Regarding the regional scale, we favourite two tectonic models for the origin of the Chukchi Borderland (Chapter 5, Figs. 5.1C-D). The interpretation of seismic reflection lines from the Canada Basin, especially east and northeast of the Northwind Ridge, could help to decide which of the models is more realistic. Furthermore, the comparison of the sediment and crustal structures as well as the Moho depth of the Mendeleev Ridge, the Makarov Basin and the Lomonosov Ridge, using seismic data and gravity modelling, maybe lead to conclusions about the origin of these three provinces. These results would also be important for the development of a final oceanic rift model for the opening of the Amerasian Basin.

Concerning the global scale, the continuing of the reconstruction of the relative sea level variations from different seismic lines in the entire Arctic Ocean would allow the elimination of local effects, e.g. variations in the sediment influx or local tectonic events. Several prograding sediment horizons were observed by Houseknecht et al. (2009) on the shelf of the Beaufort Sea, and by Sekretov (2001) on the East Siberian Shelf. How-

ever, a relative sea level curve was not reconstructed. Further relative sea level curves from different locations in the Arctic Ocean would improve the quality of the amplitude values of our Chukchi relative sea level curve (Chapter 3.5.2, Fig. 3.26). The comparison of different relative sea level curves would also provide important paleoenvironmental conditions within the Arctic Ocean such as ocean currents, sediment influx, tectonic events, erosion events as well as the influence of the Arctic Ocean on the global Earth system (e.g. quantity of the fresh water influx into the global oceans with the opening of the Fram Strait, extension of ice sheets in geologically younger time (Quaternary) by detection of ice erosion in the shelf sediments which surround the Arctic Basins).

8 References

Alvey, A., Gaina, C., Kusznir, N. J. & Torsvik, T. H. Integrated crustal thickness mapping and plate reconstructions for the high Arctic. *Earth and Planetary Science Letters* **274**, 310-321 (2008), doi:10.1016/j.epsl.2008.07.036.

Arrigoni, V. Origin and Evolution of the Chukchi Borderland. *Master Thesis*, pp. 74 (2008), Texas A&M University, http://hdl.handle.net/1969.1/ETD-TAMU-2008-12-120.

Baggeroer, A. B. & Falconer, R. Array Refraction Profiles and Crustal Models of the Canada Basin. *Journal of Geophysical Research* **87**, 5461-5476 (1982), doi:10.1029/JB087iB07p05461.

Braitenberg, C., Zadro, M., Fang, J., Wang, Y. & Hsu, H. T. Gravity Inversion in Qinghai-Tibet Plateau. *Physics and Chemistry of the Earth, Part A* **25**, 381-386 (2000a), doi:10.1016/S1464-1895(00)00060-0.

Braitenberg, C., Zadro, M., Fang, J., Wang, Y. & Hsu, H. T. The gravity and isostatic Moho undulations in Qinghai-Tibet plateau. *Journal of Geodynamics* **30**, 489-505 (2000b), doi:10.1016/S0264-3707(00)00004-1.

Brinkhuis, H., Schouten, S., Collinson, M. E., Sluijs, A., Sinninghe Damsté, J. S., Dickens, G. R., Huber, M., Cronin, T. M., Onodera, J., Takahashi, K., Bujak, J. P., Stein, R., van der Burgh, J., Eldrett, J. S., Harding, I. C., Lotter, A. F., Sangiorgi, F., van Konijnenburg-van Cittert, H., de Leeuw, J. W., Matthiessen, J., Backman, J., Moran, K. & the Expedition 302 Scientists. Episodic fresh surface waters in the Eocene Arctic Ocean. *Nature* **441**, 606-609 (2006), doi:10.1038/nature04692.

Brozena, J. M., Peters, M. F. & Salman, R. Arctic airborne gravity measurement program. In *Gravity, Geoid and Marine Geodesy, International Association of Geodesy Symposia* **Vol. 117** (eds Segawa, J., Fujimoto, H. & Okubo, S.), 131-139 (1997), Springer, New York, ISBN:9783540633525.

Bruvoll, V., Kristoffersen, Y., Coakley, B. J. & Hopper, J. R. Hemipelagic deposits on the Mendeleev and northwestern Alpha submarine Ridges in the Arctic Ocean: acoustic stratigraphy, depositional environment and an inter-ridge correlation calibrated by the ACEX results. *Marine Geophysical Research* **31**, 149-171 (2010), doi:10.1007/s11001-010-9094-9.

Catuneanu, O. Principles of sequence stratigraphy. pp. 375 (2006), Elsevier Science, Heidelberg, ISBN:9780444515681.

Chalmers, J. A., Pulvertaft, T. C. R., Christiansen, F. G., Larsen, H.C., Laursen, K. H. & Ottesen, T. G. The southern West Greenland continental margin: rifting history, basin development, and petroleum potential. *Petroleum Geology Conference series* **4**, 915-931 (1993), doi:10.1144/0040915.

Craig, J. D., Sherwood, K. W. & Johnson, P. P. Geologic Report for the Beaufort Sea Planning Area, Alaska: Regional Geology, Petroleum Geology, Environmental Geology. *OCS Report MMS 85-0111*, pp. 192 (1986), U.S. Department of the Interior, Minerals Management Service, Anchorage, ID:102-594-068.

Darby, D. A., Jakobsson, M. & Polyak, L. Icebreaker Expedition Collects Key Arctic Seafloor and Ice Data. *Eos, Transactions, American Geophysical Union* **86**, 549-556 (2005), doi:10.1029/2005EO520001.

Dinkelman, M. G., Kumar, N., Helwig, J. A., Emmet, P. A. & Granath, J. W. Highlights of Petroleum and Crustal Framework of the US Chukchi Shelf: Key Results from the ChukchiSPAN Survey. *CSEG Recorder* **33**, 35-43 (2008).

Dixon, J., Dietrich, J. R. & McNeil, D. H. Upper cretaceous to pleistocene sequence stratigraphy of the Beaufort - Mackenzie and Banks Island areas, Northwest Canada. *Geological Survey of Canada, Bulletin* **407**, pp.90 (1992), ISBN:0660138468.

Dove, D., Coakley, B., Hopper, J., Kristoffersen, Y. & HLY0503 Geophysics Team. Bathymetry, controlled source seismic and gravity observations of the Mendeleev

ridge; implications for ridge structure, origin, and regional tectonics. *Geophysical Journal International* **183**, 481-502 (2010), doi:10.1111/j.1365-246X.2010.04746.x.

Drachev, S. S., Malyshev, N. A. & Nikishin, A. M. Tectonic history and petroleum geology of the Russian Arctic Shelves: an overview. *Petroleum Geology Conference series* **7**, 591-619 (2010), doi:10.1144/0070591.

Dutro, J. T., Jr. Geology of Alaska bordering the Arctic Ocean. In *The ocean basins and margins: The Arctic Ocean* **5** (eds Nairn, A. E. M., Churkin, M. & Stehli, F. G.), 21-36 (1981), Plenum Press, New York, ISBN:0306377756.

Ebbing, J., Braitenberg, C., & Wienecke, S. Insights into the lithospheric structure and tectonic setting of the Barents Sea region from isostatic considerations. *Geophysical Journal International* **171**, 1390-1403 (2007), doi:10.1111/j.1365-246X.2007.03602.x.

Edwards, M. H. & Coakley, B. J. SCICEX Investigations of the Arctic Ocean System. *Chemie der Erde - Geochemistry* **63**, 281-328 (2003), doi:10.1078/0009-2819-00039.

Eldrett, J. S., Harding, I. C., Wilson, P. A., Butler, E. & Roberts, A. P. Continental ice in Greenland during the Eocene and Oligocene. *Nature* **446**, 176-179 (2007), doi:10.1038/nature05591.

Embry, A. F. Geological and Geophysical Evidence in Support of the Hypothesis of Anticlockwise Rotation of Northern Alaska. *Marine Geology* **93**, 317-329 (1990), doi:10.1016/0025-3227(90)90090-7.

Engen, Ø., Faleide, J. I. & Dyreng, T. K. Opening of the Fram Strait gateway: A review of plate tectonic constraints. *Tectonophysics* **450**, 51-69 (2008), doi:10.1016/j.tecto.2008.01.002.

Forsberg, R., Olesen, A. V. & Keller, K. Airborne gravity survey of the North Greenland continental shelf. In *Gravity, Geoid and Geodynamics 2000, International Association of Geodesy Symposia* **123** (ed Sideris, M. G.), 235-240 (2002), Springer, New York, ISBN:9783540424697.

Forsberg, R. & Kenyon, S. Gravity and Geoid in the Arctic Region - The Northern Polar Gap now Filled. In *GOCE, The Geoid and Oceanography, Proceedings of the Second International GOCE User Workshop, ESA SP-569* (ed Lacoste, H.), pp. 5 (2004), ESA Publication Division, Netherlands, ISBN:9290928808.

Forsberg, R. & Skourup, H. Arctic Ocean gravity, geoid and sea-ice freeboard heights from ICESat and GRACE. *Geophysical Research Letters* **32**, pp. 4 (2005), doi:10.1029/2005GL023711.

Forsyth, D. A., Morel-A-L'Huissier, P., Asudeh, I. & Green, A. Alpha ridge and Iceland-products of the same plume? *Journal of Geodynamics* **6**, 197-214 (1986), doi:10.1016/0264-3707(86)90039-6.

Franke, D. & Hinz, K. The structural style of sedimentary basins on the shelves of the Laptev Sea and western East Siberian Sea, Siberian Arctic. *Journal of Petroleum Geology* **28**, 49-66 (2005), doi:10.1111/j.1747-5457.2005.tb00083.x.

Gibbard, P. L., Head, M. J., Walker, M. J. C. & the Subcommission on Quaternary Stratigraphy. Formal ratification of the Quaternary System/Period and the Pleistocene Series/Epoch with a base at 2.58 Ma. *Journal of Quaternary Science* **25**, 96-102 (2010), doi:10.1002/jqs.1338.

Gladenkov, A. Y., Oleinik, A. E., Marincovich, L., Jr. & Barinov, K. B. A refined age for the earliest opening of Bering Strait. *Palaeogeography, Palaeoclimatology, Palaeoecology* **183**, 321-328 (2002), doi:10.1016/S0031-0182(02)00249-3.

Götze, H.-J. Ein numerisches Verfahren zur Berechnung der gravimetrischen Feldgrößen dreidimensionaler Modellkörper. *Archiv für Meteorologie, Geophysik und Bioklimatologie, Serie A* **27**, 195-215 (1978), doi:10.1007/BF02246695.

Götze, H.-J. & Lahmeyer, B. Application of three-dimensional interactive modeling in gravity and magnetics. *Geophysics* **53**, 1096 - 1108 (1988), doi:10.1190/1.1442546.

Grantz, A., Eittreim, S. & Dinter, D. A. Geology and tectonic development of the continental margin of Alaska. *Tectonophysics* **59**, 263-291 (1979), doi:10.1016/0040-1951(79)90050-7.

Grantz, A. & May, S. D. Rifting history and structural development of the continental margin north of Alaska. In *Studies in continental margin geology, American Association of Petroleum Geologists Special Volumes* **34** (eds Watkins, J. S. & Drake, C. L.), 77-100 (1982), American Association of Petroleum Geologists, Tulsa/Oklahoma, ISBN:0891813110.

Grantz, A., May, S. D., Taylor, P. T. & Lawver, L. A. The Canada Basin. In *The Arctic Ocean Region, The Geology of North America, Vol.* **L** (eds Grantz, A., Johnson, L. & Sweeney, J. F.), 379-402 (1990), The Geological Society of America, Boulder/Colorado, ISBN:0813752116.

Grantz, A., Clark, D. L., Phillips, R. L., Srivastava, S. P., Blome, C. D., Gray, L. B., Haga, H., Mamet, B. L., McIntyre, D. J., McNeil, D. H., Mickey, M. B., Mullen, M. W., Murchey, B. I., Ross, C. A., Stevens, C. H., Silberling, N. J., Wall, J. H. & Willard, D. A. Phanerozoic stratigraphy of Northwind Ridge, magnetic anomalies in the Canada basin, and the geometry and timing of rifting in the Amerasia basin, Arctic Ocean. *Geological Society of America Bulletin* **110**, 801-820 (1998), doi:10.1130/0016-7606(1998)110<0801:PSONRM>2.3.CO;2.

Grantz, A., Hart, P. E. & May, S. D. Seismic reflection and refraction data acquired in Canada Basin, Northwind Ridge and Northwind Basin, Arctic Ocean in 1988, 1992 and 1993. *U.S. Geological Survey Open-File Report* **2004-1243**, pp. 33 (2004), http://pubs.usgs.gov/of/2004/1243/index.html.

Grantz, A. & Hart, P. E. Geophysical and geological evidence that Amerasia Basin, Arctic Ocean was created by two phases of anti-clockwise rotation. *Geological Society of America Abstracts with Programs* **38(5)**, pp. 1 (2006).

Grantz, A., Scott, R. A., Drachev, S. S., Moore, T. E. & Valin, Z. C. Sedimentary successions of the Arctic Region (58–64° to 90°N) that may be prospective for hydrocarbons. In *Arctic Petroleum Geology, Memoirs* **35** (eds Spencer, A. M., Embry, A. F., Gautier, D. L., Stoupakova, A. V. & Sørensen, K.), 17-37 (2011), The Geological Society of London, ISBN:1862393281.

Hall, J. K. Arctic Ocean Geophysical Studies: The Alpha Cordillera and Mendeleyev Ridge, *PhD Thesis*, pp. 140 (1970), Columbia University New York, Accession No.: AD0715656.

Hall, J. K. Chukchi Borderland. In *The Arctic Ocean Region, The Geology of North America, Vol.* **L** (eds Grantz, A., Johnson, L. & Sweeney, J. F.), 337-350 (1990), The Geological Society of America, Boulder/Colorado, ISBN:0813752116.

Hegewald, A. & Jokat, W. Relative sea level variations in the Chukchi Region - Arctic Ocean - since the Late Eocene. (2012; in review).

Herron, E. M., Dewey, J. F. & Pitman, W. C., III. Plate Tectonics Model for the Evolution of the Arctic. *Geology* **2**, 377-380 (1974), doi:10.1130/0091-7613(1974)2<377:PTMFTE>2.0.CO;2.

Hou, Z., Sket, B., Fišer, C. & Li, S. Eocene habitat shift from saline to freshwater promoted Tethyan amphipod diversification. *Proceedings of the National Academy of Sciences of the United States of America* **108**, 14533-14538 (2011), doi:10.1073/pnas.1104636108.

Houseknecht, D. W., Bird, K. J. & Schenk, C. J. Seismic analysis of clinoform depositional sequences and shelf-margin trajectories in Lower Cretaceous (Albian) strata, Alaska North Slope. *Basin Research* **21**, 644-654 (2009), doi:10.1111/j.1365-2117.2008.00392.x.

Houseknecht, D. W. & Bird, K. J. Geology and petroleum potential of the rifted margins of the Canada Basin. In *Arctic Petroleum Geology, Memoirs* **35** (eds Spencer,

A. M., Embry, A. F., Gautier, D. L., Stoupakova, A. V. & Sørensen, K.), 509-526 (2011), The Geological Society of London, ISBN:1862393281.

Hutchinson, D. R., Jackson, H. R., Shimeld, J. W., Chapman, C. B., Childs, J. R., Funck, T. & Rowland, R. W. Acquiring Marine Data in the Canada Basin, Arctic Ocean. *Eos, Transactions, American Geophysical Union* **90**, 197-204 (2009), doi:10.1029/2009EO230001.

Jackson, H. R., Forsyth, D. A., Hall, J. K. & Overton, A. Seismic reflection and refraction. In *The Arctic Ocean region, The Geology of North America, Vol.* **L** (eds Grantz, A., Johnson, L. & Sweeney, J. F.), 153-170 (1990), The Geological Society of America, Boulder/Colorado, ISBN:0813752116.

Jakobsson, M., Backman, J., Rudels, B., Nycander, J., Frank, M., Mayer, L., Jokat, W., Sangiorgi, F., O'Regan, M., Brinkhuis, H., King, J. & Moran, K. The early Miocene onset of a ventilated circulation regime in the Arctic Ocean. *Nature* **447**, 986-990 (2007), doi:10.1038/nature05924.

Jakobsson, M., Macnab, R., Mayer, L., Anderson, R., Edwards, M., Hatzky, J., Schenke, H. W. & Johnson, P. An improved bathymetric portrayal of the Arctic Ocean: Implications for ocean modeling and geological, geophysical and oceanographic analyses. *Geophysical Research Letters* **35**, pp. 5 (2008a), doi:10.1029/2008GL033520.

Jakobsson, M., Polyak, L., Edwards, M., Kleman, J. & Coakley, B. Glacial geomorphology of the Central Arctic Ocean: the Chukchi Borderland and the Lomonosov Ridge. *Earth Surface Processes and Landforms* **33**, 526-545 (2008b), doi:10.1002/esp.1667.

Jokat, W. Seismic investigations along the western sector of Alpha Ridge, Central Arctic Ocean. *Geophysical Journal International* **152**, 185-201 (2003), doi:10.1046/j.1365-246X.2003.01839.x.

Jokat, W., Hegewald, A., Kahlberg, T., Kollofrath, J., Kessling, S., Martens, H., Pulm, P., Urlaub, M. & Winter, F. Marine Geophysics. In *The expedition of the research*

vessel "Polarstern" to the Arctic in 2008 (ARK-XXIII/3), Berichte zur Polar- und Meeresforschung (Reports on Polar and Marine Research) **597** (eds Jokat, W. & the participants), 87-94 (2009), Alfred Wegener Institute for Polar and Marine Research, Bremerhaven, hdl:10013/epic.33317.d001.

Kenyon, S., Forsberg, R. & Coakley, B. New Gravity Field for the Arctic. *EOS Transactions American Geophysical Union* **89**, 289-290 (2008), doi:10.1029/2008EO320002.

Klemperer, S. L., Miller, E.L., Grantz, A., Scholl, D.W. & the Bering-Chukchi Working Group. Crustal structure of the Bering and Chukchi shelves: Deep seismic reflection profiles across the North American continent between Alaska and Russia. In *Tectonic Evolution of the Bering Shelf-Chukchi Sea-Arctic Margin and Adjacent Landmasses* (eds Miller, E. L., Grantz, A. & Klemperer, S. L.), 1-24 (2002), The Geological Society of America Special Paper, Boulder/Colorado, ISBN:9780813723600.

Kominz, M. A., Browning, J. V., Miller, K. G., Sugarman, P. J., Mizintsevaw, S. & Scotese, C. R. Late Cretaceous to Miocene sea-level estimates from the New Jersey and Delaware coastal plain coreholes: an error analysis. *Basin Research* **20**, 211-226 (2008), doi:10.1111/j.1365-2117.2008.00354.x.

Kristofferson, Y. Eurasia Basin. In *The Arctic Ocean region, The Geology of North America, Vol.* **L** (eds Grantz, A., Johnson, L. & Sweeney, J. F.), 365-378 (1990), The Geological Society of America, Boulder/Colorado, ISBN:0813752116.

Kumar, N., Granath, J. W., Emmet, P. A., Helwig, J. A. & Dinkelman, M. G. Stratigraphic and tectonic framework of the US Chukchi Shelf: exploration insights from a new regional deep-seismic reflection survey. In *Arctic Petroleum Geology, Memoirs* **35** (eds Spencer, A. M., Embry, A. F., Gautier, D. L., Stoupakova, A. V. & Sørensen, K.), 501-508 (2011), The Geological Society of London, ISBN:1862393281.

Lane, L. S. Canada Basin, Arctic Ocean: Evidence against a rotational origin. *Tectonics* **16**, 363-387 (1997), doi:10.1029/97TC00432.

Lawver, L. A., & Scotese, C. A review of tectonic models for the evolution of the Canada Basin. In *The Arctic Ocean region, The Geology of North America, Vol.* **L** (eds Grantz, A., Johnson, L. & Sweeney, J. F.), 593-618 (1990), The Geological Society of America, Boulder/Colorado, ISBN:0813752116.

Lawver, L.A. & Müller, R.D. Iceland hotspot track. *Geology* **22**, 311-314 (1994), doi:10.1130/0091-7613(1994)022<0311:IHT>2.3.CO;2.

Lawver, L. A., Grantz, A. & Gahagan, L. M. Plate kinematic evolution of the present Arctic region since the Ordovician. In *Tectonic Evolution of the Bering Shelf-Chukchi Sea-Arctic Margin and Adjacent Landmasses* (eds Miller, E. L., Grantz, A. & Klemperer, S. L.), 333-358 (2002), The Geological Society of America Special Paper, Boulder/Colorado, ISBN:9780813723600.

Laxon, S. W. & McAdoo, D. Arctic Ocean Gravity Field Derived From ERS-1 Satellite Altimetry. *Science* **265**, 621-624 (1994), doi:10.1126/science.265.5172.621.

Lebedeva-Ivanova, N.N., Zamansky, Y. Y., Langinen, A. E. & Sorokin, M. Y. Seismic profiling across the Mendeleev Ridge at 82°N: evidence of continental crust. *Geophysical Journal International* **165**, 527-544 (2006), doi:10.1111/j.1365-246X.2006.02859.x.

Lerand, M. M. Beaufort Sea. In *The future petroleum provinces of Canada: Their geology and potential, Memoir* **1** (ed McCrossan, R. G.), 315-386 (1973), Canadian Society of Petroleum Geologists.

Marincovich, L., Jr., Brouwers, E. M., Hopkins, D. M. & McKenna, M. C. Late Mesozoic and Cenozoic paleogeographic and paleoclimatic history of the Arctic Ocean Basin, based on shallow-water marine faunas and terrestrial vertebrates. In *The Arctic Ocean region, The Geology of North America, Vol.* **L** (eds Grantz, A., Johnson, L. & Sweeney, J. F.), 403-426 (1990), The Geological Society of America, Boulder/Colorado, ISBN:0813752116.

März, C., Vogt, C., Schnetger, B. & Brumsack, H. J. Variable Eocene-Miocene sedimentation processes and bottom water redox conditions in the Central Arctic Ocean (IODP Expedition 302). *Earth and Planetary Science Letters* **310**, 526-537 (2011), doi:10.1016/j.epsl.2011.08.025.

Maus, S., Barckhausen, U., Berkenbosch, H., Bournas, N., Brozena, J., Childers, V., Dostaler, F., Fairhead, J. D., Finn, C., von Frese, R. R. B., Gaina, C., Golynsky, S., Kucks, R., Lühr, H., Milligan, P., Mogren, S., Müller, R. D., Olesen, O., Pilkington, M., Saltus, R., Schreckenberger, B., Thébault, E. & Caratori Tontini, F. EMAG2: A 2-arc min resolution Earth Magnetic Anomaly Grid compiled from satellite, airborne, and marine magnetic measurements. *Geochemistry, Geophysics, Geosystems* **10**, pp. 12 (2009), doi:10.1029/2009GC002471.

McNeil, D. H., Duk-Rodkin, A., Dixon, J., Dietrich, J.R., White, J.M., Miller, K.G. & Issler, D.R. Sequence stratigraphy, biotic change, $^{87}Sr/^{86}Sr$ record, paleoclimatic history, and sedimentation rate change across a regional late Cenozoic unconformity in Arctic Canada. *Canadian Journal of Earth Sciences* **38**, 309-331 (2001), doi:10.1139/cjes-38-2-309.

Miller, K. G., Kominz, M. A., Browning, J. V., Wright, J. D., Mountain, G. S., Katz, M. E., Sugarman, P. J., Cramer, B. S., Christie-Blick, N. & Pekar, S. F. The Phanerozoic Record of Global Sea-Level Change. *Science* **310**, 1293-1298 (2005), doi:10.1126/science.1116412.

Miller, E. L., Toro, J., Gehrels, G., Amato, J. M., Prokopiev, A, Tuchkova, M. I., Akinin, V. V., Dumitru, T. A., Moore, T. E. & Cecile, M. P. New insights into Arctic paleogeography and tectonics from U-Pb detrital zircon geochronology. *Tectonics* **25**, pp. 19 (2006), doi:10.1029/2005TC001830.

Miller, E. L. & Verzhbitsky, V. E. Structural studies near Pevek, Russia: implications for formation of the East Siberian Shelf and Makarov Basin of the Arctic Ocean.

Stephan Mueller Special Publication Series **4**, 223-241 (2009), doi:10.5194/smsps-4-223-2009.

Miller, E. L., Gehrels, G. E., Pease, V. & Sokolov S. Stratigraphy and U-Pb detrital zircon geochronology of Wrangel Island, Russia: Implications for Arctic paleogeography. *American Association of Petroleum Geologists Bulletin* **94**, 665-692 (2010), doi:10.1306/10200909036.

Militzer, H. & Weber, F. Angewandte Geophysik, Band 3: Seismik. pp. 420 (1987), Springer Wien, ISBN:3211817999.

Moore, T. E., Wallace, W. K., Bird, K. J., Karl, S. M., Mull, C. G. & Dillon, J. T. Geology of northern Alaska. In *The Geology of Alaska, The Geology of North America, Vol.* **G-1** (eds Plafker, G. & Berg, H. C.), 49-138 (1994), Geological Society of America, Boulder/Colorado, ISBN:0813752191.

Mutter, J. C. Seaward dipping reflectors and the continent-ocean boundary at passive continental margins. *Tectonophysics* **114**, 117-131 (1985), doi:10.1016/0040-1951(85)90009-5.

Oldenburg, D. W. The inversion and interpretation of gravity anomalies. *Geophysics* **39**, 526-536 (1974), doi:10.1190/1.1440444.

O'Regan, M., Moran, K., Backman, J., Jakobsson, M., Sangiorgi, F., Brinkhuis, H., Pockalny, R., Skelton, A., Stickley, C., Koç, N., Brumsack, H.-J. & Willard, D. Mid-Cenozoic tectonic and paleoenvironmental setting of the central Arctic Ocean. *Paleoceanography* **23**, pp. 15 (2008), doi:10.1029/2007PA001559.

Ostenso, N. A., & Wold, R. J. Aeromagnetic Evidence for Origin of Arctic Ocean Basin: Evolution of Arctic Ocean Basin. In *Arctic Geology, American Association of Petroleum Geologists Memoir* **19** (ed Pitcher, M. G.), 506-516 (1973).

Parker, R. L. The Rapid Calculation of Potential Anomalies. *Geophysical Journal of the Royal Astronomical Society* **31**, 447-455 (1972), doi:10.1111/j.1365-246X.1973.tb06513.x.

Plafker, G. & Berg, H. C. An overview of the geology and tectonic evolution of Alaska. In *The Geology of Alaska, The Geology of North America, Vol.* **G-1** (eds Plafker, G. & Berg, H. C.), 989-1021 (1994), The Geological Society of America, Boulder/Colorado, ISBN:0813752191.

Planke, S. & Cambray, H. Seismic properties of flood basalts from Hole 917A downhole data, southeast Greenland volcanic margin. In *Proceedings of the Ocean Drilling Program, Scientific Results* **152** (eds Saunders, A. D., Larsen, H. C. & Wise, S. W., Jr.), 453-462 (1998), College Station/Texas (Ocean Drilling Program), doi:10.2973/odp.proc.sr.152.247.1998.

Rowley, D. B. & Lottes, A. L. Plate-kinematic reconstructions of the North Atlantic and Arctic: Late Jurassic to Present. *Tectonophysics* **155**, 73-120 (1988), doi:10.1016/0040-1951(88)90261-2.

Schmidt, S. & Götze, H.-J. Integration of Data Constraints and Potential Field Modelling - an Example from Southern Lower Saxony, Germany. *Physics and Chemistry of the Earth, Part A* **24**, 191-196 (1999), doi:10.1016/S1464-1895(99)00017-4.

Schmidt, S. Interactive Gravity and Magnetic Application System (IGMAS). *Online Manual*, http://www.gravity.uni-kiel.de/igmas/ (Last update: September 13, 2004).

Schön, J. H. Physical Properties of Rocks: Fundamentals and Principles of Petrophysics. pp. 600 (2004), Elsevier, Heidelberg, ISBN:9780080443461.

Sekretov S. B. Northwestern margin of the East Siberian Sea, Russian Arctic: seismic stratigraphy, structure of the sedimentary cover and some remarks on the tectonic history. *Tectonophysics* **339**, 353-383 (2001), doi:10.1016/S0040-1951(01)00108-1.

Shaver, R. & Hunkins, K. Arctic Ocean geophysical studies: Chukchi Cap and Chukchi Abyssal Plain. *Deep-Sea Research* **11**, 905-916 (1964), doi:10.1016/0011-7471(64)90340-7.

Sherwood, K. W., Johnson, P. P., Craig, J. D., Zerwick, S. A., Lothamer, R. T., Thurston, D. K. & Hurlbert, S. B. Structure and stratigraphy of the Hanna Trough, U.S. Chukchi Shelf, Alaska. In *Tectonic Evolution of the Bering Shelf-Chukchi Sea-Arctic Margin and Adjacent Landmasses* (eds Miller, E. L., Grantz, A. & Klemperer, S. L.), 39-66 (2002), The Geological Society of America Special Paper, Boulder/Colorado, ISBN:9780813723600.

Sorokin, M. Yu., Zamansky, Yu. Ya., Langinen, A. Ye., Jackson, H. R. & Macnab, R. Crustal structure of the Makarov Basin, Arctic Ocean determined by seismic refraction. *Earth and Planetary Science Letters* **168**, 187-199 (1999), doi:10.1016/S0012-821X(99)00049-7.

Steckler, M. S., Mountain, G. S., Miller, K. G. & Christie-Blick, N. Reconstruction of Tertiary progradation and clinoform development on the New Jersey passive margin by 2-D backstripping. *Marine Geology* **154**, 399-420 (1999), doi:10.1016/S0025-3227(98)00126-1.

Steffen, R., Steffen, H. & Jentzsch, G. A three-dimensional Moho depth model for the Tien Shan from EGM2008 gravity data. *Tectonics* **30**, pp. 19 (2011), doi:10.1029/2011TC002886.

Stein, R. Arctic Ocean Sediments: Processes, Proxies, and Paleoenvironment. pp. 608 (2008), Elsevier Science & Technology, ISBN:978-0-444-52018-0.

Tolson, R. B. Structure and Stratigraphy of the Hope Basin, Southern Chukchi Sea, Alaska. In *Geology and Resource Potential of the Continental Margin of Western North America and Adjacent Ocean Basins - Beaufort Sea to Baja California* (eds Scholl, D. W., Grantz, A. & Vedder, J. G.), 59-71 (1987), Circum-Pacific Coun-

cil for Energy and Mineral Resources, Earth Sciences Series 6, Housten/Texas, ISBN:0933687060.

USGS - United States Geological Service. National Archive of Marine Seismic Surveys (NAMSS). *Online database*, http://walrus.wr.usgs.gov/NAMSS/ (Last update: April 03, 2012).

Vail, P. R., Mitchum, R. M., Jr. & Thompson, S. Seismic Stratigraphy and Global Changes of Sea Level, Part 3: Relative Changes of Sea Level from Coastal Onlap. In *Seismic Stratigraphy: Applications to Hydrocarbon Exploration, American Association of Petroleum Geologists Memoir* **26** (ed Payton, C. E.), 63-81 (1977a), American Association of Petroleum Geologists, Tulsa/Oklahoma, ISBN:0891813020.

Vail, P. R., Mitchum, R. M., Jr. & Thompson, S. Seismic Stratigraphy and Global Changes of Sea Level, Part 4: Global Cycles of Relative Changes of Sea Level. In *Seismic Stratigraphy: Applications to Hydrocarbon Exploration, American Association of Petroleum Geologists Memoir* **26** (ed Payton, C. E.), 83-97 (1977b), American Association of Petroleum Geologists, Tulsa/Oklahoma, ISBN:0891813020.

Vandamme, D., Courtillot, V., Besse, J. & Montigny, R. Paleomagnetism and age determinations of the Deccan Traps (India): Results of a Nagpur-Bombay Traverse and review of earlier work. *Reviews of Geophysics* **29**, 159-190 (1991), doi:10.1029/91RG00218.

Verschuur, D. J. Seismic multiple removal techniques: Past, present and future. pp. 191 (2006), European Association of Geoscientists & Engineers Publications, Houten/Netherlands, ISBN:90-73781-51-5.

Verzhbitsky, V., Frantzen, E., Savostina, T., Little, A., Sokolov, S. D. & Tuchkova, M. I. Russian Chukchi Sea. *GEOExpro* **5**, 36-41 (2008), www.geoexpro.com/article/Russian_Chukchi_Sea/d2f0d9b3.aspx.

Verzhbitsky, E. V., Lobkovskii, L. I., Kononov, M. V. & Byakov, A. F. Age of the Alpha-Mendeleev and Lomonosov ridges (Amerasian Basin). *Doklady Earth Sciences* **441**, 1587-1590 (2011), doi:10.1134/S1028334X11110316.

Vogt, P. R., Taylor, P. T., Kovacs, L. C. & Johnson, G. L. Detailed Aeromagnetic Investigation of the Arctic Basin. *Journal of Geophysical Research* **84**, 1071-1089 (1979), doi:10.1029/JB084iB03p01071.

Vogt, P. R., Jung, W. Y. & Brozena, J. Arctic margin gravity highs: Deeper meaning for sediment depocenters? *Marine Geophysical Researches* **20**, 459-477 (1998), doi:10.1023/A:1004775228851.

Weber, J. R., & Sweeney, J. F. Ridges and basins in the central Arctic Ocean. In *The Arctic Ocean region, The Geology of North America, Vol.* **L** (eds Grantz, A., Johnson, L. & Sweeney, J. F.), 305-336 (1990), The Geological Society of America, Boulder/Colorado, ISBN:0813752116.

Wienecke, S., Mariani, P., Ebbing, J. & Braitenberg, C. LithoFLEX Tutorial. *Online manual*, http://www.lithoflex.org/lithoflex/home/basics/Lithoflex_tutorial.pdf (Last update: June 28, 2008).

Yilmaz, Ö. *Seismic Data Analysis - Processing, Inversion and Interpretation of Seismic Data* pp. 2027 (2001), Society of Exploration Geophysics, Tulsa/Oklahoma, ISBN:1560800984.

Zachos, J., Pagani, M., Sloan, L., Thomas, E. & Billups, K. Trends, Rhythms, and Aberrations in Global Climate 65 Ma to Present. *Science* **292**, 686-693 (2001), doi:10.1126/science.1059412.

Zelt, C. A. & Smith, R. B. Seismic traveltime inversion for 2-D crustal velocity structure. *Geophysical Journal International* **108**, 16-34 (1992), doi:10.1111/j.1365-246X.1992.tb00836.x.

Acknowledgment

Finally, let me express my sincere thanks and appreciation to all people listed below for their help and support during my 3 years PhD work at the Alfred Wegener Institute in Bremerhaven and the Friedrich Schiller University in Jena. I would like to thanks in particular:

Prof. Dr. Gerhard Jentzsch (FSU Jena)	doctoral advisor; for taking over the evaluation of my thesis at the Friedrich Schiller University in Jena and for his constructive comments during my final writing phase of this thesis
Prof. Dr. Wilfried Jokat (AWI)	superior; for making it possible for me to attend several international congresses, ship expeditions to the Arctic Ocean, and a two month stay at the University of Alaska, Fairbanks
Prof. Dr. Michael Korn (University Leipzig)	external examiner; for taking over the external evaluation of my thesis
PD Dr. Thomas Jahr (FSU Jena)	internal examiner; for answering my questions concerning the 3D gravity modelling, for taking over the evaluation of my thesis, and for his constructive comments during my final writing phase of this thesis
The captain and the crew of R/V Polarstern as well as the seismic team	for their excellent job during the ARK-XXIII/3 summer expedition in 2008

WesternGeco, ION-GXT, TGS-NOPEC, USGS	for getting an insight in their seismic reflection data on the Chukchi Shelf
Prof. Dr. Bernard Coakley (UAF)	for making it possible for me to participate the American expedition MGL 11-12 in 2011 where I got a first view on the seismic data which are located in the "data gap" on the Chukchi Shelf, and for his help during my two month stay at the University of Alaska, Fairbanks
Dr. David Houseknecht (USGS)	for the interesting and helpful discussions about sediment ages and structures in the Chukchi region as well as for the insight into his interpreted seismic lines on the Chukchi Shelf and in the Beaufort Sea
Dr. Gabi Uenzelmann-Neben (AWI)	for her help with the seismic data interpretation software *LANDMARK*
AWI marine geophysics group	for the good working atmosphere and that they were always be prepared to listen to questions and to discuss problems
Stefanie Kaboth and Tobias Hermann	for the proof reading of the final thesis
Friends and **Family**	**for all the great things, activities and help**

Selbstständigkeitserklärung

Ich erkläre, dass ich die vorliegende Arbeit selbstständig und unter Verwendung der angegebenen Hilfsmittel, persönlichen Mitteilungen und Quellen angefertigt habe.

Jena, den 24. Oktober 2012

Anne Hegewald

Curriculum Vitae

Personal details

Name:	Anne Hegewald
Date of birth:	11. January 1985
Place of birth:	Erfurt
Nationality:	German

Education

08/95 to 06/03	**High School Diploma**, Neideck-Gymnasium Arnstadt
10/03 to 03/09	**Geophysics Study**, Friedrich Schiller University Jena
since 04/09	**PhD Student**, Friedrich Schiller University Jena and AWI

Employments

01/06 to 12/08	**Student Assistant**, Friedrich Schiller University Jena
07/07 to 10/07	**Trainee**, Alfred Wegener Institute Bremerhaven
since 04/09	**PhD Student**, Alfred Wegener Institute Bremerhaven

Experiences

08/08 to 10/08	**Student Assistant**, RV Polarstern expedition (ARK 23-3), charged by AWI, Chukchi region (Arctic Ocean)
08/09 to 09/09	**Research Assistant**, RV Polarstern expedition (ARK 24-3), charged by AWI, northeast Greenland and Fram Strait
07/10 to 10/10	**Research Assistant**, RV Polarstern expedition (ARK 25-3), charged by BGR, northwest Greenland and Baffin Bay
09/11 to 10/11	**Research Assistant**, RV Langseth expedition (MGL11-12), charged by UAF, Chukchi region (Arctic Ocean)
10/11 to 11/11	**Stay at the UAF**, University of Alaska, Fairbanks

Conference Presentations

09/08 Old versus New: The mechanical LaCoste & Romberg gravimeter ET18 in comparison with the superconducting gravimeter CD-034 at the broad-band observatory Moxa.
Earth Tide Symposium, Jena

03/09 Analyse der Daten des LaCoste und Romberg Gravimeters ET18 und Vergleich mit dem supraleitenden Gravimeter CD-034.
DGG Conference, Kiel

10/09 Variations along the continental margin from Alaska to the Lomonosov Ridge.
Penrose Conference, Banff

12/10 Relative sea-level variations in the Amerasia Basin since the Lower Cretaceous.
AGU Fall Meeting, San Francisco

06/11 Sedimentary structures and horizon ages in the Amerasian Basin between the Chukchi Plateau and Mendeleev Ridge.
Internationale Conference on Arctic Margins, Fairbanks
(Student recognition award for outstanding oral presentation)

12/11 Sediment structures and sediment ages of the Chukchi region, Amerasia Basin.
AGU Fall Meeting, San Francisco

Jena, den 24. Oktober 2012

Anne Hegewald